National Library of Canada
Bibliothèque nationale du Canada

Canadian Theses Service
Service des thèses canadiennes

Ottawa, Canada
K1A 0N4

NOTICE

The quality of this microform is heavily dependent upon the quality of the original thesis submitted for microfilming. Every effort has been made to ensure the highest quality of reproduction possible.

If pages are missing, contact the university which granted the degree.

Some pages may have indistinct print especially if the original pages were typed with a poor typewriter ribbon or if the university sent us an inferior photocopy.

Reproduction in full or in part of this microform is governed by the Canadian Copyright Act, R.S.C. 1970, c. C-30, and subsequent amendments.

AVIS

La qualité de cette microforme dépend grandement de la qualité de la thèse soumise au microfilmage. Nous avons tout fait pour assurer une qualité supérieure de reproduction.

S'il manque des pages, veuillez communiquer avec l'université qui a conféré le grade.

La qualité d'impression de certaines pages peut laisser à désirer, surtout si les pages originales ont été dactylographiées à l'aide d'un ruban usé ou si l'université nous a fait parvenir une photocopie de qualité inférieure.

La reproduction, même partielle, de cette microforme est soumise à la Loi canadienne sur le droit d'auteur, SRC 1970, c. C-30, et ses amendements subséquents.

NL-339 (r. 88/04) c

Canada

HORIZONTAL WELL TESTING UNDER THERMAL AND NON-THERMAL SITUATIONS

BY

MOHAMMED BEN ISSAKA

C

A THESIS

SUBMITTED TO THE FACULTY OF GRADUATE STUDIES AND RESEARCH IN PARTIAL FULFILLMENT OF THE REQUIREMENTS FOR THE DEGREE OF

MASTER OF SCIENCE

IN

PETROLEUM ENGINEERING

DEPARTMENT OF MINING, METALLURGICAL AND PETROLEUM ENGINEERING

EDMONTON, ALBERTA

SPRING, 1992

National Library of Canada
Bibliothèque nationale du Canada

Canadian Theses Service
Service des thèses canadiennes

Ottawa, Canada
K1A 0N4

The author has granted an irrevocable non-exclusive licence allowing the National Library of Canada to reproduce, loan, distribute or sell copies of his/her thesis by any means and in any form or format, making this thesis available to interested persons.

L'auteur a accordé une licence irrévocable et non exclusive permettant à la Bibliothèque nationale du Canada de reproduire, prêter, distribuer ou vendre des copies de sa thèse de quelque manière et sous quelque forme que ce soit pour mettre des exemplaires de cette thèse à la disposition des personnes intéressées.

The author retains ownership of the copyright in his/her thesis. Neither the thesis nor substantial extracts from it may be printed or otherwise reproduced without his/her permission.

L'auteur conserve la propriété du droit d'auteur qui protège sa thèse. Ni la thèse ni des extraits substantiels de celle-ci ne doivent être imprimés ou autrement reproduits sans son autorisation.

ISBN 0-315-73199-0

Canada

RELEASE FORM

NAME OF AUTHOR: Mohammed Ben Issaka

TITLE OF THESIS: Horizontal Well Testing Under Thermal and Non-Thermal Situations

DEGREE FOR WHICH THESIS WAS PRESENTED: MASTER OF SCIENCE

YEAR THE DEGREE WAS GRANTED: SPRING, 1992

Permission is hereby granted to THE UNIVERSITY OF ALBERTA LIBRARY to reproduce single copies of this thesis and to lend or sell such copies for private, scholarly or scientific research purposes only.

The author reserves other publication rights, and neither the thesis nor extensive extracts from it may be printed or otherwise reproduced without the author's written permission.

(SIGNED)---[redacted] B Issaka

PERMANENT ADDRESS:

P. 0. BOX 245

TARKWA, GHANA

DATED: November 14 , 1991

THE UNIVERSITY OF ALBERTA

FACULTY OF GRADUATE STUDIES AND RESEARCH

The undersigned certify that they have read, and recommend to the Faculty of Graduate Studies and Research for acceptance, a thesis entitled "HORIZONTAL WELL TESTING UNDER THERMAL AND NON-THERMAL SITUATIONS" submitted by MOHAMMED BEN ISSAKA in partial fulfillment of the requirements for the degree of MASTER OF SCIENCE in PEROLEUM ENGINEERING.

A. K. Ambastha (Supervisor)

J. M. Whiting

S. M. Farouq Ali

K. T. Chuang

DATED: October 17, 1991

ABSTRACT

Horizontal wells are becoming popular for primary and enhanced oil recovery operations because of unique advantages of horizontal wells in comparison to those for vertical wells. Monitoring the progress of a steam injection process requires a knowledge of the steam-swept volume, as this provides a measure of the heat loss from the heated zone. Well testing offers a relatively quick and inexpensive way of estimating the steam-swept volume. The pseudosteady state method has been used to estimate the swept volume, from pressure falloff testing of vertical wells, with a good degree of success. However, horizontal well testing is considerably more complex than vertical well testing.

To gain an insight into the pressure transient behaviour of a horizontal well under steam injection, an analytical study of the transient pressure behaviour of horizontal wells has been conducted. This study uses numerical integration to evaluate an analytical solution for the transient pressure response of a horizontal well located in a closed, box-shaped, anisotropic reservoir. Results from this study show that numerical integration can be used to evaluate the solution with a comparative degree of accuracy, while avoiding the convergence problems associated with the analytical integration. Both drawdown and buildup responses have been studied.

New time criteria, based on the semi-log pressure derivative response, are proposed for well test analysis and design purposes. These time criteria generally suggest shorter flow period durations than those corresponding to the time criteria based on the pressure response. The effects of well radius, well location and reservoir size on the drawdown pressure derivative response are discussed. Producing time effects on the buildup pressure derivative responses are also investigated. Results show that for a horizontal well in a

closed reservoir, the late linear flow period will not occur on the buildup response for any case, even when the late linear flow period is present on the drawdown response.

To evaluate the accuracy and applicability of the pseudosteady state method in the estimation of swept volume for steam injection through a horizontal well, a thermal numerical simulator is used to generate the pressure falloff data. Results of the study show that the pseudosteady state method may be used to estimate the swept volume for steam injection through a horizontal well. However, swept volume may be overestimated by 10 to 60 per cent. Injection time effects on the estimated swept volume are also studied. Results indicate that longer injection times prior to shut-in appear to have an adverse effect on the estimated swept volume because of a more irregular swept region shape for longer injection time cases. Analyses of the well test data show that steam chamber mobility can be accurately estimated from pressure falloff tests of horizontal wells. Irregular swept region shape does not appear to have a noticeable effect on the early time well test data.

ACKNOWLEDGEMENTS

The author wishes to express his sincere gratitude and appreciation to Professor A. K. Ambastha for his guidance and support throughout this study. Financial support for this work and my graduate studies was provided by the Alberta Oil Sands Technology and Research Authority (AOSTRA), for which I am very thankful. I also wish to acknowledge the use of the In Situ Combustion and Steam Reservoir Simulator (ISCOM) developed by the Computer Modelling Group of Calgary, Alberta. Finally, I would like to thank my wife, Esi, and my daughters, Fauzia and Sharifah for their patience, understanding and support during my graduate studies.

TABLE OF CONTENTS

Page

1. INTRODUCTION 1
2. LITERATURE REVIEW 3
   - 2.1 Transient Pressure Behaviour of Horizontal Wells 3
     - 2.1.1 Drawdown Response 3
     - 2.1.2 Buildup Response 7
     - 2.1.3 Producing Time Effects on Buildup Response 7
   - 2.2 Thermal Well Testing for a Horizontal Well 8
     - 2.2.1 Estimating Swept Volume 9
       - 2.2.1.1 Deviation Time Method 10
       - 2.2.1.2 Intersection Time Method 10
       - 2.2.1.3 Type Curve Matching Method 11
       - 2.2.1.4 Pseudosteady State Method 13
3. STATEMENT OF THE PROBLEM 17
4. TRANSIENT PRESSURE BEHAVIOUR OF HORIZONTAL WELLS 19
   - 4.1 Drawdown Response 19
     - 4.1.1 Model Description 19
     - 4.1.2 Mathematical Formulation 21
     - 4.1.3 General Solution 21
     - 4.1.4 Transient Flow Regime Description 27
       - 4.1.4.1 Early Radial Flow 27
       - 4.1.4.2 Early Linear Flow 27
       - 4.1.4.3 Late Pseudo-Radial Flow 28

4.1.4.4 Late Linear Flow 28
4.1.5 Time Criteria Based on Pressure Derivative Response 29
4.1.6 Sensitivity Study 31
4.1.6.1 Well Radius 31
4.1.6.2 Well Location 33
4.1.6.3 Reservoir Size 36
4.2 Buildup Response 39
4.2.1 Mathematical Development 39
4.2.2 Producing Time Effects on Buildup Response 41
5. THERMAL WELL TESTING FOR A HORIZONTAL WELL 50
5.1 Theory 50
5.2 Reservoir Model 54
5.2.1 Reservoir Size 54
5.2.2 Reservoir Properties 56
5.2.3 Fluid Properties 58
5.2.4 Simulator 59
5.3 Cases Studied 59
5.4 Simulation Results and Discussion 60
5.4.1 Results of Run 1 60
5.4.1.1 Identification of Flow Regimes 62
5.4.1.2 Estimation of Swept Volume 64
5.4.1.3 Estimation of Steam Chamber Mobility 67
5.4.2 Possible Causes of Swept Volume and Mobility Overestimation 70
5.4.2.1 Effect of Wellbore Gridblock Size 71
5.4.2.2 Injection Time Effects on Swept Volume Estimation .. 74
5.4.2.3 Injection Rate Effect on Swept Volume Estimation 78

5.4.2.4 Effect of Isotropy on Swept Volume Estimation.....78

5.4.2.5 Results of Steam Chamber Mobility Estimation 79

6. CONCLUSIONS AND RECOMMENDATIONS 81

6.1 Conclusions 81

6.2 Recommendations 83

REFERENCES 84

APPENDIX A Computer programs.....89

APPENDIX B Sample input data and results..... 100

APPENDIX C Development of Design Equations.....102

APPENDIX D Further Analysis Equations.....111

APPENDIX E Figures for Analysis of Thermal Well Test Data.....113

LIST OF TABLES

Page

Table 4.1: Comparison of time criteria based on pressure response with those based on pressure derivative response....30

Table 5.1: Reservoir parameters used in simulation....56

Table 5.2: Viscosity-temperature relationships for reservoir fluids....58

Table 5.3: Cases studied....60

Table 5.4: Conditions at the start of falloff test simulation....70

Table 5.5: Steam chamber mobility and skin factor....74

Table 5.6: Simulated falloff test results....75

Table C1: Data for estimating time to the end of early radial flow period....103

Table C2: Data for estimating time to the start of early linear flow period....104

Table C3: Data for estimating time to the end of early linear flow period....104

Table C4: Data for estimating time to the start of late pseudo-radial flow period....105

Table C5: Data for estimating time to the end of late pseudo-radial flow period....106

Table C6: Data for estimating time to the start of late linear flow period....107

Table C7: Data for estimating time to the end of late linear flow period....107

Table C8: Comparison of deviation times predicted by Eq. (C-8) with the actual deviation times (MDH slope within 5% of drawdown slope)....108

Table C9: Comparison of deviation times predicted by Eq. (C-9) with the actual deviation times (MDH slope within 5% of drawdown slope)....109

Table C10: Comparison of deviation times predicted by Eq. (C-10) with the actual deviation times (MDH slope within 5% of drawdown slope)....110

LIST OF FIGURES

Page

Figure 4.1: Schematic of a horizontal well in a box-shaped reservoir.....20

Figure 4.2: Dimensionless pressure and semi-log pressure derivative response for a horizontal well in closed, box-shaped reservoir.....26

Figure 4.3: Comparison of pressure response from this study with the response from the Odeh and Babu study for the early radial flow period.....26

Figure 4.4: Effect of well radius on the semi-log pressure derivative response for a horizontal well.....32

Figure 4.5: Effect of x-direction well location on the semi-log pressure derivative response for a horizontal well.....34

Figure 4.6: Effect of y-direction well location on the semi-log pressure derivative response for a horizontal well.....35

Figure 4.7: Effect of z-direction well location on the semi-log pressure derivative response for a horizontal well.....35

Figure 4.8: Effect of reservoir length on the semi-log pressure derivative response for a horizontal well.....37

Figure 4.9: Effect of reservoir width on the semi-log pressure derivative response for a horizontal well.....38

Figure 4.10: Effect of reservoir height on the semi-log pressure derivative response for a horizontal well.....38

Figure 4.11: Comparison of MDH and Agarwal slopes for a short producing time.....43

Figure 4.12: Effect of t_{pDA} on MDH slope for a_D=1, b_D=1, and h_D=1.....44

Figure 4.13: Effect of t_{pDA} on Agarwal slope for a_D=1, b_D=1, and h_D=1.....44

Figure 4.14: Effect of t_{pDA} on MDH slope for a_D=4, b_D=1, and h_D=1.....46

Figure 4.15: Effect of t_{pDA} on Agarwal slope for a_D=4, b_D=1, and h_D=1.....46

Figure 4.16: Effect of t_{pDA} on MDH slope for a_D=10, b_D=4, and h_D=0.2.....48

Figure 4.17: Effect of t_{pDA} on Agarwal slope for a_D=10, b_D=4, and h_D=0.2.....48

Figure 5.1: Schematic of 3-D reservoir model used for simulation.....55

Figure 5.2: Water/oil relative permeability.....57

Figure 5.3: Gas/oil relative permeability.....57

Figure 5.4: Falloff response from simulator for Run 1.....61

Figure 5.5: Semi-log pressure derivative response from simulator for Run 1....63

Figure 5.6: Semi-log pressure derivative response from analytical solution for Run 1.....63

Figure 5.7: Cartesian graph of falloff data for Run 1.....66

Figure 5.8: Semi-log graph of falloff data for Run 1.....69

Figure 5.9: Pressure falloff data for Runs 1 and 2.....72

Figure 5.10: Semi-log pressure derivative data for Runs 1 and 2.....72

Figure 5.11: Semi-log graph of falloff data for Runs 1 and 2.....73

Figure 5.12: Pressure falloff data for Runs 2, 3, 4 and 5.....77

Figure 5.13: Swept region shapes for Runs 4, 5, 6, 8 and 10.....77

Figure 5.14: Comparison of simulated and calculated semi-log slopes for all simulation runs.....80

Figure E1a: Falloff response from simulator for Run 1.....114

Figure E1b: Semi-log pressure derivative response from simulator for Run 1..114

Figure E1c: Cartesian graph of falloff data for Run 1.....115

Figure E1d: Semi-log graph of falloff data for Run 1.....115

Figure E2a: Falloff response from simulator for Run 2.....116

Figure E2b: Semi-log pressure derivative response from simulator for Run 2..116

Figure E2c: Cartesian graph of falloff data for Run 2.....117

Figure E2d: Semi-log graph of falloff data for Run 2.....117

Figure E3a: Falloff response from simulator for Run 3.....118

Figure E3b: Semi-log pressure derivative response from simulator for Run 3..118

Figure E3c: Cartesian graph of falloff data for Run 3.....119
Figure E3d: Semi-log graph of falloff data for Run 3.....119
Figure E4a: Falloff response from simulator for Run 4.....120
Figure E4b: Semi-log pressure derivative response from simulator for Run 4....120
Figure E4c: Cartesian graph of falloff data for Run 4.....121
Figure E4d: Semi-log graph of falloff data for Run 4.....121
Figure E5a: Falloff response from simulator for Run 5.....122
Figure E5b: Semi-log pressure derivative response from simulator for Run 5....122
Figure E5c: Cartesian graph of falloff data for Run 5.....123
Figure E5d: Semi-log graph of falloff data for Run 5.....123
Figure E6a: Falloff response from simulator for Run 6.....124
Figure E6b: Semi-log pressure derivative response from simulator for Run 6....124
Figure E6c: Cartesian graph of falloff data for Run 6.....125
Figure E6d: Semi-log graph of falloff data for Run 6.....125
Figure E7a: Falloff response from simulator for Run 7.....126
Figure E7b: Semi-log pressure derivative response from simulator for Run 7....126
Figure E7c: Cartesian graph of falloff data for Run 7.....127
Figure E7d: Semi-log graph of falloff data for Run 7.....127
Figure E8a: Falloff response from simulator for Run 8.....128
Figure E8b: Semi-log pressure derivative response from simulator for Run 8....128
Figure E8c: Cartesian graph of falloff data for Run 8.....129
Figure E8d: Semi-log graph of falloff data for Run 8.....129
Figure E9a: Falloff response from simulator for Run 9.....130
Figure E9b: Semi-log pressure derivative response from simulator for Run 9....130
Figure E9c: Cartesian graph of falloff data for Run 9.....131
Figure E9d: Semi-log graph of falloff data for Run 9.....131
Figure E10a: Falloff response from simulator for Run 10.....132

Figure E10b: Semi-log pressure derivative response from simulator for Run 10...132
Figure E10c: Cartesian graph of falloff data for Run 10.....133
Figure E10d: Semi-log graph of falloff data for Run 10.....133

NOMENCLATURE

a = reservoir length (x-direction), ft

b = reservoir width (y-direction), ft

B_g = gas formation volume factor, ft^3/SCF

c = compressibility, psi^{-1}

c_t = total compressibility, 1/psi

c_{thw} = total hot water zone compressibility, psi^{-1}

c_{ts} = total steam zone compressibility, psi^{-1}

$c_{2\phi}$ = two-phase compressibility, psi^{-1}

C = heat capacity, BTU/lb-^oF

C_D = dimensionless storage constant

d_x = the shortest distance between the well and the x-boundary, ft

d_y = the shortest distance between the well and the y-boundary, ft

d_z = the shortest distance between the well and the z-boundary, ft

D_y = the longest distance between the well and the y-boundary, ft

D_z = the longest distance between the well and the z-boundary, ft

f_{st} = steam quality, fraction

h = reservoir thickness(z-direction), ft

k_{rg} = gas relative permeability

k_x = permeability in the x-direction, md

k_y = permeability in the y-direction, md

k_z = permeability in the z-direction, md

L = length of well, ft

L_D = dimensionless well length

L_v = latent heat of vaporization, BTU/lb

m' = slope of pressure vs square root of time graph, $psi/hr^{1/2}$

$minm$ = minimum

$maxm$ = maximum

m_c = Cartesian slope corresponding to pseudosteady state flow, psi/hr

m_{cw} = Cartesian slope corresponding to wellbore-dominated flow, psi/hr

m_s = semi-log slope, psi/cycle

p = pressure, psi

p_i = initial pressure, psi

p_{wD} = dimensionless wellbore pressure

p_{wDs} = dimensionless well shut-in pressure

p_{wf} = well flowing pressure, psi

p_{wfs} = wellbore grid block pressure at the instant of shut-in, psi

p_{ws} = wellbore grid block shut-in pressure, psi

q = flow rate, STB/day

q_s = steam flow rate, SCF/day

r_w = wellbore radius, ft

r_{we} = effective wellbore radius, ft

s = wellbore skin, dimensionless

S = saturation, fraction

t = time, hours

t_D = dimensionless time

t_{DA} = dimensionless time based on area

t_{pD} = dimensionless producing time

t_{pDA} = dimensionless producing time based on area

T = temperature, ^oF

V_{hw} = hot water-swept pore volume, ft^3

V_s = swept pore volume, ft^3

V_{st} = steam-swept pore volume, ft^3

Greek Symbols

α = $3790.85\phi\mu c_t$, hr

β = formation volume factor, ft^3/SC

Δp_w = well pressure drop, psi

Δt = shut-in time, hr

Δt_D = dimensionless shut-in time

Δt_{DA} = dimensionless shut-in time = $\Delta t_D/(a_D b_D)$

Δt_{eD} = dimensionless equivalent drawdown time

$(\Delta t_{DA})_{dev}$ = dimensionless deviation time

Δx = grid block length, ft

Δy = grid block width, ft

Δz = grid block height, ft

μ = viscosity, cp

ρ = density, lb/ft^3

θ = angle

ϕ = porosity, fraction

ϑ_s = specific volume of steam, ft^3/lb

$(\vartheta_s)_{std.}$ = specific volume of steam at standard conditions, ft^3/lb

Subscripts

c = Cartesian

D = dimensionless

dev = deviation

f = formation

g = gas

hw = hot water

i = initial

o = oil

pss = pseudosteady state

s = swept, steam or semi-log

std. = standard conditions

t = total

w = water or wellbore

x = x-direction

y = y-direction

z = z-direction

0 = well location

1 = first

2 = second

2ø = two-phase

1. INTRODUCTION

As the world's reserves of conventional (light) oil are depleted, the exploitation of heavy oil is becoming more and more important. Currently, thermal recovery by steam injection is the dominant method for producing heavy oil around the world. To monitor the progress of a steam injection process, a knowledge of the steam-swept volume is required. The volume occupied by steam, after a period of injection, will provide a measure of the heat loss from the heated zone, and the technical and economic feasibility of the project.

Over the years, various methods have been used to estimate swept volume for both steam injection and in-situ combustion projects. In field operations, coring, as well as temperature observations made at wells during the passage of the displacement front, have been used. These methods are, however, very expensive and time consuming. Well testing offers a relatively quick and inexpensive way of estimating the steam swept volume.

The most common well test used for estimating swept volume has been the pressure falloff test. Pressure transient analysis of falloff data to estimate swept volume is based on the pseudosteady state method. This method is independent of the geometry of the swept region, and has been used to estimate swept volume for both steam injection and in-situ combustion processes involving vertical wells with apparent success. Due to the large contrast in mobility between the swept zone and the unswept zone, the flood front tends to behave like a closed boundary. Thus, when pressure falloff data are graphed against time, the data, for a vertical well, indicate an initial semi-log straight line, characteristic of fluid mobility in the swept region. This semi-log straight line is followed by a Cartesian straight line, which is related to the volume of the swept region. The Cartesian straight line

represents a period when the front behaves as a closed boundary. Another semi-log straight line may follow, corresponding to the mobility in the unswept region.

The ability of horizontal wells to provide large surface areas of contact with the reservoir makes a horizontal well suitable for the efficient recovery of oil, especially from thin reservoirs. While a significant amount of research has been carried out in the area of pressure transient analysis for horizontal wells located in a homogeneous or a naturally-fractured reservoir, the applicability of the pseudosteady state method to the estimation of swept volume from horizontal wells has not been studied. Consequently, the main purpose of this study is to investigate the applicability of the pseudosteady state method to estimate swept volume for a horizontal well under steam injection.

To gain insight into the pressure transient behaviour of a horizontal well under steam injection, an analytical study of the transient pressure behaviour of a horizontal well located in a box-shaped reservoir has been conducted. The effects of some important variables on the transient pressure derivative response are studied. The effects of producing time, prior to shut-in, on the pressure buildup behaviour have also been investigated. Chapter 2 presents the literature survey conducted for the study, while the statement of the problem is presented in Chapter 3. Chapter 4 presents a detailed study of the transient pressure behaviour of a horizontal well in a box-shaped reservoir. Both the pressure drawdown and buildup responses are considered. In Chapter 5, the results of a numerical simulation study, conducted to determine the swept volume when steam is injected through a horizontal well, is presented. Finally, Chapter 6 presents conclusions drawn from this study and recommendations for further studies.

2. LITERATURE REVIEW

2.1 Transient Pressure Behaviour of Horizontal Wells

The use of horizontal wells in the oil industry began in the early 1940's[1]. Their development has, however, been slow due to excessive drilling costs as well as competition with hydraulic fracturing. While recent advances in technology have lowered drilling costs considerably, both laboratory and field studies have demonstrated the unique advantages of horizontal wells in:[2]

1. some naturally fractured reservoirs,
2. reservoirs with gas and/or water coning problems,
3. thin reservoirs, and
4. reservoirs with high vertical permeability.

Consequently, there has been a considerable interest in the research related to the reservoir engineering aspects of horizontal well technology. A number of analytical solutions for the pressure transient behaviour of horizontal wells have been presented in the literature [1-7].

2.1.1 Drawdown Response

Deviau, Mouronval, Bourdarot and Curutchet[3] have presented analytical solutions for analyzing the behaviour of horizontal wells, with and without wellbore storage and skin, in infinite homogeneous reservoirs. They considered both uniform-flux and infinite-conductivity inner boundary conditions, and noted that the infinite-conductivity

approximation related more closely to the real case than the uniform flux approximation. Solutions were developed for infinite, closed and constant pressure outer boundary conditions. Deviau et al.[3] identified two transient flow regimes as distinctive features of horizontal well behaviour. These include an early time circular radial flow in a vertical plane perpendicular to the well, and a late time horizontal pseudo-radial flow. They proposed time criteria to determine the beginning and the end of the transient flow periods, which can serve as a guide to semi-log analysis and well test design.

Another study by Clonts and Ramey[4] presented an analytical solution for the transient pressure response of a uniform-flux horizontal drainhole in an anisotropic reservoir of finite thickness, but infinite horizontal extension. The solution, which also applies for a reservoir with multiple drainholes in a vertical array, showed the possible occurrence of two transient flow types:[4]

1. For a short drainhole relative to the reservoir height, an initial radial flow perpendicular to the drainhole axis occurs,which is then followed by a transition to pseudo-radial flow.

2. For a long drainhole, the initial radial flow ends rapidly, and is followed by a linear flow idendical to that of uniform-flux vertical fracture.

Clonts and Ramey[4] presented a set of log-log type curves of dimensionless pressure versus dimensionless time for various drainhole radii, which can be used to determine reservoir characteristics. They also presented conditions under which horizontal drainholes may give greater productivity than vertical wells or hydraulic fractures.

Goode and Thambynayagam[1] have also presented an analytical solution for the transient pressure response during drawdown and buildup tests on a horizontal well. They considered an infinite-conductivity horizontal well located in a semi-infinite, homogeneous and anisotropic reservoir of uniform thickness and width. The three-dimensional diffusivity equation describing fluid flow in the reservoir model was solved with successive integral transforms. Goode and Thambynayagam[1] presented simplified solutions for the short, intermediate and long time flow behaviours. They validated their solution method by comparing their results with those from a numerical simulator as well as an analogous analytical solution by Hantush[8]. Predictions of the Goode and Thambynayagam[1] solution were found to be in good agreement with those of the numerical simulator and the Hantush[8] analytic solution.

Kuchuk, Goode, Wilkinson and Thambynayagam[5] extended the previously published works[1,3,4] on pressure transient behaviour of horizontal wells, to include analytic solutions for reservoirs with and without the effect of a gas cap and/or an aquifer. Treating the horizontal well as a uniform-flux line source, Kuchuk et al.[5] computed the pressure response at the well by averaging the pressure along the length of the well, rather than using an equivalent pressure point. They pointed out that averaging the pressure along the length of the well instead of using an equivalent pressure point, was the main difference between their solution scheme and other previously published solutions.[1,3,4] The Kuchuk et al.[5] solutions were presented in both Laplace space and real time. The pressure solution in the Laplace space was used to obtain solutions that account for wellbore storage and skin effects. Simpler equations and existence criteria were also presented for the flow periods that can occur during a pressure transient test.

Further analysis of the pressure transient behaviour of a horizontal well or drainhole has been presented by Ozkan and Raghavan[2], who compared the performances of horizontal

wells and fully penetrating vertical fractures. Wellbore pressures were computed for both infinite-conductivity and uniform-flux boundary conditions. Their conclusions were:

1. for a single horizontal well or drainhole, the infinite-conductivity idealization was the only viable boundary condition,

2. for two drainholes drilled in diametrically opposite directions from a single vertical well, either the infinite-conductivity or the uniform-flux idealization was appropriate, and

3. at long times, the pressure responses for long horizontal wells are almost identical to the responses for fully-penetrating vertically fractured wells.

Another analytical study of the transient pressure behaviour of horizontal wells has been presented by Odeh and Babu[6]. They noted that the infinite or semi-infinite extension assumption of the reservoir in the x-y plane could lead to the occurrence or non-occurrence of some of the transient flow periods. Therefore, they assumed their reservoir model to be completely sealed in all three directions. The three-dimensional differential equation describing fluid flow in the reservoir model was solved by using the method of separation of variables and Fourier series. Odeh and Babu[6] identified four possible transient flow periods for a horizontal well in a closed, box-shaped reservoir. They presented simplified equations describing the pressure-time relations during each flow period as well as the durations of the periods. They also presented methods for analyzing data obtained from testing the well, to determine permeability anisotropy in the drainage volume as well as the skin factor. Odeh and Babu[6] concluded that both the uniform-flux and uniform-pressure inner boundary condition assumptions lead to approximately the same pressure solution.

Analytical solutions for the pressure behaviour of horizontal wells, such as that presented by Odeh and Babu[6], involve a product of three infinite series, which tend to converge very slowly. Thompson and Manrique[7] have presented efficient algorithms for generating the uniform-flux horizontal well pressure response, that significantly reduce the computing time required. Using Laplace transforms and subsequent numerical inversion, Thompson and Manrique[7] generated the variable-rate pressure response from the uniform-flux pressure response, for both homogeneous and dual porosity systems. Thompson and Manrique[7] also generated the pressure response for a sequence of constant rates, and included the buildup response as a special case of multiple-step-rate pressure response.

2.1.2 Buildup Response

In the preceding section, the drawdown responses for horizontal wells were discussed. In addition to the drawdown responses, the various authors[1-7] presented the corresponding buildup responses. These buildup solutions were derived from the drawdown solutions by using the principle of superposition in time. The buildup equations should provide identical results as the drawdown equations when used to analyze well test data, as long as the time criteria requirements for the occurrence of the particular flow regime are met and producing time prior to shut-in is long.

2.1.3 Producing Time Effects on Buildup Response

A problem arises when drawdown type curves are used to analyze buildup data. In such situations, unless the producing time prior to shut-in is taken into account, it may result in erroneous interpretation of the buildup test. Agarwal[9] has presented a method to account for producing time effects when drawdown type curves are used to analyze pressure buildup test data. Agarwal's[9] method was developed for a vertical well in an infinite,

circular reservoir. Using the concept of an equivalent drawdown time, pressure buildup data are normalized in such a way that existing drawdown type curves may be used in place of a family of buildup curves. When wellbore storage and skin effects are present, however, there is a minimum time before which it is not possible to normalize the buildup data. Aarstad[10] has also shown that the Agarwal[9] method is not applicable to vertical wells in square or rectangular drainage areas. Ambastha and Ramey[11] have shown that for finite, circular reservoirs, pressure buildup data can be correlated with pressure drawdown data, except during early times when wellbore storage effects are predominant and at late times when the effect of the finite reservoir size are felt. Ambastha and Ramey[11] concluded that for proper type curve matching analysis of buildup derivative data obtained from a vertical well in a finite, circular reservoir, producing time effects and outer boundary condition should be taken into account. To the best of our knowledge, there has not appeared in the literature any studies on the producing time effects on the pressure buildup response for horizontal wells.

2.2 Thermal Well Testing for a Horizontal Well

As more oil companies turn to enhanced oil recovery to produce additional oil from existing reservoirs, the unique advantages offered by horizontal wells are being put to use. Horizontal wells for thermal recovery have been drilled in Fort McMurray[12], Cold Lake[13] and Kern River[14]. In 1978, Esso Resources Canada drilled horizontal wells at the Cold Lake Leming pilot to field test thermally-aided gravity drainage processes. Joshi[15], in 1986, conducted a laboratory study of thermal oil recovery using horizontal wells. His experiments showed a significant increase in oil recovery and sweep efficiency when a horizontal well was used. Research has shown that steam-assisted gravity drainage is the main recovery mechanism when using horizontal wells for thermal recovery.[15-17] Using data from thermal simulation of a steam drive process for the Athabasca McMurray

formation, Jain and Khosla[18] have presented production performance predictions for horizontal wells drilled from a tunnel (drainhole) as well as surface deviated horizontal wells in combination with vertical wells. Rial[19] has also compared the production performance of a horizontal well with that of a vertical well using thermal numerical simulation, with input data representative of the Kern River Field. During the 15-year simulation period, the horizontal wellbore model produced 71% of the original oil in place (OOIP), while the vertical wellbore model produced 58% OOIP. Using temperature and oil saturation distributions, Rial[19] showed that the horizontal wellbore had a higher sweep efficiency than the vertical wellbore during steamflooding. Thus, a considerable development has been reported in the modelling of horizontal well performance for thermal oil recovery. However, when a recovery process is initiated in the field, it is important to monitor the technical and economic performance of the process as it proceeds. For a steam injection process, the actual volume occupied by steam after a period of injection, as compared to the cumulative amount of injected steam, can provide a measure of the heat loss from the heated zone. Thus, a knowledge of the steam-swept pore volume is very important.

2.2.1 Estimating Swept Volume

Well testing is a relatively quick and inexpensive way of finding swept volume in thermal recovery processes. The literature reports several attempts to determine swept volume from pressure falloff data on vertical wells in both steam injection and in-situ combustion processes[20-33]. These investigations treat the reservoir undergoing thermal recovery as a composite system consisting of two zones with different rock and/or fluid properties. Determining the swept volume is, therefore, analogous to finding the volume (or front radius) of the inner region. For vertical wells, many authors[20-33] have applied different methods to estimate the swept or burned volume from pressure falloff data. These include

the deviation time, intersection time, type curve matching, and pseudosteady state methods[20].

2.2.1.1 Deviation Time Method

When pressure transient data from a falloff test are graphed versus time, the data may indicate an initial semi-log straight line, characteristic of fluid mobility in the inner (swept) zone. A deviation from the straight line occurs when the effects of the interface or front separating the inner and outer zones are felt. The time at the end of the semi-log straight line is used to calculate the front radius, based on a theoretical dimensionless deviation time. van Poollen[21] used a radius of drainage concept with the deviation time method to locate the flood front in an in-situ combustion process. Kazemi[22] also used the deviation time method to calculate the distance to a burning front from pressure falloff data of an in-situ combustion process. Kazemi[22] generated his pressure falloff data from a numerical model and also considered the effect of temperature variations on the thermodynamic properties of the reservoir fluids. The deviation time method assumes the flood front to be cylindrical. This is often not the case in thermal recovery processes because of gravity effects. The front radius calculated using the deviation time method is, thus, an average one. Consequently, the swept volume will only be approximate. Another drawback of the deviation time method is that it is possible for wellbore storage effects to mask the initial semi-log straight line, thus, making the method inapplicable.

2.2.1.2 Intersection Time Method

When pressure falloff data deviate from the initial semi-log straight line, it is possible, after some transition period, to have a second semi-log straight line, if the falloff test is run long enough. This second semi-log straight line is characteristic of fluid mobility in the outer

zone. The time at which the two semi-log lines intersect can be used to calculate the front radius, based on a theoretical dimensionless intersection time. This method, proposed by Bixel and van Poollen[23] and Merrill, Hossein and Gogarty[24], is among the earliest methods used to calculate the front radius. Merrill et al.[24] showed that the dimensionless intersection time of the two straight lines is a constant, for mobility ratios close to and and less than unity. However, for mobility ratios much greater than unity, the dimensionless intersection time is a function of both the mobility ratio and the specific storage ratio. They presented a correlation of the dimensionless intersection time as a function of the slope ratio, with specific storage ratio as a parameter. However, if the time criterion for the start of the second semi-log straight line[20] is used on the Merrill et al.[24] data, the Merrill et al.[24] second semi-log line is, in reality, a line drawn through transition data after the first semi-log line. Thus, the Merrill et al.[24] correlation may not be correct. The main drawback of the intersection time method in thermal recovery methods is that in most cases, either the falloff test will not be run long enough to see the second semi-log straight line, or outer boundary effects will mask the second semi-log line[20].

2.2.1.3 Type Curve Matching Method

The type curve matching method involves fitting the entire falloff data to a set of theoretical dimensionless type curves computed from a mathematical model. Typically, the type curves are dimensionless functions of pressure or pressure derivative versus time, with mobility and storativity ratios as parameters. Bixel and van Poollen[23] proposed a type curve matching method to calculate the distance to the radial discontinuity in a composite reservoir. They presented several type curves of dimensionless pressure as a function of dimensionless time, with mobility ratio as a parameter. The type curves were developed for different storage capacity ratios ranging between 0.001 and 1000. The Bixel and van Poollen[23] method uses the slope of the first semi-log straight line to calculate a

pseudodimensionless pressure from the observed pressure data. A graph of the pseudodimensionless pressure versus time is then matched onto the type curve. The time match point is used to calculate the distance to the radial discontinuity. This method, however, requires a knowledge of the type of radial discontinuity involved to select the appropriate chart for the storage capacity ratio. Lack of prior knowledge of the storage capacity ratio can present difficulties in getting a unique match.

Noting the non-uniqueness problem often encountered in visual type curve matching, Barua and Horne[25] presented an automated type-curve matching technique in which the observed data is fitted to the theoretical solution mathematically, using a least-squares method on a computer. They demonstrated their technique for both field and simulated pressure falloff tests of in-situ combustion and steam injection processes. Barua and Horne[25] noted that it was not possible to find all the necessary parameters of the two-zone reservoir by one automated type curve match, because of the large number of parameters involved. Thus, the pressure transient data was analyzed in sections. They concluded that the automated type curve matching method could be used to find the average swept zone radius in a two-zone reservoir, even when mobility ratio is low.

Recently, Ambastha and Ramey[20] have presented a type curve matching method for thermal recovery well tests, using an infinitely large composite reservoir model without wellbore storage. The type curve is based on the relationship between the dimensionless semi-log pressure derivative and the dimensionless time, with mobility and storativity ratios as parameters. The time match point is used to calculate the front radius, while the pressure derivative match point yields the mobility of the inner (swept) zone. Ambastha and Ramey[20] recommend that wellbore storage should be small to use their type curve. Also the test should be run long enough for a graph of the semi-log pressure derivative versus

time to show a typical bending over the maximum semi-log derivative value. Limiting equations are provided for the appropriate use of the type curve.

2.2.1.4 Pseudosteady State Method

The pseudosteady state method derives from the mobility and storativity contrasts between the inner and the outer zones of a composite reservoir. The method was proposed by Eggenschwiler, Ramey, Satman and Cinco-Ley[26]. They solved a composite reservoir model analytically, and showed that if the mobility and storativity contrasts are large, the inner (swept) region could behave like a closed system for a short period of time after the end of the first semi-log straight line. A Cartesian graph of pressure versus time during this period may indicate a straight line whose slope can be related to the swept volume. This analysis method is referred to as the pseudosteady state method. As the pseudosteady state method is independent of the geometry of the swept region, it is not necessary for the flood front to be cylindrical to get a good estimate of the swept volume. Eggenschwiler et al.[26] demonstrated the applicability of the pseudosteady state method by analyzing the previously published falloff data of van Poollen[21] and Kazemi[22]. The results were in close agreement.

Several investigators[27-33] have attempted to confirm the existence of the pseudosteady state period. Walsh, Ramey and Brigham[27] proposed guidelines for evaluating pressure falloff tests for both steam injection and in-situ combustion wells to determine the swept volume as well as the heat distribution within the reservoir. They showed that for a steam injection process, accurate determination of the swept volume requires the use of a two-phase effective compressibility instead of the steam compressibility for the steam-swept zone. The use of the two-phase compressibility accounts for volumetric changes caused by phase shifts when steam condenses.

Using the Walsh et al.[27] analysis procedure, Messner and Williams[28] analyzed falloff test data from several steamflood projects. Temperature observation wells were included in most of the steam flood projects to aid in the verification of the analysis procedure. In addition, Messner and Williams[28] used a fully-implicit thermal simulator to generate falloff data for a comparative analysis. They concluded that in both the field and the simulated cases, the estimated swept volumes appeared reasonable. There was a difference of about 10% between calculated and actual swept volumes in the simulated cases. Thermal efficiencies were rather low, indicating larger overburden heat losses and more channeling than expected. They stated that the low thermal efficiencies could also be due to the inability of present analysis methods to accurately assess the reservoir heat content ahead of the steam zone. Messner and Williams[28] also found that both field and simulated test results indicated consistently low estimates of the permeability in the swept region. They attributed the low permeability estimates to relative permeability effects.

Further investigations of the applicability of the pseudosteady state method to in-situ combustion projects have been carried out by Onyekonwu, Ramey, Brigham and Jenkins[29] and Da Prat, Bockh and Prado[30]. Onyekonwu et al.[29] simulated pressure falloff tests of in-situ combustion processes in a one-dimensional radial reservoir. Analysis of the data using the Walsh et al.[27] procedure yielded calculated swept volumes that were in good agreement with the simulated swept volumes. They, however, found that the swept volume included both the burned volume and the high gas saturation zone ahead of the combustion front. Da Prat et al.[30] applied the pseudosteady state method to the locating of the burning front in an in-situ combustion project in Eastern Venezuela. Two pressure falloff tests were conducted on one air injector. Examination of the falloff data showed that some initial stabilization time was required for the pressure probe to adjust to the ambient temperature. After that the falloff behaviour matched theoretical predictions.

Da Prat et al.[30] concluded that the calculated front radius, derived from the burned volume, assuming it to be cylindrical, was consistent with the actual locations of the injector and the producer.

Stanislav, Easwaran and Kokal[31] have investigated the effect of heat losses on the estimation of swept volume based on the pseudosteady state concept. In analytical solutions of the composite reservoir model for steam injection, the steam zone is assumed to be at a constant temperature. However, heat losses to both overburden and underburden can lead to a drop in temperature, resulting in steam condensation. It is, therefore, possible to underestimate the swept volume from analysis of falloff data. Stanislav et al.[31] modified the Eggenschwiler et al.[26] solution to the composite reservoir model by including a term which accounts for heat losses from the steam chamber. They carried out a sensitivity study of the solution to the heat loss term. Stanislav et al.[31] concluded that under certain conditions, heat losses could have a significant effect on the pressure falloff behaviour and dominate the pseudosteady state period. Consequently, they proposed a new analysis procedure for falloff data interpretation, when heat loss effect is significant.

Recently, Fassihi[32] has conducted a study to evaluate the applicability of the pseudosteady state method for estimating swept volume from thermal pressure falloff tests in heterogeneous systems. He used a numerical simulator to simulate injection falloff testing of steamflood and in-situ combustion processes in both radial and areal reservoir models. Fassihi[32] investigated the effect of such parameters as wellbore grid size, non-uniform permeability, layering and oil vaporization, on the estimated swept volume. For steamfloods in relatively homogeneous reservoirs, Fassihi[32] determined that the calculated swept volumes using the pseudosteady state method were in agreement with the simulated volumes. Differences between calculated and simulated swept volumes ranged from 6 to 20 per cent. However, for very heterogeneous reservoirs, there was a very long transition

period that masked the pseudosteady state data. This made it impossible to estimate the swept volume.

Ambastha and Kumar[33] have reported an attempt to calculate swept volume from pressure falloff data of steam injection wells in a low-permeability reservoir with steam-induced vertical fractures. They reported that the estimated swept volumes using the pseudosteady state method were unrealistically large. Ambastha and Kumar[33] suggested that the swept volume overestimation may have been caused by short injection time effects on the falloff responses for the rectangular swept region. They could not verify this hypothesis directly since there is no analytical solution available for the reservoir configuration under study. Ambastha and Kumar[33], however, pointed out that a study by Ambastha and Ramey[34] showed that for a cylindrical swept region, pseudosteady state data may overestimate the swept volume by orders of magnitude, if injection time prior to shut-in is short.

From the preceding literature review, it appears that the application of the pseudosteady state method to determine swept volume in thermal recovery processes has met with a good degree of success for vertical wells. However, to the best of our knowledge, the literature does not contain any reference to the application of the pseudosteady state method to horizontal wells under steam injection.

3. STATEMENT OF THE PROBLEM

The transient pressure behaviour of a horizontal well can be quite different from that of a vertical well. For a vertical well in a homogeneous, unfractured reservoir, flow is essentially radial in the horizontal direction. For a horizontal well, it is possible to have up to four different flow regimes prior to pseudosteady state, in a closed reservoir with anisotropy. Thus, transient pressure data may not necessarily appear as a semi-log straight line (indicating radial flow) for the swept region mobility. It is possible to have linear flow.

The literature review also shows that the application of the pseudosteady state method to swept volume determination has, thus far, been concentrated to vertical wells. For a horizontal well in a homogeneous, isotropic reservoir, the steam-swept volume is ellipsoidal in shape[15]. Under the influence of gravity, anisotropy and reservoir heterogeneity, it can be expected that the ellipsoidal swept region will not be symmetric around the wellbore. Such asymmetries, if severe, could mask the appearance of the pseudosteady state straight line. It is also not clear how steam-assisted gravity drainage will affect the well test. There is also the question of whether it will be possible to obtain steam chamber mobility from the well test data. Thus, the main objectives of this study are:

1. to evaluate the accuracy and applicability of the pseudosteady state method in the estimation of swept volume for a horizontal well under steam injection.

2. to investigate how steam-assisted gravity drainage affects horizontal well tests, and

3. to obtain steam chamber mobility from the well test.

To achieve the stated objectives, the study is conducted in two stages:

1. An analytical study of the pressure behaviour of a horizontal well in a closed reservoir with anisotropy is conducted. The aim is to find out the various possible flow regimes and how to calculate the fluid mobility. Knowledge gained in this part of the study is used to determine the steam chamber mobility in the next part. The effect of producing time on the pressure buildup behaviour is also investigated.

2. A numerical simulation study of the pressure falloff behaviour of a horizontal well under steam drive conditions is conducted. The ISCOM (version 4.0)[35] In-Situ Combustion and Steam Reservoir Simulator is used to generate the pressure falloff data for analysis to determine the swept volume and steam chamber mobility.

4. TRANSIENT PRESSURE BEHAVIOUR OF HORIZONTAL WELLS

This chapter considers the pressure transient behaviour of a horizontal well in a closed reservoir, with anisotropy. The solution presented by Odeh and Babu[6], for the transient pressure behaviour of a horizontal well in a closed, box-shaped reservoir with anisotropy, is cast in dimensionless form and evaluated numerically. The dimensionless pressure derivative is also evaluated. A sensitivity study is then conducted to determine the effect of the system parameters on the pressure derivative response. The effect of producing time prior to shut-in on the buildup derivative response is also investigated in detail.

4.1 Drawdown Response

The pressure drawdown response of a horizontal well in a closed, box-shaped reservoir is studied in this section. The reservoir model used is the same as that in Ref. 6.

4.1.1 Model Description

Figure 4.1 shows a box-shaped reservoir of length, *a*, in the x-direction; width, *b*, in the y-direction; and thickness, *h*, in the z-direction. The horizontal well, of radius , r_w and length, L, is drilled in the y-direction and extends between y_1 and y_2. The well is located at (x_o,z_o), and produces at a rate, q, from an anisotropic reservoir with permeabilities k_x, k_y, and k_z in the x-, y-, and z-directions, respectively. The fluid is slightly compressible and all reservoir boundaries are closed. The reservoir pressure is initially at p_i.

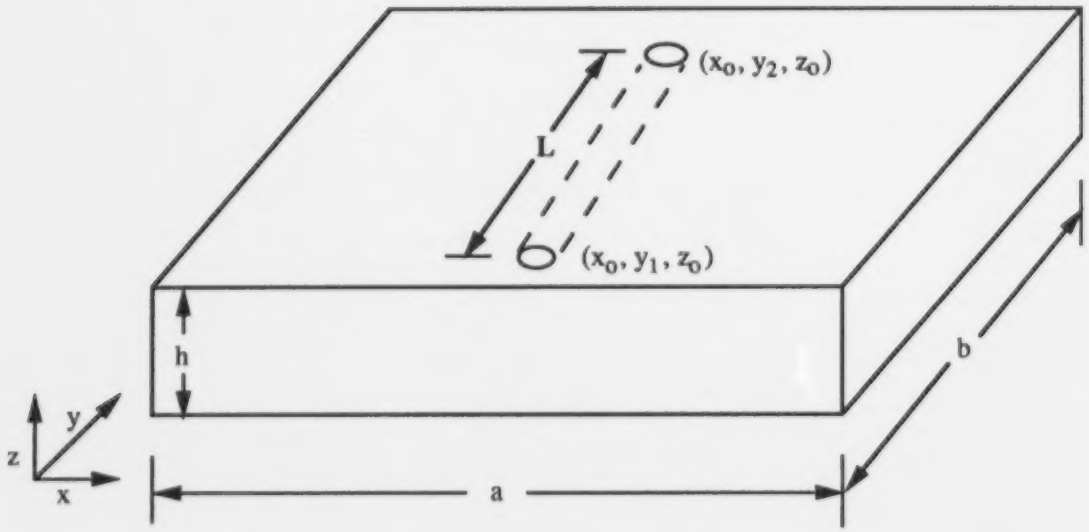

Fig. 4.1 - Schematic of a horizontal well in a box-shaped reservoir

4.1.2 Mathematical Formulation

The differential equation describing a single-phase fluid flow in the reservoir, can be written as:

$$k_x \frac{\partial^2 p}{\partial x^2} + k_y \frac{\partial^2 p}{\partial y^2} + k_z \frac{\partial^2 p}{\partial z^2} = \phi \mu c_t \frac{\partial p}{\partial t}. \quad (4.1)$$

The initial condition is:

$$p\,(x, y, z, 0) = p_i\,. \quad (4.2)$$

For the closed outer boundaries:

$$\frac{\partial p}{\partial x} = \frac{\partial p}{\partial y} = \frac{\partial p}{\partial z} = 0\,, \text{ and} \quad (4.3)$$

for the uniform-flux inner boundary condition:

$$\frac{\partial p}{\partial x} = \text{constant}; \frac{\partial p}{\partial y} = \text{constant}; \frac{\partial p}{\partial z} = \text{constant}. \quad (4.4)$$

4.1.3 General Solution

In Reference 6, the pressure drop, Δp, at any arbitrary point (x,y,z) was obtained by analytical integrations of the appropriate Green's functions. The well was represented as a line sink parallel to the y-axis and located along the line $x=x_o$, $y_1 \le y \le y_2$, $z=z_o$. This

resulted in double and triple infinite series, which were extremely slow to converge near the wellbore. Consequently, Odeh and Babu[6] introduced certain closed form expressions and formulas[36] to reduce the infinite sums to forms that converge faster. Babu and Odeh[36] noted that the errors resulting from using these formulas are often quite small. However, errors of up to 10% could occur if the well is very close to any of the reservoir boundaries. To avoid the convergence problem of Odeh and Babu[6], the integrations are carried out numerically in this study.

Before solving Eq. (4.1), subject to the preceding boundary conditions, the following dimensionless variables were introduced:

$$t_D = \frac{k_x t}{\alpha L^2} , \tag{4.5}$$

where:

$$\alpha = 3790.85 \phi \mu c_t , \tag{4.6}$$

$$p_D = \frac{0.00708 h k_x \Delta p}{\beta \mu q} , \tag{4.7}$$

$$x_D = \frac{x}{L} , \tag{4.8}$$

$$y_D = \frac{y}{L}\sqrt{\frac{k_x}{k_y}} , \text{ and} \tag{4.9}$$

$$z_D = \frac{z}{L}\sqrt{\frac{k_x}{k_z}} \, . \tag{4.10}$$

All dimensions in the x-direction are made dimensionless in a manner similar to Eq. (4.8). Similarly, Eq. (4.9) is used for dimensions in the y-direction, while Eq. (4.10) is used for the z-direction. By definition, the dimensionless well length is:

$$L_D = y_{2D} - y_{1D} \tag{4.11}$$

In dimensionless form, Eq. (4.1) becomes:

$$\frac{\partial^2 p_D}{\partial x_D^2} + \frac{\partial^2 p_D}{\partial y_D^2} + \frac{\partial^2 p_D}{\partial z_D^2} = \frac{\partial p_D}{\partial t_D} \, . \tag{4.12}$$

A solution for the dimensionless pressure drop, following the technique presented in Ref. 6, is:

$$p_D = \frac{2\pi}{a_D b_D} \int_0^{t_D} \int_{y_{1D}}^{y_{2D}} (S_{1D} \cdot S_{2D} \cdot S_{3D}) \, dy_{0D} \, dt_D \, , \tag{4.13}$$

where:

$$S_{1D} = 1 + 2 \sum_{n=1}^{\infty} \cos \frac{n\pi x_D}{a_D} \cos \frac{n\pi x_{0D}}{a_D} \exp\left[- \frac{n^2\pi^2}{a_D^2} t_D \right] \, , \tag{4.14}$$

$$S_{2D} = 1 + 2 \sum_{m=1}^{\infty} \cos \frac{m\pi y_D}{b_D} \cos \frac{m\pi y_{0D}}{b_D} \exp \left[- \frac{m^2\pi^2}{b_D^2} t_D \right] , \text{ and} \tag{4.15}$$

$$S_{3D} = 1 + 2 \sum_{l=1}^{\infty} \cos \frac{l\pi z_D}{h_D} \cos \frac{l\pi z_{0D}}{h_D} \exp \left[- \frac{l^2\pi^2}{h_D^2} t_D \right] . \tag{4.16}$$

S_{1D}, S_{2D} and S_{3D} are the dimensionless instantaneous Green's functions located at the point (x_{0D}, y_{0D}, z_{0D}) and satisfying zero flux boundary conditions at $x_D = 0$, a_D; $y_D = 0$, b_D; and $z_D = 0$, h_D, respectively.

Differentiating Eq. (4.13) with respect to t_D, the dimensionless pressure derivative can be written as:

$$\frac{dp_D}{dt_D} = \frac{2\pi}{a_D b_D} \int_{y_{1D}}^{y_{2D}} (S_{1D} \cdot S_{2D} \cdot S_{3D}) \, dy_{0D} . \tag{4.17}$$

To compute the pressure drop at the wellbore, the point (x, y, z) must be on the well perimeter, r_w. However, for an anisotropic reservoir, the pressure drop at the wellbore will depend on the angle, θ, in the vertical (x-z) plane at which the pressure is computed. Thus, the pressure has to be averaged to obtain a representative wellbore pressure drop. In Ref. 36, it is shown that such an average pressure drop is equivalent to the pressure drop measured at an angle, θ, from the x-axis, where θ is given by:

$$\theta = \arctan \left(\frac{k_z}{k_x} \right)^{\frac{1}{4}} . \tag{4.18}$$

Thus, at the wellbore:

$$x = x_0 + r_w \cos\theta \ , \tag{4.19}$$

$$z = z_0 + r_w \sin\theta \ , \text{ and} \tag{4.20}$$

$$y = y_0 \ ; \ y_1 \leq y_0 \leq y_2 \ . \tag{4.21}$$

Equation (4.13) was solved in two steps. In the first step, the dimensionless pressure derivative (Eq. 4.17) was computed using a Simpson's 1/3-rule algorithm. It was found that 1,000 equally-spaced intervals between y_{1D} and y_{2D} were adequate for convergence. Also, the series in S_{1D} was assumed to have converged when the absolute value of the ratio of the sum of the *n-2*, *n-1*, and *n* terms to the total sum was less than 10^{-15}. A similar convergence criterion was used for the series in S_{2D} and S_{3D}.

With the dimensionless pressure derivative (dp_{wD}/dt_D) results from the first step, a trapezoidal rule algorithm was used to evaluate p_{wD}. A lower-bound value of $t_D = 10^{-7}$ was found to result in the correct values of p_{wD}. The computer program and a sample result sheet are shown in Appendices A and B, respectively. Input data for these results are from Example 1 of Ref. 6. Figure 4.2 shows p_{wD} and $dp_{wD}/dlnt_D$ graphed against t_D. In Fig. 4.3, the results of this study are compared with those of Example 1 of Ref. 6 on a graph of Δp_w vs. log(t), for the early radial flow regime.

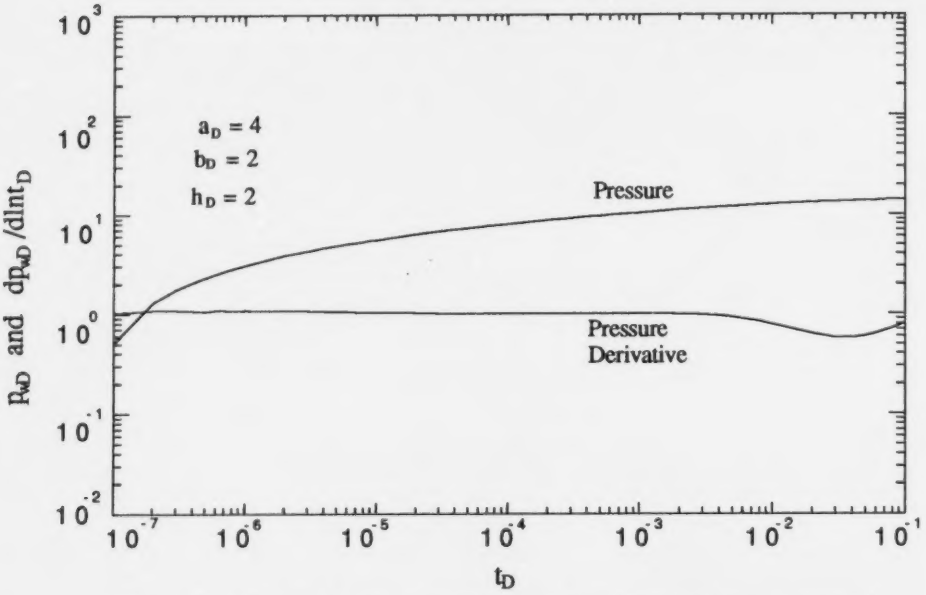

Fig. 4.2 - Dimensionless pressure and semi-log pressure derivative responses for a horizontal well in a closed, box-shaped reservoir.

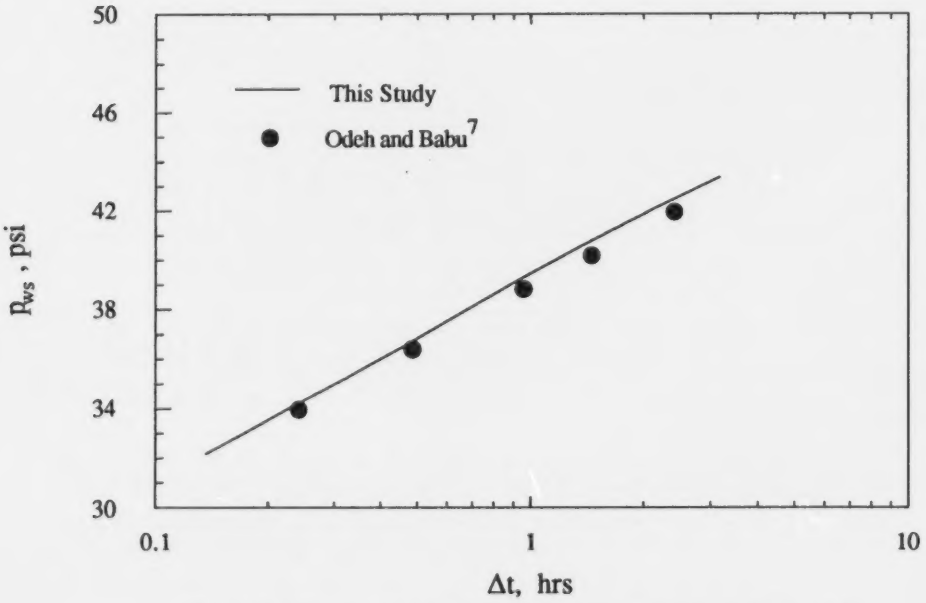

Fig. 4.3 - Comparison of the pressure response from this study with the response from the Odeh and Babu study for the early radial flow period.

4.1.4 Transient Flow Regime Description

Depending on reservoir properties and dimensions, well length and well location, one, two, three, or four transient flow periods may occur prior to pseudosteady state for a horizontal well in a closed reservoir. The following presents the criteria for the times for the start and/or end of the various transient flow regimes as presented in Ref. 6, but written in dimensionless forms. The transient flow regimes are:

4.1.4.1 Early Radial Flow

This period occurs immediately after the well starts to flow. Flow to the well occurs radially, in the vertical x-z plane. Graphical analysis of pressure transient data (Δp_w vs. log(t)) in this period yields $\sqrt{k_x k_z}$, if other reservoir properties are known.

The time to the end of early radial flow period is:

$$(t_{end})_D = \text{minm}\left[0.4748\ dz_D^2\ ,\ 0.033 L_D^2\right]. \tag{4.22}$$

4.1.4.2 Early Linear Flow

This period may follow the early radial period, if the well is significantly longer than the reservoir thickness. Flow to the well occurs linearly in the x-direction. A graph of Δp_w vs. $\sqrt{t}$ for data in this period yields k_x. The dimensionless times for the start and end of this period are:

$$(t_{start})_D = 0.4748\, D_{zD}^2, \text{ and} \tag{4.23}$$

$$(t_{end})_D = 0.0422 L_D^2 . \tag{4.24}$$

4.1.4.3 Late Pseudo-Radial Flow

The occurrence of the late pseudo-radial flow period depends on the ratio of the well length to the width of the reservoir or the penetration ratio (L/b). Flow occurs radially in the horizontal x-y plane. A graph of Δp_w vs. log(t) yields $\sqrt{k_x k_y}$, other reservoir properties being known.

Dimensionless times for the start and end of the late pseudo-radial flow period are given by:

$$(t_{start})_D = 0.3904 L_D^2, \text{ and} \tag{4.25}$$

$$(t_{end})_D = \text{minm}\left[0.5276\left(d_{yD} + \frac{L_D}{4}\right)^2, 0.4353\, d_{xD}^2\right] . \tag{4.26}$$

4.1.4.4 Late Linear Flow

The late linear flow period will occur, if the reservoir length is significantly larger than the width. Flow is linear in the x-direction. A graph of Δp_w vs. $\sqrt{t}$ will yield k_x. Dimensionless time for the start of this flow period is:

$$(t_{start})_D = \text{maxm}\left[1.26\, D_{yD}^2,\ 0.475\, D_{zD}^2\right], \tag{4.27}$$

and the time to the end of the late linear flow period is:

$$(t_{end})_D = 0.4353\ d_{xD}^2 \tag{4.28}$$

4.1.5 Time Criteria Based on Pressure Derivative Response

The dimensionless times for the start and/or end of the transient flow regimes discussed in the preceding sections are based on the pressure solution presented by Odeh and Babu[6]. Using the dimensionless semi-log pressure derivative as the basis, it is possible to get different times for the occurrence of the various transient flow regimes. Table 4.1 compares the time criteria for the occurrence of the transient flow regimes based on the dimensionless semi-log pressure derivative response with those based on the dimensionless pressure response. Details of the development of the time criteria based on the dimensionless semi-log pressure derivative response are presented in App. C

Table 4.1 indicates significant differences between the two time criteria. The various flow regimes tend to start later, and end earlier if the times are based on the semi-log pressure derivative. Thus, the durations of the transient flow periods will tend to be shorter when deduced from the semi-log pressure derivative. These results are consistent with the findings regarding time criteria based on pressure or pressure derivative solution for composite reservoirs.[20]

Table 4.1: Comparison of time criteria based on pressure response with those based on pressure derivative response

Flow Regime	Dimension-less Time	Time Criteria Based on	
		Dimensionless Pressure	Dimensionless Pressure Derivative
Early Radial	$(t_{end})_D$	minm $[0.4748 d_{zD}^2 , 0.033 L_D^2]$	minm $[0.25 d_{zD}^2 , 0.033 L_D^2]$
Early Linear	$(t_{start})_D$	$0.4748 D_{zD}^2$	$0.6 D_{zD}^2$
	$(t_{end})_D$	$0.0422 L_D^2$	$0.02 L_D^2$
Late pseudo-radial	$(t_{start})_D$	$0.3904 L_D^2$	$0.4 L_D^2$
	$(t_{end})_D$	minm$[0.528(d_{yD}+L_D/4)^2, 0.453 d_{xD}^2]$	minm$[0.33(d_{yD}+L_D/4)^2, 0.27 d_{xD}^2]$
Late linear	$(t_{start})_D$	maxm $[1.26 D_{yD}^2 , 0.4748 D_{zD}^2]$	maxm $[0.88 D_{yD}^2 , 0.63 D_{zD}^2]$
	$(t_{end})_D$	$0.435 d_{xD}^2$	$0.162 d_{xD}^2$

4.1.6 Sensitivity Study

A sensitivity study was conducted to determine the effect of the various system parameters on the dimensionless semi-log pressure derivative response. The effects of well radius, well location and reservoir size are discussed.

4.1.6.1 Well Radius

The effect of well radius was studied by considering three dimensionless well radii (r_{wD} = 0.00025, 0.0005, 0.001). These correspond to actual well radii of 0.25 ft, 0.5 ft and 1 ft, respectively. Figure 4.4 shows the dimensionless semi-log pressure derivative ($dp_{wD}/dlnt_D$) graphed against dimensionless time (t_D) on a log-log scale. The well is centrally-located in all cases. Figure 4.4 shows that the dimensionless semi-log pressure derivative responses correlate well for all r_{wD}. Thus, r_{wD} need not be considered as a parameter for further sensitivity study.

Figure 4.4 also shows a zero-slope line from $t_D = 10^{-4}$ to about 0.002. This indicates early radial flow regime. After a short transition period, a half-slope line emerges and continues to $t_D = 0.2$, indicating early linear flow. A second zero-slope line from $t_D = 0.2$ to about 0.8 follows, indicating late pseudo-radial flow. The late linear flow regime is not observed, as there is no noticeable second half-slope line. Finally, a unit-slope line appears after $t_D = 3$, indicating pseudosteady state flow.

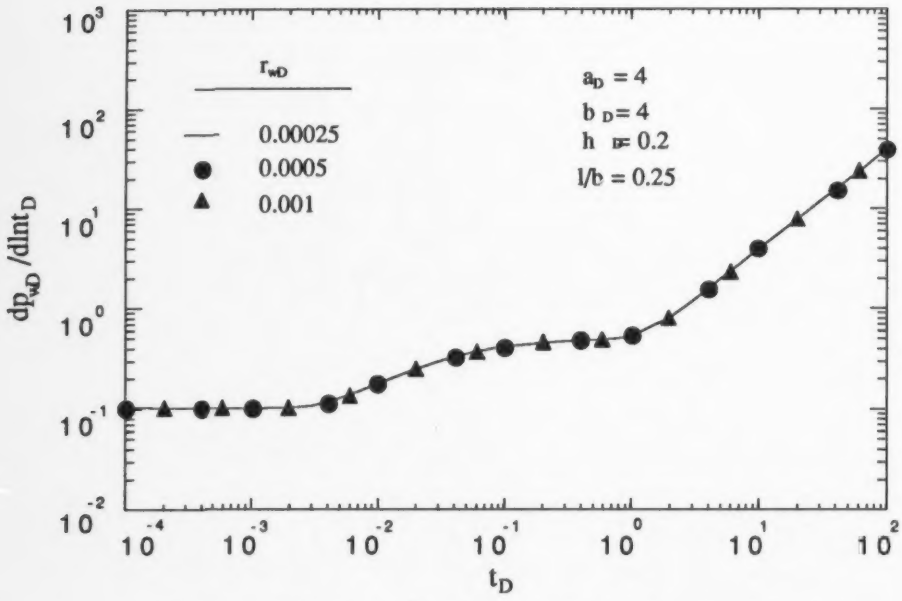

Fig. 4.4 - Effect of well radius on the semi-log pressure derivative response for a horizontal well.

4.1.6.2 Well Location

The effect of well location on the occurrence of the various flow regimes was investigated by changing the location of the well along the x-, y- and z-directions, one at a time. The base case was that consisting of a centrally-located well of $r_{wD} = 0.00025$ and a penetration ratio of 0.25. Figure 4.5 shows the dimensionless semi-log pressure derivative responses for various x_{0D}/a_D. The well was centrally-located with respect to the y- and z-axes. Figure 4.5 shows that varying the well location along the length of the reservoir affects mainly the late-time flow behaviour. For x_{0D}/a_D =0.5, there is a significant late pseudo-radial flow period (t_D = 0.2 to about 0.8). However, as x_{0D}/a_D increases to 0.9, the late-linear flow regime (half-slope line) begins to dominate all late-time transient flow behaviour, to the exclusion of the late pseudo-radial flow regime.

For the effect of well location along the width of the reservoir, four cases of y_{1D} (0, 0.5, 1, 1.5) were considered. y_{1D} is the starting point of the well along the reservoir width. Figure 4.6 shows the dimensionless semi-log pressure derivative graph for the four cases. Here also the effect lies mainly in the late-time flow behaviour. As the starting point of the well moves closer to the reservoir boundary (y_D = 0), the length of the late pseudo-radial flow period decreases. For y_{1D} = 0, the late pseudo-radial flow regime does not occur. Instead, the early linear flow period continues, with only a short transition, to the late linear flow period.

Figure 4.7 shows the effect of z-direction well location. Three cases of z_{0D}/h_D (0.5, 0.7, 0.9) were studied. The graph shows that varying the well location in the vertical direction affects the early-time flow behaviour. Increasing z_{0D}/h_D tends to reduce the length of the early radial flow period. For z_{0D}/h_D = 0.9, the early radial flow regime is practically non-existent. Due to symmetry, similar flow behaviour will be exhibited for cases of z_{0D}/h_D

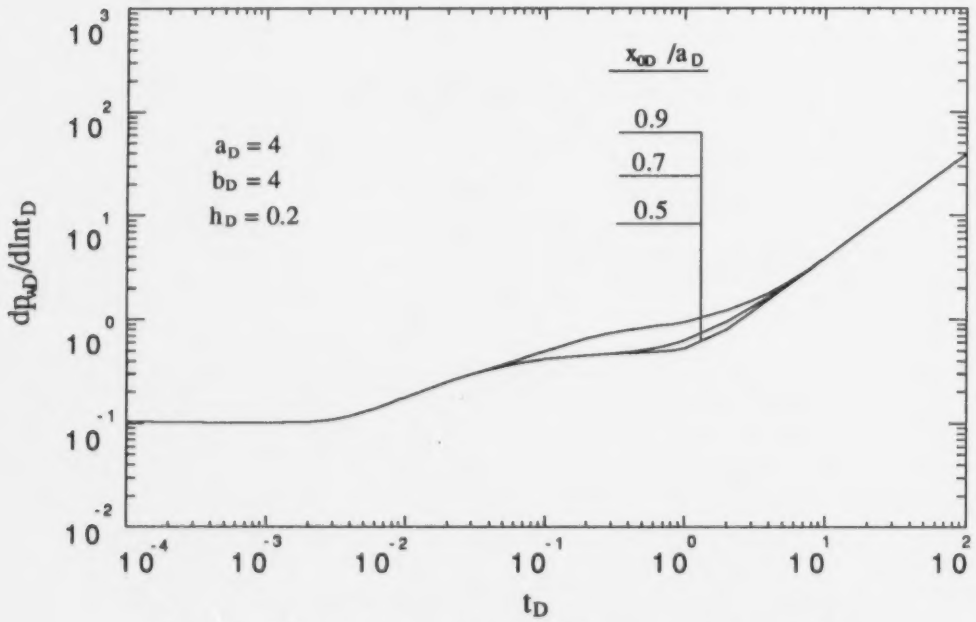

Fig. 4.5 - Effect of x-direction well location on the semi-log pressure derivative response for a horizontal well.

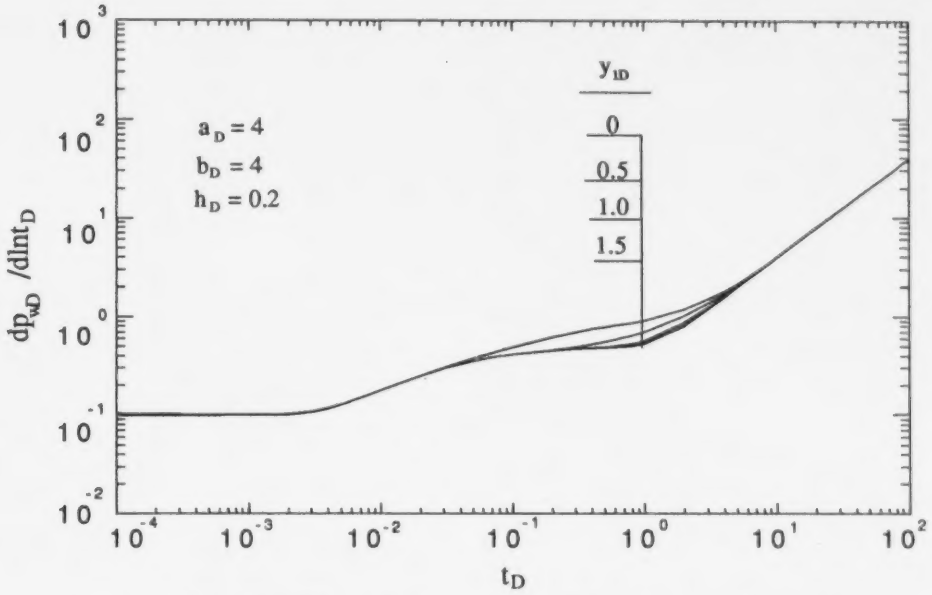

Fig. 4.6 - Effect of y-direction well location on the semi-log pressure derivative response for a horizontal well.

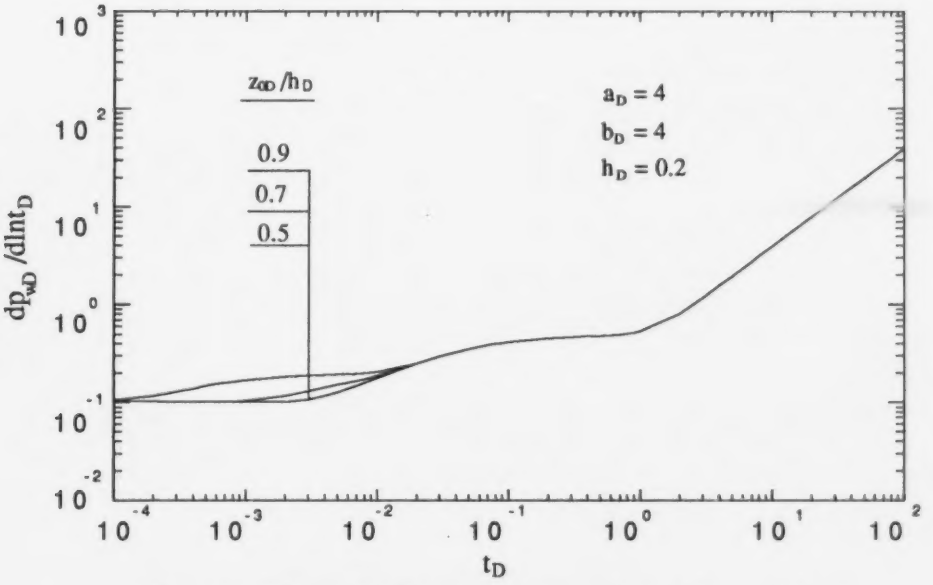

Fig. 4.7 - Effect of z-direction well location on the semi-log pressure derivative response for a horizontal well.

less than 0.5. For example, $z_{0D}/h_D = 0.3$ response will be the same as the response for $z_{0D}/h_D = 0.7$ case.

4.1.6.3 Reservoir Size

The reservoir size effect was investigated by varying the length, width and height of the reservoir. The base case was that of a centrally-located well with penetration ratio of 0.25 and $r_{wD} = 0.00025$.

Figure 4.8 shows the effect of the reservoir length on the occurrence of the various flow regimes. Figure 4.8 indicates that changing the reservoir length affects only the late-linear flow behaviour. As the reservoir length increases, the length of the late-linear flow period also increases.

The effect of reservoir width is shown in Fig. 4.9. Figure 4.9 shows that changing the reservoir width affects the late-time flow behaviour. For $b_D = 1$, i.e., when the well is fully penetrating, the late pseudo-radial flow does not occur. Instead, the early linear flow continues until boundary effects are felt (unit-slope line). As the reservoir width increases, the length of the late pseudo-radial flow period also increases.

In Fig. 4.10, the dimensionless semi-log pressure derivative response for four different cases of reservoir height ($h_D = 0.1, 0.2, 0.3, 0.4$) are graphed. Figure 4.10 indicates that as the reservoir height increases, the length of the early radial flow period also increases. Correspondingly, the length of the early linear flow period decreases.

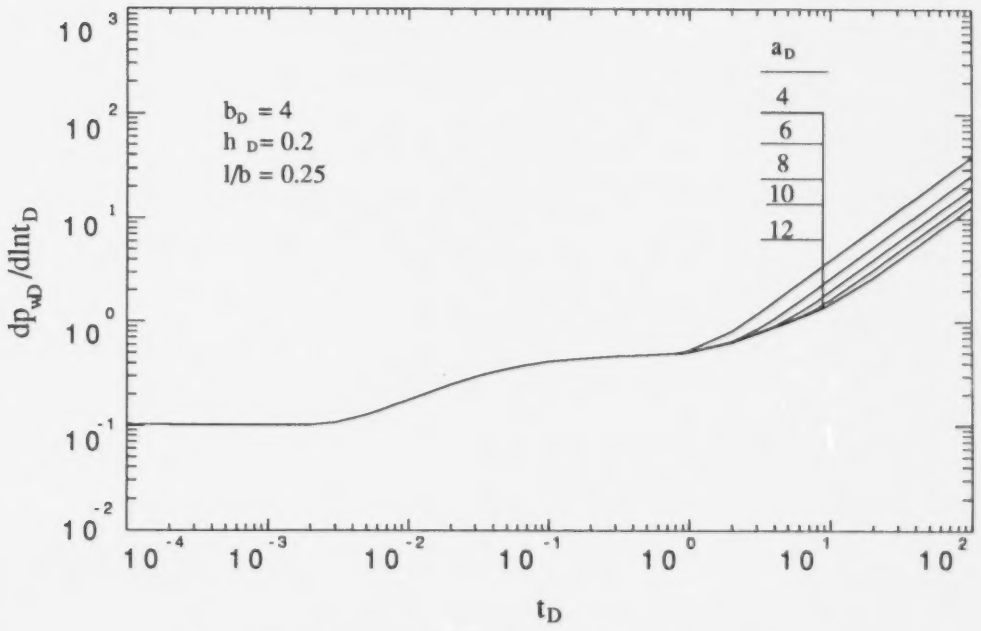

Fig. 4.8 - Effect of reservoir length on the semi-log pressure derivative response for a horizontal well.

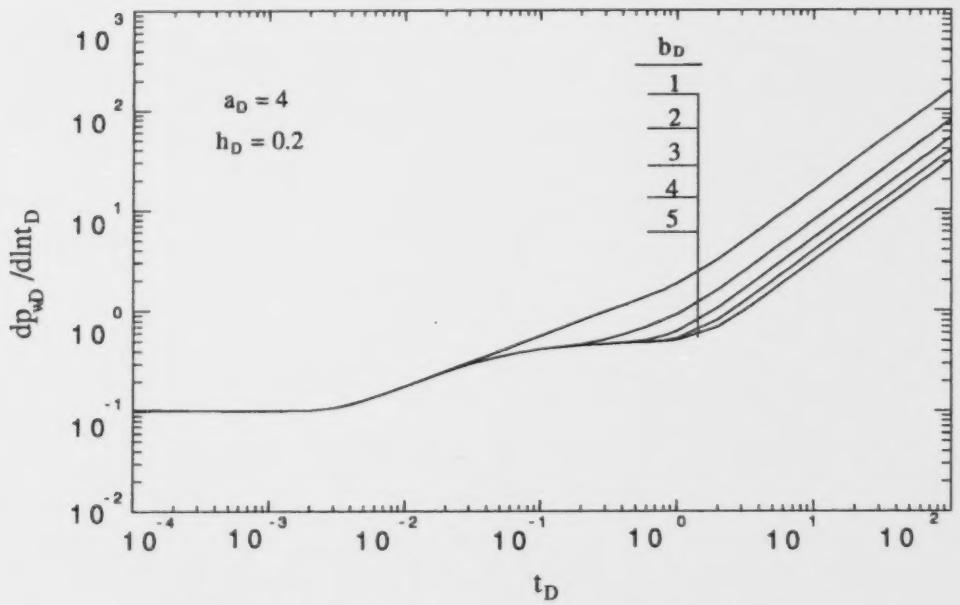

Fig. 4.9 - Effect of reservoir width on the semi-log pressure derivative response for a horizontal well.

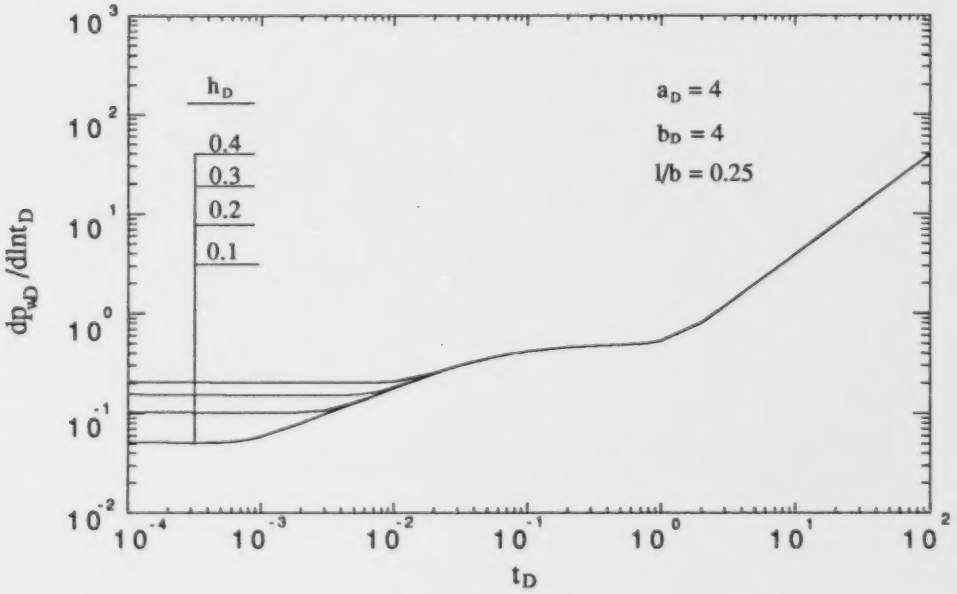

Fig. 4.10 - Effect of reservoir height on the semi-log pressure derivative response for a horizontal well.

4.2 Buildup Response

This section considers the buildup response from a horizontal well in a closed, box-shaped reservoir, with anisotropy. Using the principle of superposition in time, the drawdown solution is transformed into a buildup solution. The computer program for the drawdown solution (see App. A) is modified to incorporate producing time prior to shut-in. Producing time effects on the buildup derivative responses are investigated using the slope of dimensionless Agarwal[9] and MDH[37] graphs.

4.2.1 Mathematical Development

The principle of superposition in time can be used to transform a pressure drawdown solution into a pressure buildup solution. The resulting dimensionless shut-in pressure is:

$$p_{wDs}(\Delta t_D) = p_{wD}(t_{pD}) + p_{wD}(\Delta t_D) - p_{wD}(t_{pD} + \Delta t_D)\,, \tag{4.29}$$

where:

$$p_{wDs}(\Delta t_D) = \frac{0.00708 k_x h (p_{ws} - p_{wfs})}{q\mu\beta}\,. \tag{4.30}$$

Differentiating Eq. (4.29) with respect to Δt_D, the dimensionless shut-in pressure derivative is:

$$\frac{dp_{wDs}(\Delta t_D)}{d(\Delta t_D)} = \frac{dp_{wD}(\Delta t_D)}{d(\Delta t_D)} - \frac{dp_{wD}(t_{pD} + \Delta t_D)}{d(\Delta t_D)}\,. \tag{4.31}$$

To compute the buildup pressure derivative response of a horizontal well in a closed, box-shaped reservoir using Eq. (4.31), the portion of the computer program (Program # 1 of App. A) for the drawdown pressure derivative response (Eq. 4.17) was modified to incorporate a producing time. The modified computer program is shown as Program # 2 of App. A.

It is customary to analyze pressure buildup data using either the MDH[37] method or the Horner[38] method. While the MDH[37] method is simpler, it is applicable for long producing times prior to shut-in. The Horner[38] method, however, is applicable for all producing times. Both methods use a semi-log graph of pressure as a function of some time variable to analyze buildup data.

The slope of a dimensionless MDH[37] graph is:

$$\text{MDH Slope} = \frac{dp_{wDs}}{d\ln(\Delta t_D)} = \Delta t_D \frac{dp_{wDs}(\Delta t_D)}{d(\Delta t_D)} \quad . \tag{4.32}$$

For a dimensionless Horner[38] graph, the slope is:

$$\text{Horner Slope} = \frac{dp_{wDs}}{d\ln\left(\frac{t_{pD} + \Delta t_D}{\Delta t_D}\right)} = -\Delta t_D \frac{(t_{pD} + \Delta t_D)}{t_{pD}} \cdot \frac{dp_{wDs}(\Delta t_D)}{d(\Delta t_D)} \quad . \tag{4.33}$$

4.2.2 Producing Time Effects on Buildup Response

To consider producing time effects when drawdown type curves are used to analyze buildup data, Agarwal[9] introduced the concept of an equivalent drawdown time, defined as:

$$\Delta t_{eD} = \frac{t_{pD}\Delta t_D}{t_{pD} + \Delta t_D} \quad . \tag{4.34}$$

Agarwal[9] showed that if pressure buildup data are graphed as p_{wDs} vs. Δt_{eD} for an infinitely large, homogeneous or fractured reservoir, then all pressure buildup responses can be correlated with the drawdown response, regardless of the producing time before shut-in.

The slope of a dimensionless Agarwal buildup graph is:

$$\text{Agarwal Slope} = \frac{dp_{wDs}}{d\ln(\Delta t_{eD})} = \Delta t_D \frac{(t_{pD} + \Delta t_D)}{t_{pD}} \cdot \frac{dp_{wDs}(\Delta t_D)}{d(\Delta t_D)} \quad . \tag{4.35}$$

A comparison of Eqs. (4.33) and (4.35) indicates that:[11]

$$\text{Agarwal Slope} = \text{- Horner Slope} \quad . \tag{4.36}$$

Thus, either slope can be used to study producing time effects. The Agarwal slope is used in this study.

Figure 4.11 compares the MDH and Agarwal buildup slopes with the drawdown response for a short producing time. A short producing time is considered to be any time shorter than the time to reach pseudosteady state on the drawdown response. Data in Fig. 4.11 are for a centrally-located, fully-penetrating horizontal well in a closed, box-shaped reservoir. Wellbore storage and skin are ignored. Reservoir dimensions are shown on the figure. The dimensionless producing time prior to shut-in (t_{pDA}) is 0.01, while the dimensionless time to pseudosteady state, $(t_{DA})_{pss}$, for the drawdown solution is 0.1. For a bounded reservoir, both MDH and Agarwal slopes should go to zero during pseudosteady state flow. However, Fig. 4.11 shows that the MDH slope deviates from the drawdown solution much earlier than the Agarwal slope. Defining the dimensionless deviation time, $(\Delta t_{DA})_{dev}$, as the time at which the buildup slope deviates by 5% from the drawdown slope, $(\Delta t_{DA})_{dev}$ is 0.00055 for the MDH slope. For the Agarwal slope $(\Delta t_{DA})_{dev}$ is 0.035.

Figures 4.12 and 4.13 show the effect of producing time, t_{pDA}, on the MDH slope and the Agarwal slope, respectively. Values of t_{pDA} range between 0.001 and 1.0. Reservoir parameters are similar to those in Fig. 4.11, and are chosen to result in only one transient flow period prior to pseudosteady state flow. Figure 4.12 shows that the dimensionless deviation time, $(\Delta t_{DA})_{dev}$, depends on t_{pDA}. The smaller t_{pDA} is, the earlier the deviation from the drawdown solution. For the reservoir configuration of Fig. 4.12, $(\Delta t_{DA})_{dev}$ for an MDH graph is approximately related to t_{pDA} by:

$$(\Delta t_{DA})_{dev} = 0.00407 + 0.00172 \log (t_{pDA}) , \quad \text{for} \quad 0.001 \le t_{pDA} \le 0.1 . \qquad (4.37)$$

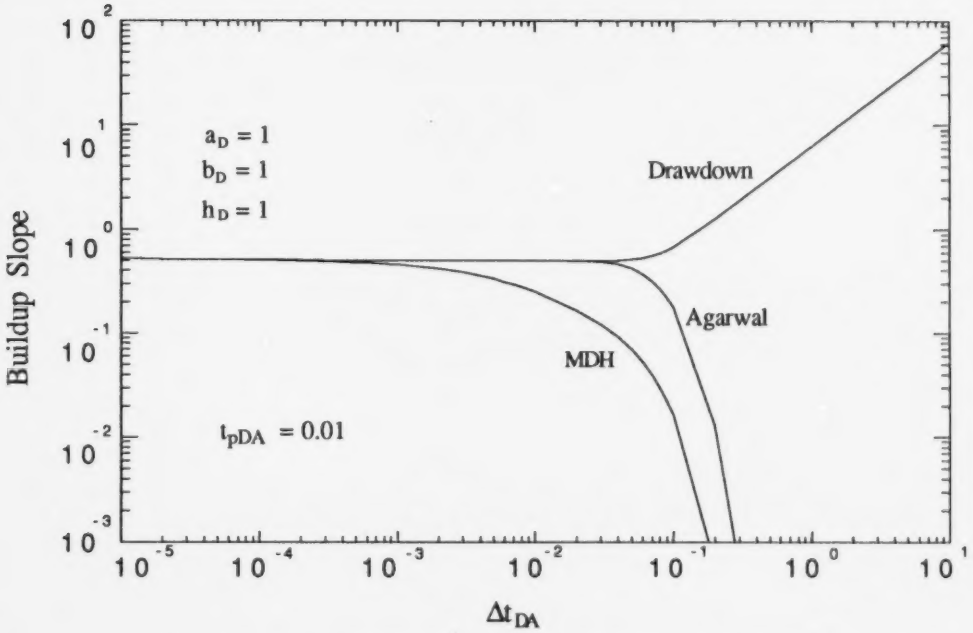

Fig. 4.11 - Comparison of MDH and Agarwal slopes for short producing times.

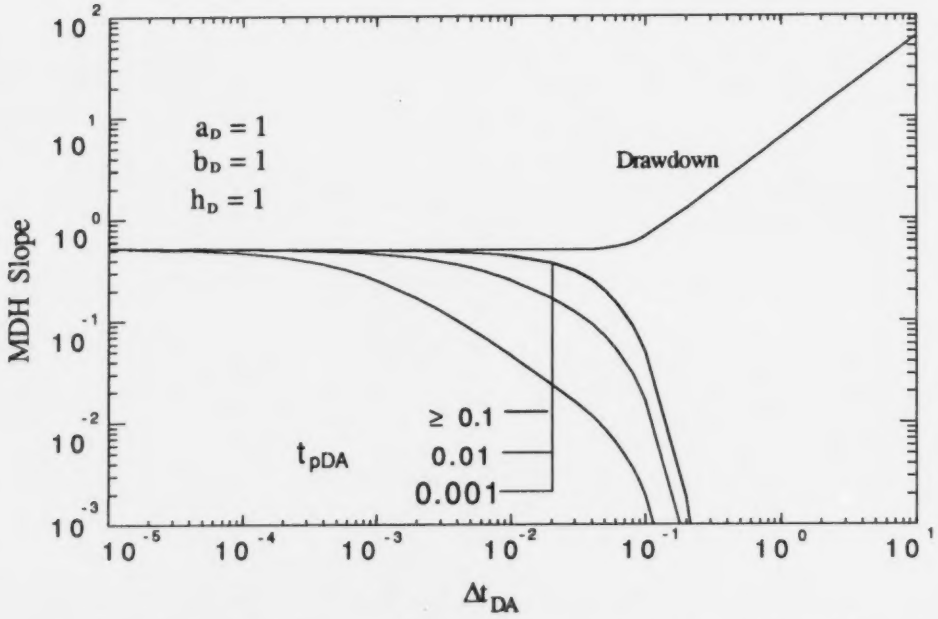

Fig. 4.12 - Effect of t_{pDA} on MDH Slope for $a_D = 1$, $b_D = 1$, and $h_D = 1$.

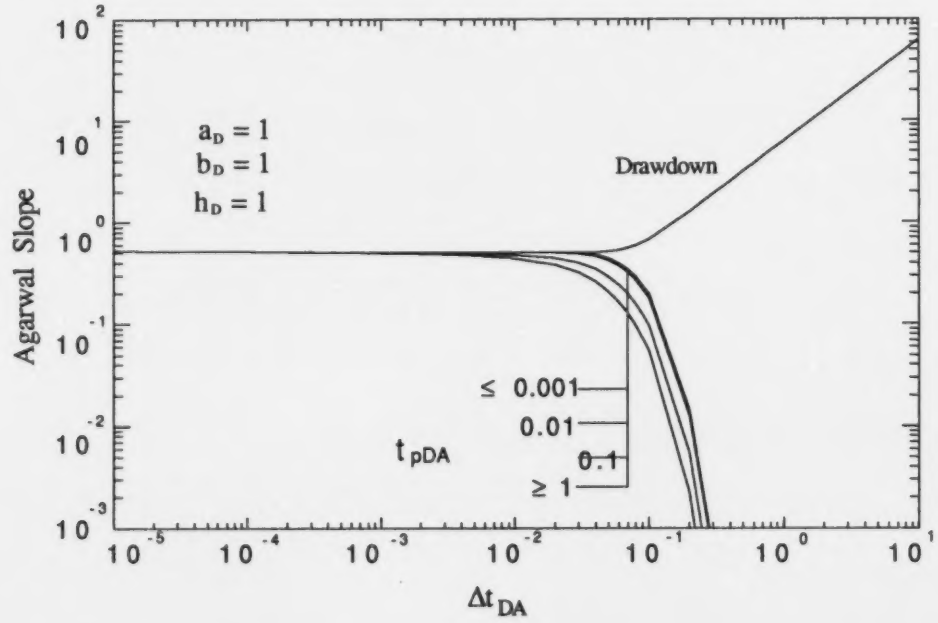

Fig. 4.13 - Effect of t_{pDA} on Agarwal Slope for $a_D = 1$, $b_D = 1$, and $h_D = 1$.

Deviation time is calculated as the time at which the buildup slope deviates by 5% from the drawdown slope. Accuracy of the design equations for predicting deviation time are investigated in App. C. Figure 4.12 also shows that for $t_{pDA} \geq 0.1$, all buildup responses form a single curve. Noting that $(t_{DA})_{pss}$ for this reservoir configuration is 0.1, it implies that all buildup responses correlate for $t_{pDA} \geq (t_{DA})_{pss}$.

For the dimensionless Agarwal graph, Fig. 4.13 shows that the early transients correlate for all producing times, which is in agreement with Ref. 9. However, during the late transient, the Agarwal slope does not result in a single curve for all producing times. Similar results have been reported by Aarstad[10] for buildup responses from a vertical well in a square or rectangular region. Ambastha and Ramey[11] have also reported the lack of correlation of the Agarwal slope during the late transient period for buildup responses from a vertical well in both closed and constant-pressure circular reservoirs. The lack of correlation at late times is, therefore, due to the finite reservoir size, rather than the shape of the reservoir.

Figures 4.14 and 4.15 show the effect of t_{pDA} on the MDH and Agarwal slopes, respectively, for an off-centered, fully-penetrating horizontal well. The reservoir dimensions and well location have been chosen to result in two transient flow regimes. The drawdown curve in Fig. 4.14 shows sequentially, a radial flow period, a linear flow period, and the pseudosteady state period. $(t_{DA})_{pss}$ for the drawdown response is 4.0. Figure 4.14 also shows different buildup responses for different values of t_{pDA}. However, for $t_{pDA} \geq 10$, all buildup responses form a single curve. None of the buildup responses shows the late linear flow period. For this reservoir configuration, $(\Delta t_{DA})_{dev}$ for an MDH graph is approximately related to t_{pDA} by:

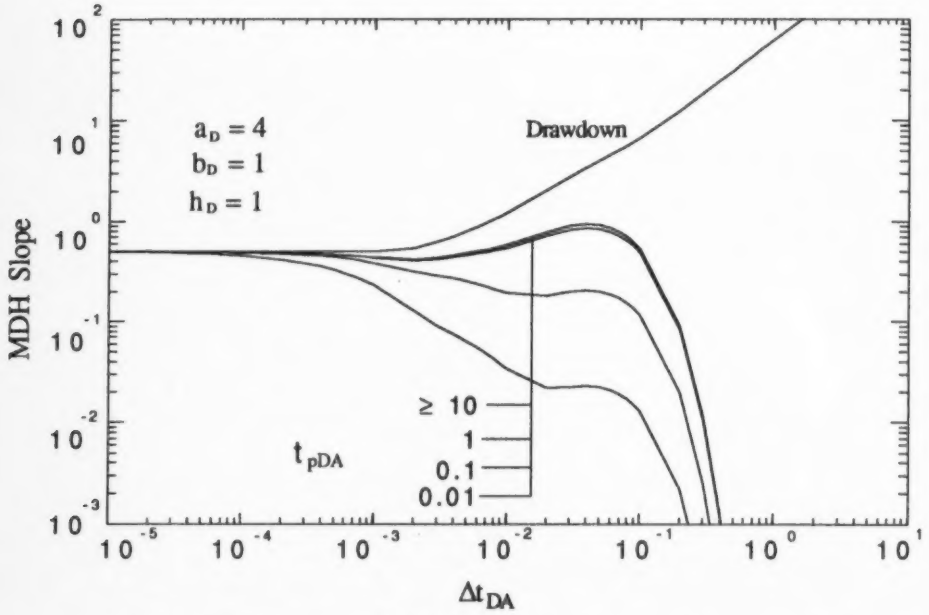

Fig. 4.14 - Effect of t_{pDA} on MDH Slope for $a_D = 4$, $b_D = 1$, and $h_D = 1$.

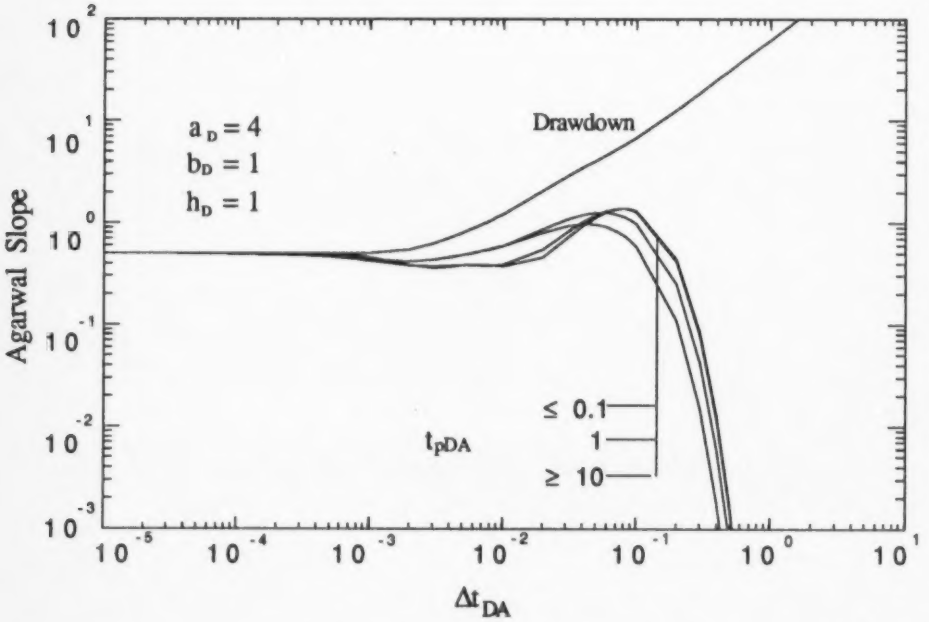

Fig. 4.15 - Effect of t_{pDA} on Agarwal Slope for $a_D = 4$, $b_D = 1$, and $h_D = 1$.

$$(\Delta t_{DA})_{dev} = 0.0035 + 0.0015 \log (t_{pDA}) , \qquad \text{for } 0.01 \leq t_{pDA} \leq 4 . \qquad (4.38)$$

In Fig. 4.15, the Agarwal slopes once again correlate for all t_{pDA} during the early transient period (the radial flow period). The late transient period, however, shows different curves for different t_{pDA}. Figure 4.15 also shows that regardless of the t_{pDA}, all buildup curves deviate from the drawdown curve long before pseudosteady state is reached. None of the buildup curves shows the linear flow period prior to pseudosteady state. It has been expected that for very long producing times ($t_{pDA} \geq (t_{DA})_{pss}$), the buildup responses will correlate with the drawdown response until pseudosteady state is reached. Figure 4.15, however, shows that the reservoir boundaries begin to affect the buildup response well before pseudosteady state is reached. To find out if the preceding observation was an isolated case or a common occurrence, more buildup responses were generated for various reservoir configurations.

Figures 4.16 and 4.17 show the effect of t_{pDA} on the MDH and Agarwal slopes, respectively, for a reservoir configuration to produce all four possible transient flow regimes preceding pseudosteady state flow. The drawdown response in Fig. 4.16 shows sequentially, an early radial, an early linear, a late pseudo radial, a late linear, and pseudosteady state flow periods. For this reservoir, $(t_{DA})_{pss}$ is 0.6. As expected, Fig. 4.16 shows that the buildup responses deviate earlier from the drawdown response as t_{pDA} decreases. The buildup responses show fewer transient flow regimes with decreasing t_{pDA}. None of the buildup responses shows the late linear flow regime. $(\Delta t_{DA})_{dev}$ for an MDH graph is approximately related to t_{pDA} by:

$$(\Delta t_{DA})_{dev} = 0.00347 + 0.00127 \log (t_{pDA}), \qquad \text{for } 0.001 \leq t_{pDA} \leq 0.6 . \qquad (4.39)$$

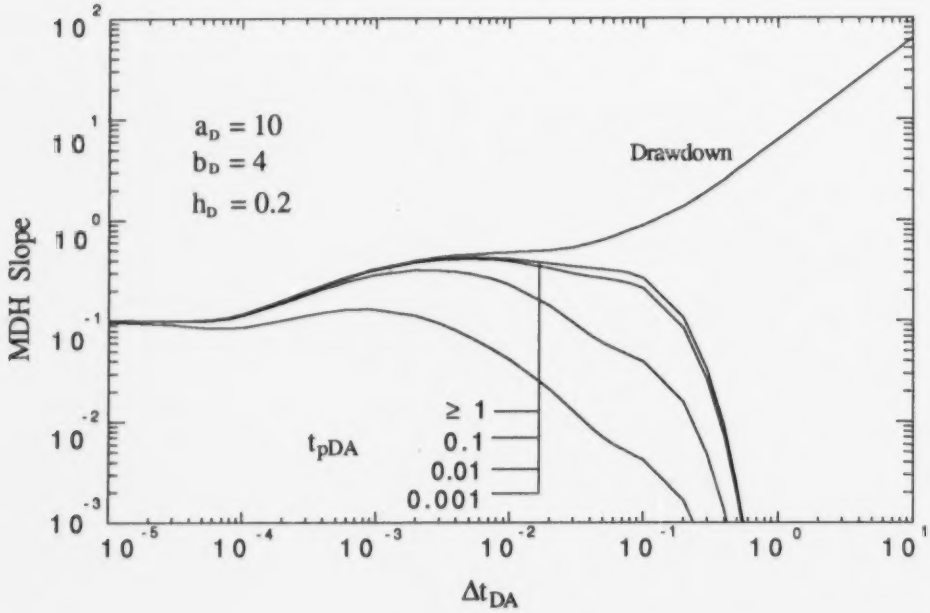

Fig. 4.16 - Effect of t_{pDA} on MDH Slope for a_D=10, b_D = 4, and h_D = 0.2.

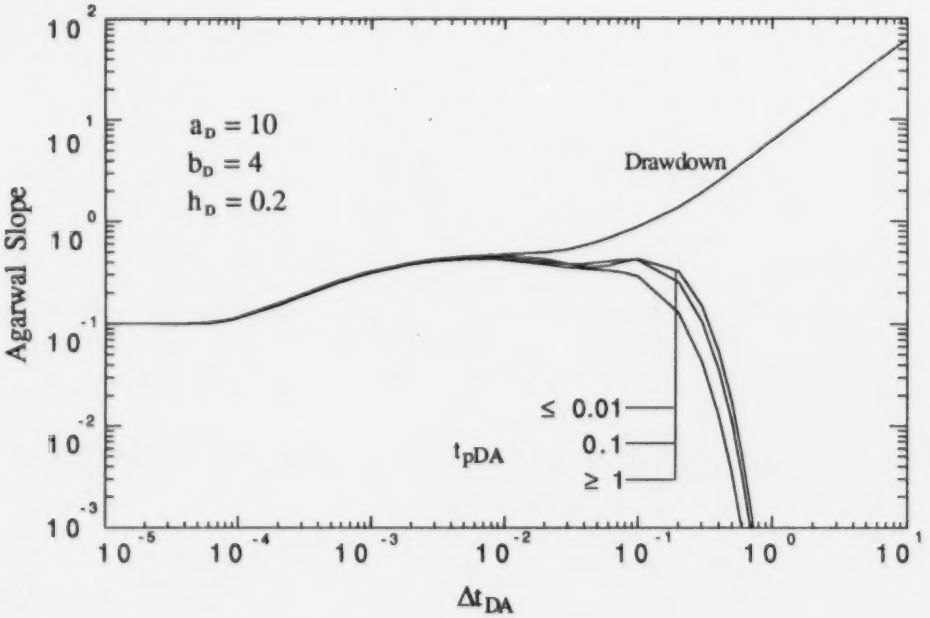

Fig. 4.17 - Effect of t_{pDA} on Agarwal Slope for a_D=10, b_D = 4, and h_D = 0.2.

The Agarwal buildup slopes in Fig. 4.17 confirm the observation made earlier that the buildup responses do not show the late linear flow regime regardless of how long the well has been producing prior to shut-in. Similar results were observed for all the reservoir configurations investigated. This finding has important implications for well test design involving horizontal wells. The preceding observation implies that no matter how long the well is produced prior to shut-in, the late linear flow regime will not occur on a pressure buildup derivative response. Thus, if wellbore storage and/or skin effects were to mask the early time data, it may not be possible to determine reservoir permeability from a buildup test of a horizontal well. For a drawdown test, however, reservoir permeability may be determined from the late transient (late linear period) data even when the early transients are masked by wellbore storage and/or skin effects. Under such circumstances, a drawdown test may be the only possible well test.

5. THERMAL WELL TESTING FOR A HORIZONTAL WELL

This study considers the application of the pseudosteady state method in the determination of swept volume for a horizontal well under steam injection. Attempts are also made to obtain steam chamber mobility from the well test data.

A steam reservoir simulator is used to simulate steam injection into the reservoir model until appreciable volumes are swept. Falloff tests are then simulated by shutting in the injector and noting the wellbore gridblock pressure with time. The main assumption in this study is that the simulator accurately depicts the pressure transient effects in the reservoir model.

5.1 Theory

Depending on reservoir properties and size of swept volume, well length and location, a pressure falloff test on a horizontal well may show one or more of the following transient flow periods leading to pseudosteady state flow corresponding to the swept volume. These are:

1. A wellbore storage-dominated flow period,

2. An early radial flow period,

3. An early linear flow period,

4. A late pseudoradial flow period,

5. A late linear flow period, and

6. A pseudosteady state flow corresponding to the swept volume.

As discussed in Chapter 4, a log-log graph of semi-log pressure derivative ($dp_{WS}/d\ln t$) versus shut-in time (Δt) may be used to identify the various flow regimes. The different flow regimes are identified by:

1. A unit-slope line for wellbore storage-dominated flow,

2. A zero-slope line for early radial flow in the swept region,

3. A half-slope line for early linear flow in the swept region,

4. A zero-slope line for pseudoradial flow,

5. A half-slope line for late linear flow, and

6. A unit-slope line for pseudosteady state flow.

The slope, m_c, of the Cartesian straight line of p_{WS} versus Δt corresponding to pseudosteady state flow is related to the swept pore volume, V_S, by:

$$m_c = \frac{q_s B_g}{24 V_s c_t}. \qquad (5.1)$$

For steam, the flow rate, q_s, is the actual steam injection rate given by:

$$q_s = 5.615\, q\rho_w f_{st}(\vartheta_s)_{std.}\,, \tag{5.2}$$

where, q is the total fluid injection rate in STB/day Cold Water Equivalent (CWE) and f_{st} is the steam quality.

For the steam-swept region, the total compressibility, c_t, is approximately equal to the two-phase compressibility. The two-phase compressibility, $c_{2\phi}$, is calculated using:[27]

$$c_{2\phi} = 0.18513\, \frac{<\rho C>}{\phi}\, \left(\frac{\rho_w - \rho_s}{L_v \rho_w \rho_s}\right)^2 (T + 460), \tag{5.3}$$

where:

$$<\rho C> = (1 - \phi)\rho_f C_f + \phi S_w \rho_w C_w\,. \tag{5.4}$$

The variables C_f and C_w are heat capacities for formation and water in BTU/lb-^{o}F. The gas (steam) formation volume factor, B_g, is given by:

$$B_g = \frac{\vartheta_s}{(\vartheta_s)_{std.}}\,. \tag{5.5}$$

Transient falloff data prior to pseudosteady state may be used to obtain an estimate of the mobility in the steam chamber. The slope, m_{s1}, of the first semi-log straight line of p_{ws} versus Δt corresponding to early radial flow is related to reservoir and fluid properties in the steam-swept region by:[6]

$$m_{s1} = \frac{28.96 q_s \mu B_g}{L k_{rg} \sqrt{k_x k_z}} \quad . \tag{5.6}$$

Another estimate of the swept region mobility could be obtained from the early linear flow period. The slope, m'_1, of the Cartesian straight line of p_{ws} versus $\sqrt{t}$ for transient data in this period is related to reservoir and fluid properties in the swept region by:

$$m'_1 = \frac{1.45 q_s \mu B_g}{L h \sqrt{\phi \mu c_t k_x k_{rg}}} \quad . \tag{5.7}$$

For the late pseudoradial flow period, the slope, m_{s2}, of the semi-log straight line of p_{ws} versus Δt gives:

$$m_{s2} = \frac{28.96 q_s \mu B_g}{h k_{rg} \sqrt{k_x k_y}} \quad . \tag{5.8}$$

The late linear flow, if it exists, should graph as a straight line of p_{ws} versus $\sqrt{t}$. The slope, m'_2, should give:

$$m'_2 = \frac{1.45 q_s \mu B_g}{b h \sqrt{\phi \mu c_t k_x k_{rg}}} \quad . \tag{5.9}$$

Except for early radial flow, none of the flow regimes corresponding to Eqs. 5.7, 5.8 and 5.9 were observed in simulated falloff data in this study. Additional equations used to analyze simulated falloff data of this study are provided in App. D.

5.2 Reservoir Model

The reservoir and fluid data used in this study are similar to those used in Ref. 39 for heavy oil reservoirs. Modifications were made to the reservoir size and grid.

5.2.1 Reservoir Size

Figure 5.1 shows a schematic of the 3-D reservoir model used in the study. For the first two simulation runs, the reservoir is 70 ft [21 m] long, 80 ft [24 m] wide and 35 ft [11 m] thick. Subsequently, the reservoir size is increased to 200 ft [61 m] long, 100 ft [31 m] wide, and 45 ft [14 m] thick, to simulate larger swept volumes. To achieve a reasonable injectivity and hence the advancement of the steam front, a producing well is added to the model[32]. Both injector and producer are parallel to the y-direction. The injector is centrally-located in the reservoir while the producer is centrally-located in the bottom layer. Due to symmetry in the y-direction, only half of the reservoir has been simulated with respect to the y-direction. Simulated well length in the y-direction was 40 ft [12 m] for Runs 1 and 2, and 50 ft [15 m] for all other runs. Note that the simulated well length refers to only half of the real well length because of symmetry in the y-direction. Short well lengths and small reservoirs were simulated in this study because of a compromise made between the number of gridblocks that could be used in the executable version of ISCOM[35] we have and the detailed discretization necessary for a pressure transient analysis study.

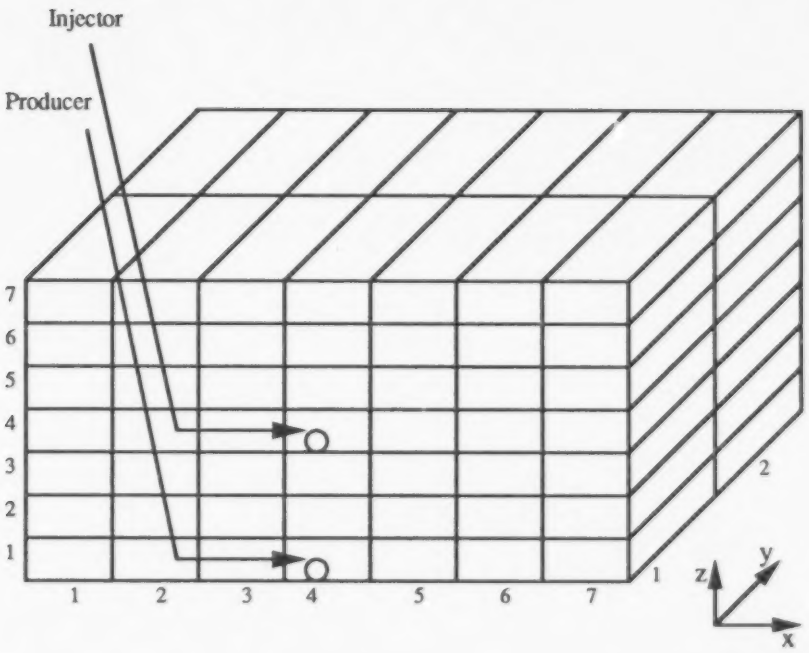

Fig. 5.1 - Schematic of 3-D reservoir model used for simulation

5.2.2 Reservoir Properties

Table 5.1 shows the important reservoir parameters used in the simulator. The reservoir properties are assumed to be uniform throughout the reservoir model at the start of steam injection. The water/oil and gas/liquid relative permeabilities used in the study are shown in Figures 5.2 and 5.3, respectively. The saturation end points are temperature-independent.

Table 5.1: Reservoir parameters used in simulation

Initial water saturation	0.51
Initial oil saturation	0.49
Reservoir pressure, psia	700
Reservoir temperature, ^{o}F	93
Oil viscosity at reservoir temperature, cp	2028
Oil gravity at reservoir temperature, ^{o}API	15.4
Oil compressibility, psi^{-1}	0.0000073
Water compressibility, psi^{-1}	0.000004
Rock compressibility, psi^{-1}	0.00003
Porosity, %	20
Horizontal permeability, md	700
Vertical permeability, md	70
Wellbore radius, ft	0.3
Rock thermal conductivity, BTU/ft-D-^{o}F	77.85
Rock specific heat, BTU/ft^{3}-^{o}F	112.7
Steam injection temperature, ^{o}F	400
Steam quality, %	80
Injection rate, STB/D CWE	200
Producer back pressure, psia	700

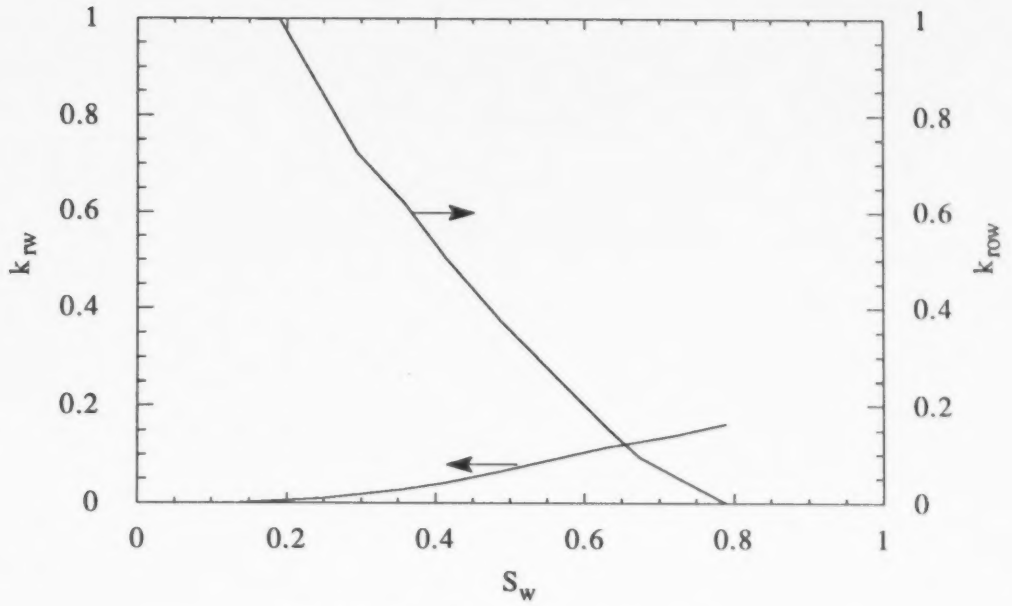

Fig. 5.2 - Water/oil relative permeability

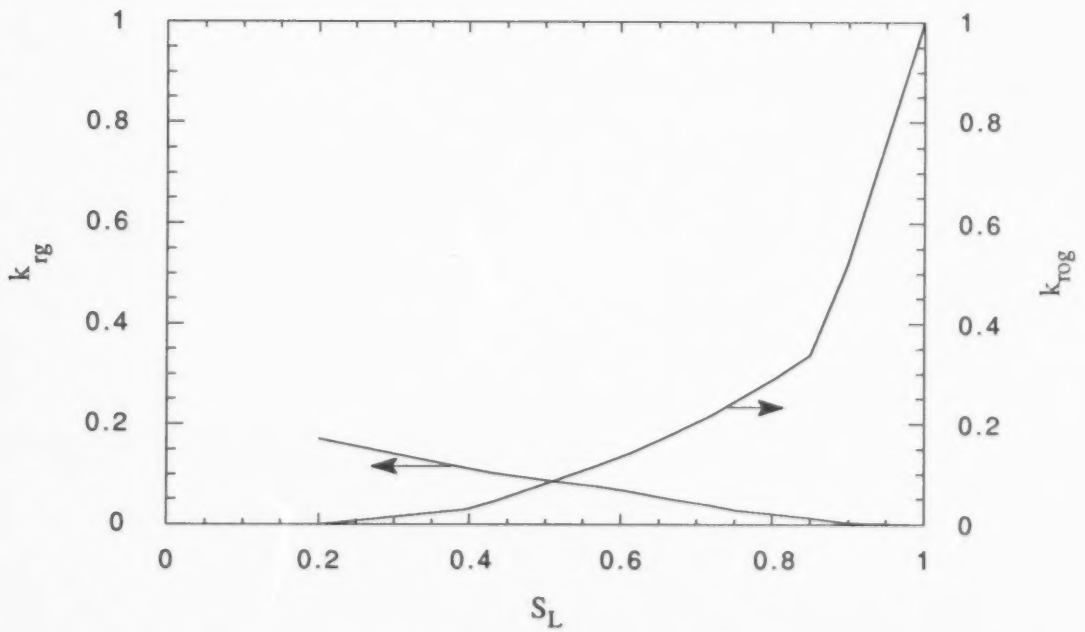

Fig. 5.3 - Gas/oil relative permeability

5.2.3 Fluid Properties

The heavy oil is assumed to be a single-component dead oil with a gravity of 15.4 ^{o}API [0.962 g/cm^3] and a molecular weight of 500. The viscosities of oil, water and gas (steam) as functions of temperature are given in Table 5.2.

Table 5.2: Viscosity-temperature relationships for reservoir fluids

Temperature (^{o}F)	Water (cp)	Oil (cp)	Steam (cp)
10	0.9314	5780	0.01752
20	0.9314	5780	0.01792
30	0.9314	5780	0.01833
40	0.9314	5780	0.01873
50	0.9314	5780	0.01883
60	0.9314	5780	0.01913
70	0.9314	5780	0.01994
80	0.8731	4278	0.02034
90	0.7714	2401	0.02075
100	0.6846	1377	0.02116
200	0.3081	47.04	0.02525
300	0.1820	8.494	0.02938
400	0.1486	3.960	0.03356
500	0.1265	2.501	0.03777
600	0.1265	2.500	0.04202
700	0.1265	2.500	0.04630
800	0.1265	2.500	0.05060
900	0.1265	2.500	0.05493
1000	0.1265	2.500	0.05930
2000	0.1265	2.500	0.1039
3000	0.1265	2.500	0.1499

5.2.4 Simulator

The ISCOM (version 4.0)[35] model is used for the numerical simulation in this study. The model is a multi-component, four-phase simulator developed for thermal recovery operations. It includes gravity and capillary terms as well as a general chemical reaction scheme, and models heat transfer by both conduction and convection. The model operates in 1-, 2- or 3-dimensional Cartesian, cylindrical, or curvilinear coordinates, and is capable of simulating well completions in directions parallel to any of the coordinate axes.

5.3 Cases Studied

Table 5.3 presents a summary of the cases investigated in this study. Ten simulation runs were conducted. Runs 1 and 2 are used to investigate the wellbore gridblock size effect on the pressure falloff data. Runs 2 through 5 are used to study the effect of injection time on the estimation of the swept volume. Except for Run 6, all other runs consider permeability anisotropy in the horizontal and vertical directions. For the anisotropic runs, horizontal permeability is maintained at 700 md, while the vertical permeability is 70 md. Isotropy is introduced in Run 6 to find out what difference it will make to the estimation of the swept volume. Runs 7 through 10 are used to study the effect of steam injection rate on the swept volume estimation.

Table 5.3: Cases studied

Run Number	Description	
1 and 2	Wellbore gridblock size	Homogeneous, anisotropic reservoir
3, 4, 5	Injection time effect	Homogeneous, anisotropic reservoir
6	Effect of isotropy	Homogeneous, isotropic reservoir
7, 8, 9, 10	Injection rate effect	Homogeneous, anisotropic reservoir

5.4 Simulation Results and Discussion

Results of the pressure falloff simulation are discussed in two parts. In the first part, the results of Run 1 are presented, detailing the calculation procedure for the swept volume estimation as well as the steam chamber mobility. In the second part, a discussion of the effect of some important parameters on the estimation of swept volume and steam chamber mobility is presented.

5.4.1 Results of Run 1

For Run 1, the reservoir was divided into 7 equal gridblocks in the x-direction, 2 in the y-direction, and 7 in the z-direction. Steam was injected into the reservoir model at the rate of 200 STB/D [0.00036 m^3/s] CWE for 20 days. This injection time was calculated to result in an appreciable swept volume while ensuring that the flood front did not reach the producer. To simulate the falloff test, the injector was then shut in for 50 hours while the producer was left open to flow. Figure 5.4 shows the wellbore gridblock pressure during the falloff test graphed against shut-in time (Δt).

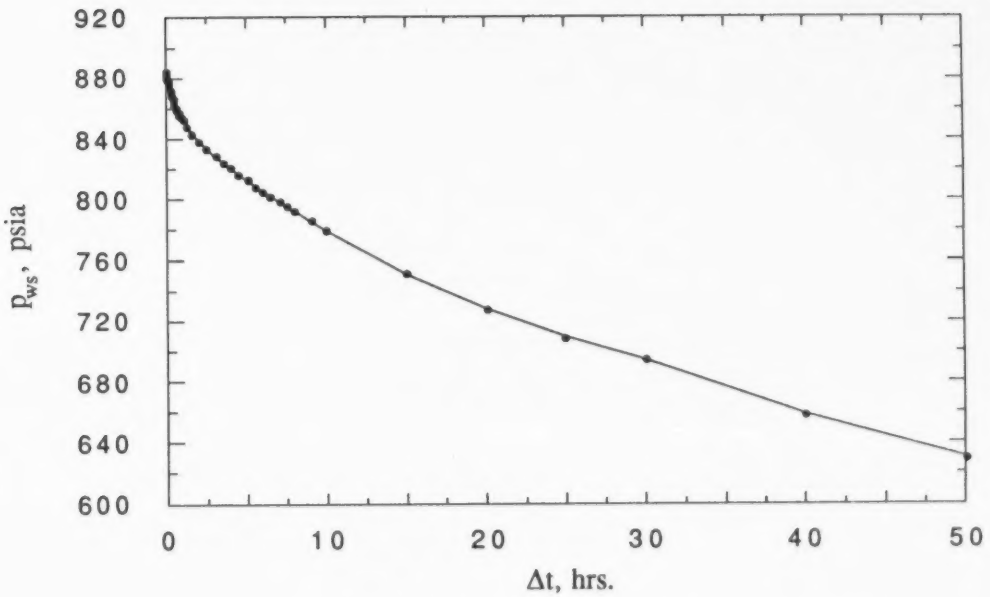

Fig. 5.4 - Falloff response from simulator for Run 1

5.4.1.1 Identification of Flow Regimes

To identify the various flow regimes, semi-log pressure derivatives were calculated from the falloff data using a differentiation algorithm.[40] A log-log graph of the semi-log pressure derivative ($dp_{WS}/dlnt$) versus shut-in time (Δt) is shown in Figure 5.5. The figure shows an early-time unit-slope line that indicates wellbore-dominated flow lasting till about 0.1 hours. After a transition time of about half a log cycle, the semi-log pressure derivative tends to flatten to a zero-slope line, indicating radial flow between 0.5 and 0.8 hours. This radial flow regime is very short in duration. However, this choice of radial flow regime appears justified based on the results of Run 2 to be discussed later. Semi-log pressure derivative rises beyond 0.8 hours, and a second unit slope line corresponding to pseudosteady state for the swept volume, is seen between 6 and 10 hours. Thus, only one transient flow period occurs prior to pseudosteady state.

Based on the assumption that the buildup (falloff) solution can be approximated by the drawdown (injection) solution, an attempt was made to corroborate the flow regimes shown in Figure 5.5 by using the analytical solution presented in Chapter 4 to calculate the semi-log pressure derivatives for a horizontal well in a closed reservoir of the same shape and size as the simulated swept volume. Figure 5.6 compares the semi-log pressure derivative response, as calculated from the analytical solution, with that from the simulated falloff data (Fig. 5.5). For the analytical response, Fig. 5.6 shows sequentially, an early radial flow period, a transition period, and a pseudosteady state flow period. It should be noted that the analytical solution neglects wellbore storage and skin. Thus, the analytical solution confirms the existence of the one transient flow regime from simulation. If the times for the start and/or end of a flow period are defined as the times for which the semi-log pressure derivative is within 5% of the correct slope for that period, then, from the analytical solution, pseudosteady state is observed to begin after 6.1 hours.

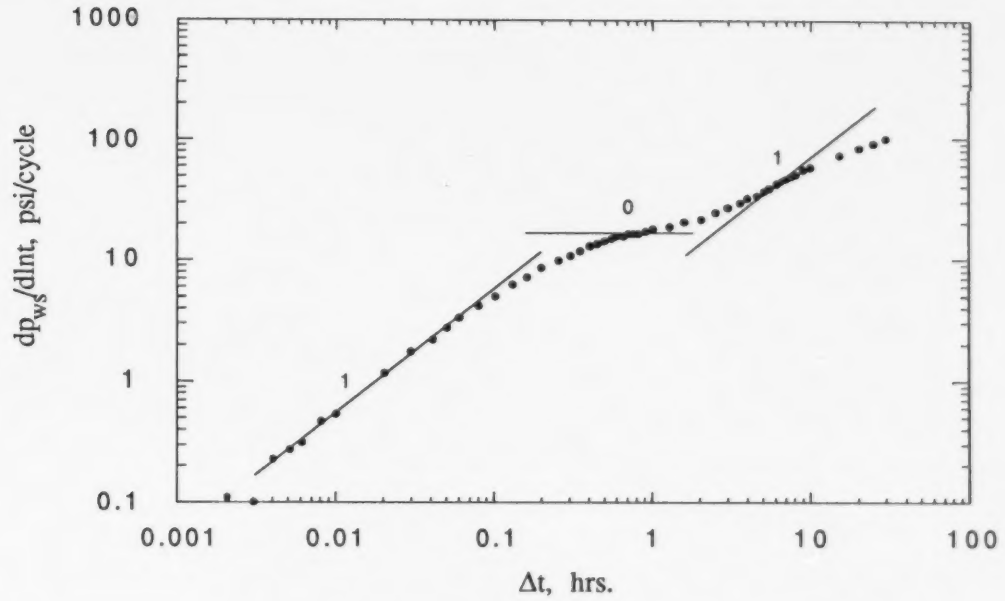

Fig. 5.5 - Semi-log pressure derivative response from falloff data for Run 1

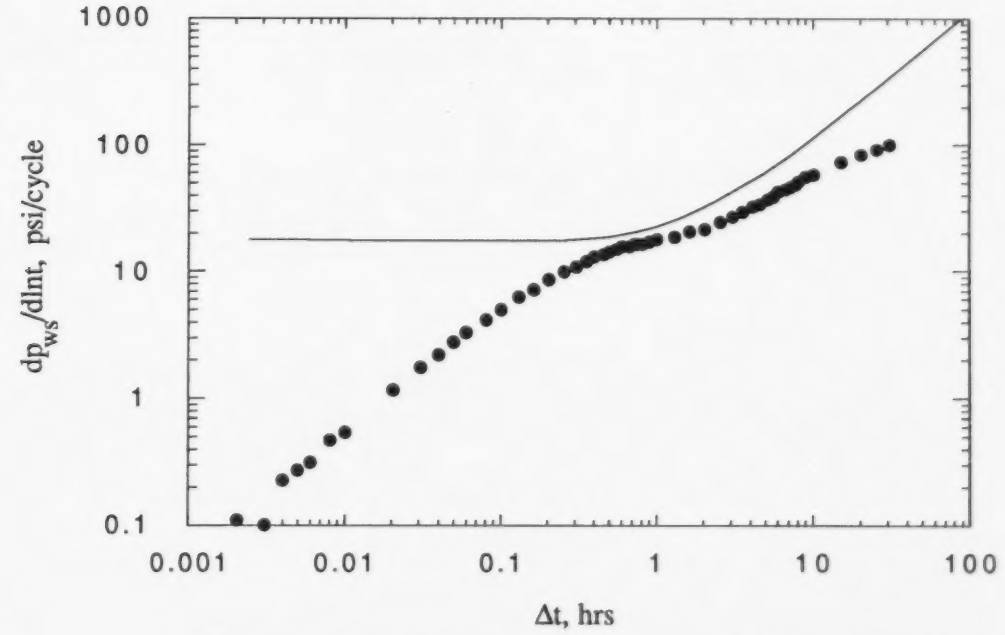

Fig. 5.6 - Comparison of semi-log pressure derivative response from analytical solution with the response from simulated falloff data for Run 1

This compares very well with the 6 hours shown in Figure 5.5, for the start of pseudosteady state flow. However, for the early radial flow regime, the analytical solution indicates that early radial flow ends at 0.45 hours, a little earlier than the 0.8 hours shown in Figure 5.5. Thus, while the analytical solution shows the same flow regimes as the simulated test of Fig. 5.5, and predicts reasonably well the time for the start of pseudosteady state flow for simulated falloff data, analytical solution does not provide a good estimate for the time to the end of the early radial flow regime.

To investigate further the wellbore storage effect, a Cartesian graph of p_{ws} vs Δt corresponding to the early time unit slope line on the derivative graph was drawn. The slope, m_{cw}, of the Cartesian straight line is 56.49 psi/hr. Using Equation D-1, the dimensionless wellbore storage constant, C_D, is 0.6. The wellbore storage effect may have been caused by changing fluid volume in the wellbore gridblock during the falloff test. An examination of the wellbore gridb'ock gas saturation during the falloff test showed that the gas saturation increased by about 4% due to the pressure drop.

5.4.1.2 Estimation of Swept Volume

The simulated swept volume at the end of steam injection into the reservoir model was calculated by adding the gridblock volumes within the swept region. The swept region was identified as the region of non-zero gas (steam) saturation[32]. This resulted in a box-shaped, steam-swept pore volume of 2400 ft^3 [67.96 m^3]. The average temperature in the swept region was calculated by taking the volumetric average of the gridblock temperatures in the swept region. The average pressure and gas saturation were also volume-averaged. Using the average temperature, the gas viscosity is calculated by interpolation from the

viscosity-temperature relationship of Table 5.2. The gas relative permeability, k_{rg}, is that corresponding to the average gas saturation within the swept volume.

The swept volume was also calculated from the falloff data using the pseudosteady state method. Figure 5.7 shows a Cartesian graph of p_{ws} versus Δt. For data between 6 and 10 hours, the slope, m_c, is 6.57 psi/hr. At an average swept volume temperature of 522 ^oF, the formation volume factor, calculated from the saturated-steam-property functional correlations of Ref. 41 and Eq. (5.5), is 0.000414 ft^3/SCF. The two-phase compressibility calculated from Eq. (5.3), is 0.0432 psi^{-1} [0.2979 kpa^{-1}]. Using Eq. (5.2), the injection rate of 200 STB/D CWE at 80% steam quality, converts to 67.65 MMSCF/D of steam. From Eq. (5.1), the swept volume is calculated as:

$$V_s = \frac{(67.65x10^6)(0.000414)}{(24)(6.57)(0.0432)} = 4111\ ft^3 . \qquad (5.10)$$

A comparison of the calculated swept volume to the simulated swept volume shows that the calculated volume is 1.71 times larger than the simulated volume. The swept volume is thus overestimated by 71%. The overestimation of the swept volume by the pseudosteady state method may possibly be the result of injection time effects[34] on falloff responses for a box-shaped region. Currently, no analytical solution is available for the reservoir configuration considered in this study. This hypothesis is investigated later by varying the steam injection time prior to shut-in.

Another possible explanation for the overestimation of the swept volume by the pseudosteady state method may be that the simulated swept volume includes not only the

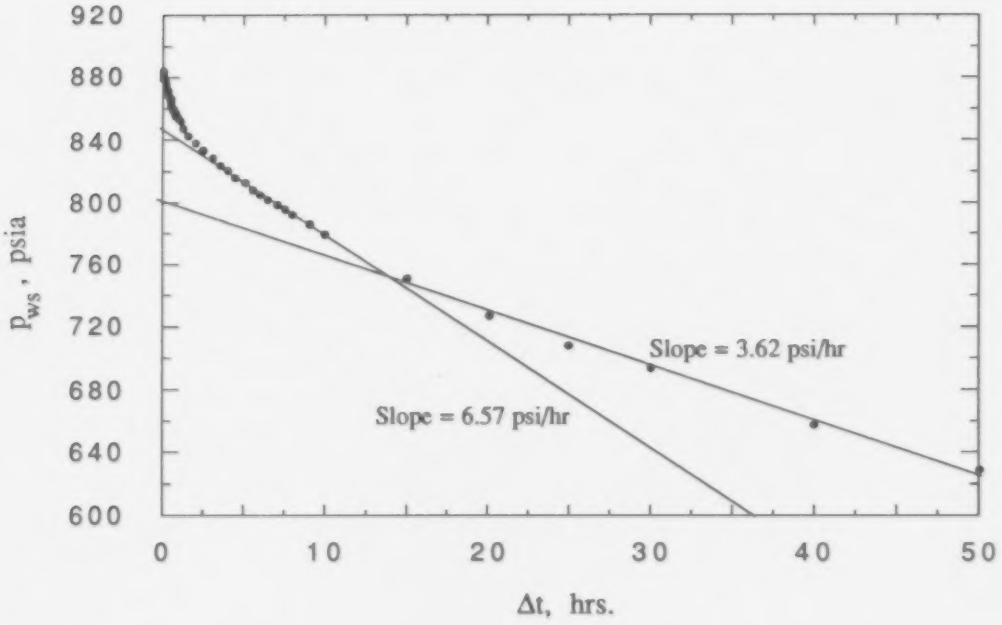

Fig. 5.7 - Cartesian graph of falloff data for Run 1

region with non-zero gas saturation, but also the hot water (condenced steam) zone ahead of the front. To investigate this hypothesis, the simulated swept volume was redefined to include all portions of the reservoir where the total effective mobility was ten or more times the original total effective mobility. This resulted in a new simulated swept volume of 6800 ft^3 [192.55 m^3]. To calculate a new swept volume based on the pseudosteady state method, the total system compressibility, c_t, had to be recalculated to reflect the fact that portions of the swept volume have zero gas saturation. Using Equation D-3, the new c_t is 0.01526 psi^{-1} [0.1052 kpa^{-1}]. The corresponding calculated swept volume is 11460 ft^3 [324.5 m^3], which is also 1.71 times the simulated swept volume. Because the total compressibility in the hot water zone (c_{thw}) is negligible compared to the total compressibility in the steam zone (c_{ts}), $c_t \approx (V_{st}/V_s)c_{ts}$ (see Eq. D-3). This is why the ratio of the calculated swept volume to the simulated swept volume remains the same for the two analyses of the data for Run 1.

Figure 5.7 also shows that another straight line could be drawn through data from 20 to 50 hours. The slope of this line is 3.6 psi/hr. If this slope is used in Eq. (5.10), the swept volume is 7502.6 ft^3 [212.4 m^3], which is about three times the simulated steam-swept pore volume of 2400 ft^3 [67.96 m^3]. Thus, the calculated swept volume is quite sensitive to the selection of the correct straight line. The correct straight line should be the one suggested by the pressure derivative graph, and by the time to pseudosteady state based on an appropriate analytical solution, if available.

5.4.1.3 Estimation of Steam Chamber Mobility

Based on average values of viscosity and gas (steam) relative permeability, as well as other reservoir and fluid properties in the swept region, the expected slope of the semi-log straight line corresponding to early-radial flow (see Eq. 5.6) is:

$$m_{s1} = \frac{28.96(67.65x10^6)(0.03871)(0.000414)}{40(0.08855)\sqrt{(700)(70)}} = 40.1 \text{ psi/cycle}. \qquad (5.10)$$

Figure 5.8 shows a semi-log graph of p_{ws} versus Δt. A straight line through data between 0.5 and 0.8 hours, corresponding to early-radial flow from Figure 5.5, gives a slope of 33.2 psi/cycle. Thus, the slope calculated from the falloff data is about 83 per cent of the actual slope from simulation. The steam chamber mobility is, thus, overestimated by about 20 per cent. The skin factor, s, calculated from Eq. D-6, is 0.73. The calculated skin factor compares favourably with the input skin factor of zero. A possible explanation for the overestimation of the steam chamber mobility is the wellbore storage effect which masked portions of the early-radial flow period. In a similar study to estimate the swept volume for a vertical well under steam injection, Fassihi[32] reported that early pressure transient data from the simulator appeared to be masked by some wellbore storage that was radius dependent. Possible near-wellbore effects on the estimation of the steam chamber mobility will be investigated by varying the gridblock size around the wellbore. Figure 5.8 also shows that another straight line could be drawn through the early time data on the semi-log graph, with a slope of 5.25 psi/cycle. Thus, the estimation of the steam chamber mobility is also shown to be quite sensitive to the selection of the correct straight line.

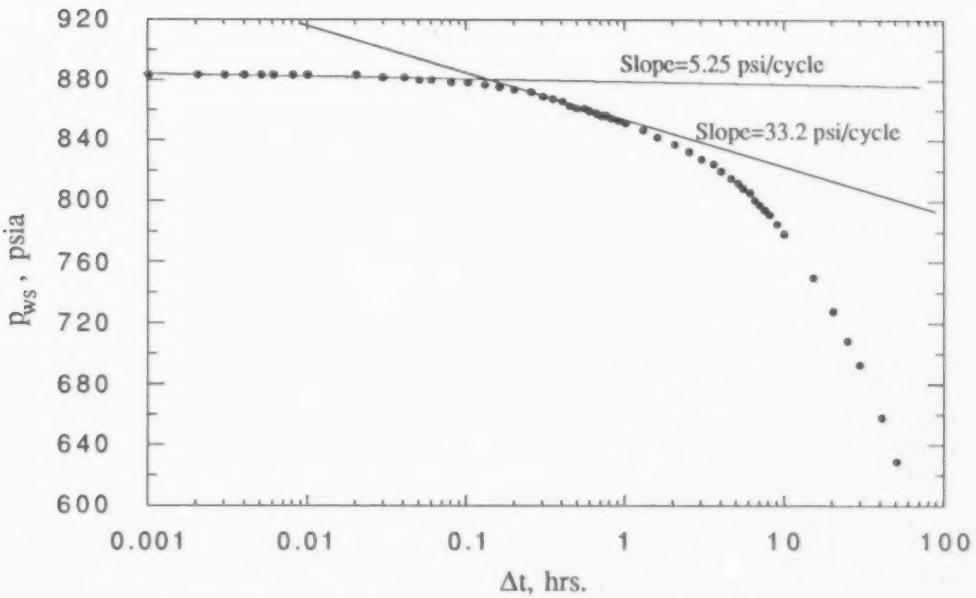

Fig. 5.8 - Semi-log graph of falloff data for Run 1

5.4.2 Possible Causes of Swept Volume and Mobility Overestimation

To investigate the possible causes of swept volume and steam chamber mobility overestimation, several pressure falloff tests were simulated. Table 5.4 shows the run conditions at the start of pressure falloff test simulation.

Table 5.4: Conditions at the start of falloff test simulation

Run Number	Injection Rate (STB/D)	Injection Duration (days)	Cumulative Injection (MSTB)	Well Gridblock Pressure (psia)
1	200	20	4.0	884.7
2	200	20	4.0	839.2
3	200	40	8.0	817.9
4	200	80	16.0	825.8
5	200	160	32.0	792.5
6	200	20	4.0	1112.3
7	400	20	8.0	932.9
8	400	10	4.0	975.2
9	800	20	16.0	1217.0
10	800	10	8.0	1183.9

5.4.2.1 Effect of Wellbore Gridblock Size

The effect of gridblock size around the wellbore was studied with falloff data from Runs 1 and 2. In Run 1, the wellbore gridblock was 10 x 5 ft [3 x 1.5 m]. The wellbore gridblock size was reduced to 3 x 3 ft [0.9 x 0.9 m] for Run 2. In addition, while the block sizes in Run 1 were all equal, those in Run 2 were made to increase telescopically away from the centre of the reservoir. The well length in both runs was 40 ft [12.2 m]. Steam injection rate was constant at 200 STB/D [0.00036 m^3/s] cold water equivalent (CWE), with 80% quality. The duration of injection was 20 days. Figure 5.9 shows the resulting pressure falloff data for the two runs. In Fig. 5.10, the semi-log pressure derivative for both runs are graphed versus time to aid in the identification of the flow regimes. Figure 5.10 shows that wellbore storage affects the early pressure transient data of both runs. The wellbore storage is, however, dependent on the size of the wellbore gridblock. The dimensionless wellbore storage coefficient, C_D, is 0.6 for Run 1. C_D for Run 2 is 0.1. Figure 5.10 also shows a flattening (zero-slope) of the semi-log pressure derivative data between 0.1 and 1 hr for Run 2. In Run 1, the flattening of the semi-log pressure derivative data occurs just between 0.5 and 0.8 hr, a much shorter duration. This makes the radial flow period more clearly identified in Run 2 than in Run 1. Figure 5.11 presents a semi-log graph of the falloff pressure versus time for the two runs. Straight lines are shown through data between 0.5 and 0.8 hours for Run 1, and between 0.1 and 1 hour for Run 2. As shown in Table 5.5, there is a better agreement between the simulated and calculated slopes for Run 2 than that for Run 1. The difference between the simulated and calculated slopes is 12% for Run 2 and 17% for Run 1. Table 5.5 also shows that the skin factor for Run 2 (s = 0.43) is closer to the input skin factor of zero, than that for Run 1 (s = 0.73). Thus, analysis of the falloff data indicates that the early-time pressure behaviour is modelled better in Run 2 than in Run 1. Consequently, for the rest of the simulation runs, the wellbore gridblock size is maintained at 3 x 3 ft [0.9 x 0.9 m].

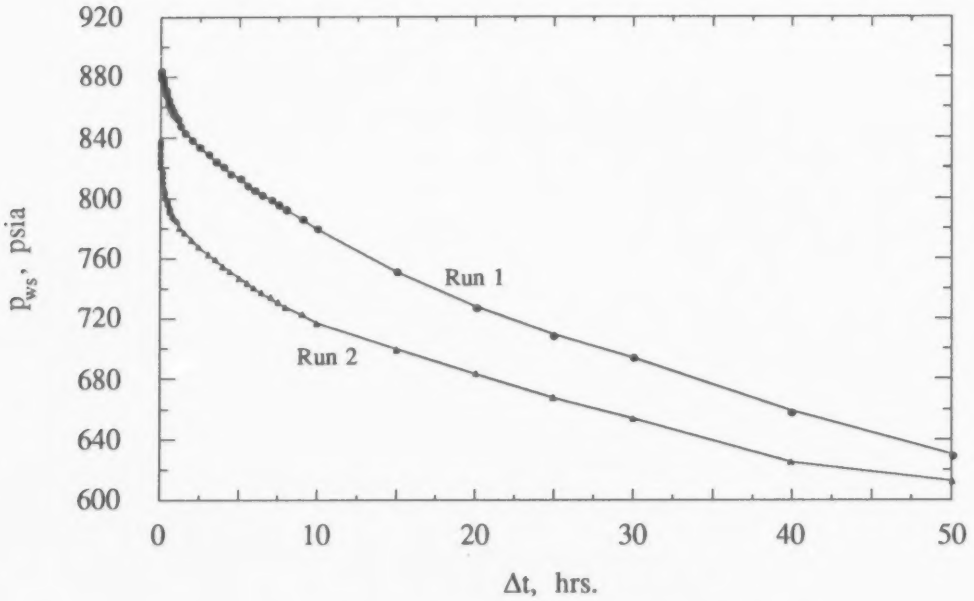

Fig. 5.9 - Pressure falloff data for Runs 1 and 2

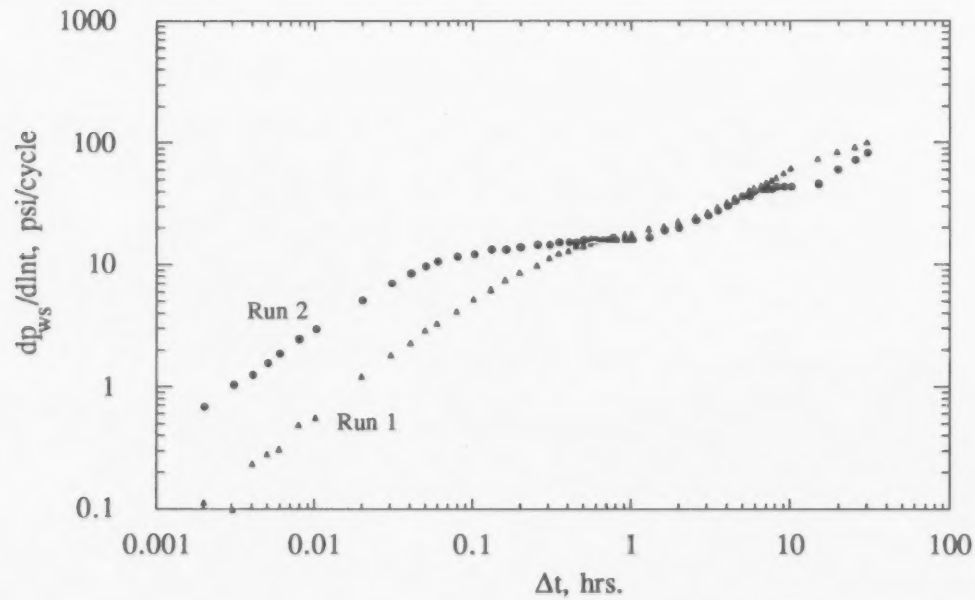

Fig. 5.10 - Semi-log pressure derivative data for Runs 1 and 2.

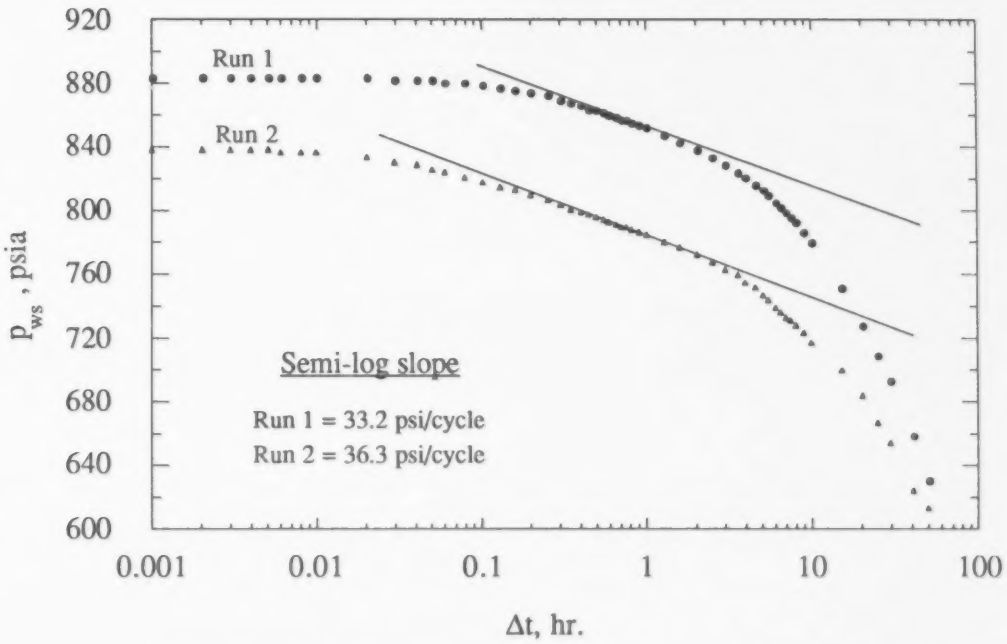

Fig. 5.11 - Semi-log graph of falloff data for Runs 1 and 2.

Table 5.5: Steam chamber mobility and skin factor for all runs

Run Number	S_g (%)	Simulated slope (psi/cycle)	Calculated slope (psi/cycle)	Calculated skin
1	50.0	33.20	40.10	0.73
2	65.8	36.28	31.93	0.43
3	63.5	36.21	35.16	0.58
4	66.0	30.20	25.86	0.38
5	61.7	25.27	24.98	0.51
6	62.2	118.0	93.90	0.56
7	67.4	66.25	59.32	0.55
8	66.5	63.30	57.40	0.49
9	61.5	85.20	87.30	0.99
10	60.8	93.00	119.4	1.3

Results of steam chamber mobility and skin factor from all simulation runs are presented in Table 5.5. Also shown in Table 5.5 are the average steam saturations in the steam-swept region at the start of the falloff test simulations.

5.4.2.2 Injection Time Effects on Swept Volume Estimation

It was suggested earlier that the swept volume overestimation by the pseudosteady state method may have been caused by short injection time prior to conducting the falloff test. To investigate this hypothesis, four simulation runs with injection durations of 20, 40, 80 and 160 days were analyzed. These correspond to Runs 2, 3, 4 and 5, respectively

(see Table 5.4). For these runs, the reservoir dimensions were 200 ft long, 100 ft wide, and 45 ft thick, to allow for the increased swept volume. The grid block sizes increased telescopically away from the centre. The steam injection rate was maintained at 200 STB/D [0.00063 m^3/s] CWE for all four runs. Figure 5.12 shows the pressure falloff data for these runs. The simulated falloff test results are shown in Table 5.6. Also shown in Table 5.6 are the volume-weighted average temperature and pressure values at the start of falloff test simulation.

Table 5.6: Simulated falloff test results

Run Number	m_c (psi/hr)	T (^oF)	p (psia)	Simulated volume (Mscf)	Calculated volume (Mscf)	Swept volume overestimation
1	6.57	522.0	834.6	2.400	4.111	1.17
2	7.72	515.9	786.4	2.152	3.222	1.50
3	4.16	511.8	758.4	3.808	5.814	1.53
4	2.74	514.4	776.0	5.840	8.977	1.54
5	1.19	509.5	744.0	12.30	20.134	1.64
6	13.44	535.7	931.0	1.784	2.015	1.13
7	9.84	520.9	821.4	3.904	5.174	1.33
8	19.43	528.1	872.9	2.272	2.703	1.19
9	11.69	549.2	1039.1	7.360	9.893	1.34
10	20.32	540.0	964.9	4.992	5.499	1.10

Contrary to expectation, the simulated falloff test results show that increasing the injection time prior to shut-in leads to worse estimates of the swept volume. Table 5.6 shows that the swept volume was overestimated by a factor of 1.50 to 1.64 when injection time increased from 20 to 160 days, respectively. This observation is further confirmed by results from Runs 8 and 10. The injection time for both these runs is 10 days. The injection rates, however, had to be increased for an appreciable volume to be swept. The rate for Run 8 is 400 STB/D [0.00126 m^3/s] CWE while for Run 10, it is 800 STB/D [0.00252 m^3/s] CWE. Results from Table 5.6 show that reducing the injection time to 10 days reduced the swept volume overestimation to 1.19 for Run 8 and 1.10 for Run 10.

Figure 5.13 shows vertical cross-sections, normal to the injector, for the swept volume shapes of Runs 4, 5, 6, 8 and 10. A study of the swept volume shapes for these runs indicates that in the runs that gave better estimates of the swept volume (Runs 6, 8 and 10), the swept regions were more uniformly shaped. Thus, it appears that the longer the injection time, the more irregular the swept volume shape becomes. Furthermore, graphs of semi-log pressure derivative versus time for these runs (Figures E4b, E5b, E6b, E8b and E10b) show that the unit slope line, indicating pseudosteady state type flow, is more clearly identified in the runs with short injection time than those with longer injection times. Thus, it appears that irregularities in the shape of the swept volume, caused by increased injection time, affect the occurrence and slope (and consequently, calculated swept volume) of the pseudosteady straight line.

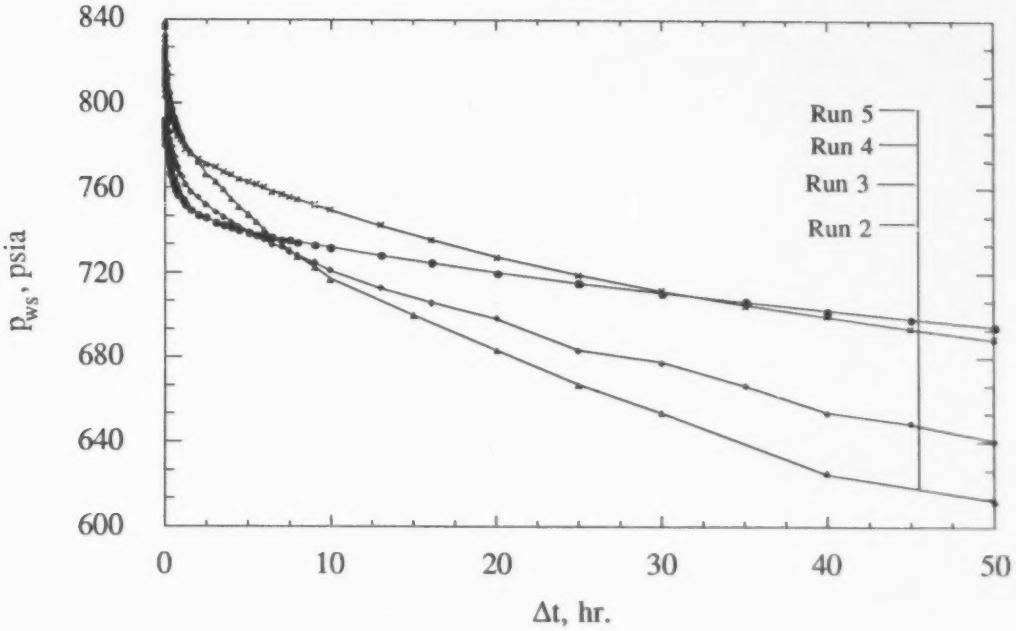

Fig. 5.12 - Pressure falloff data for Runs 2, 3, 4 and 5.

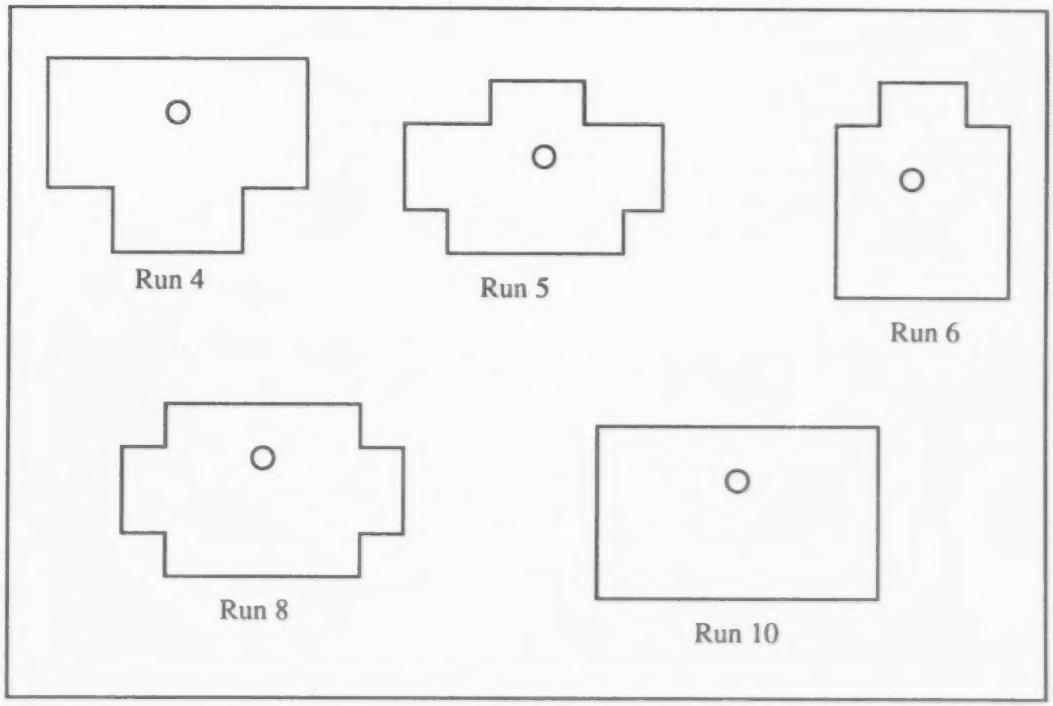

Fig. 5.13 - Swept region shapes for Runs 4, 5, 6, 8 and 10

5.4.2.3 Injection Rate Effect on Swept Volume Estimation

The effect of injection rate on the estimation of the swept volume is investigated with the results from Runs 2, 7 and 9. The injection time in all three runs is maintained at 20 days. The injection rates for Runs 2, 7 and 9 are 200, 400 and 800 STB/D [0.00063, 0.00126 and 0.00252 m^3/s] CWE, respectively. Table 5.6 shows that the swept volume overestimation for Runs 2, 7 and 9 are 1.50, 1.33 and 1.34, respectively. From the preceding results, there seems to be no established trend between the steam injection rate and the estimated swept volume. However, when viewed in conjunction with the results for Runs 8 and 10, it appears that the higher the injection rate, the better the swept volume estimation.

5.4.2.4 Effect of Isotropy on Swept Volume Estimation

Run 6 was conducted for a homogeneous and isotropic reservoir, with a permeability of 70 md. The injection rate for this run is 200 STB/D [0.00063 m^3/s] CWE. The duration of injection is 20 days. Results from Table 5.6 show that the swept volume is overestimated even when the reservoir is isotropic. The swept volume overestimation is 1.13 for this run. However, on comparing with results of Run 2, which has the same injection rate and duration, but is anisotropic, it is observed that isotropy improves the estimation of the swept volume.

A look back at Fig. 5.13 reveals that none of the swept regions is symmetrical around the wellbore for the runs shown, as well as others not shown here. These asymmetries were expected, because of the effect of gravity and the location of the producer. It is possible that the swept volume overestimation, even for the best case (10% for Run 10), may have

been caused by steam-assisted gravity drainage and/or the location of the producer. The simulation of a cyclic steam injection, without an additional producer, will confirm or eliminate the effect of the producer. Such a simulation will, however, require a much larger reservoir and more grid blocks, if an appreciable reservoir volume is to be swept prior to the falloff test. As a result, the simulation time required could be large. Because of limitations regarding the number of grid blocks that could be used in the executable version of ISCOM[35] that we have, the preceding idea was not incorporated in this study.

5.4.2.5 Results of Steam Chamber Mobility Estimation

Table 5.5 shows that the calculated semi-log straight line slopes agree quite well with the simulated slopes. Figure 5.14 shows a comparison between the calculated (expected) semi-log straight line slopes and simulated slopes. The agreement is much better for the lower values of semi-log straight line slopes (< 50 psi/cycle) than for the higher slopes. The higher slopes correspond to runs with shorter injection times. Thus, while short injection times may improve the swept volume estimation, they tend to adversely affect the estimation of the steam chamber mobility.

The calculated skin factors (Table 5.5) compare favourably with the input skin factor of zero. The results of the skin factors, together with the good agreement between the calculated and the simulated semi-log straight line slopes indicate that the early-time pressure behaviour is quite accurately modelled by the simulator. Steam-assisted gravity drainage does not appear to have any effect on the early-time well test data. Thus, steam chamber mobility can be estimated quite accurately from the well test.

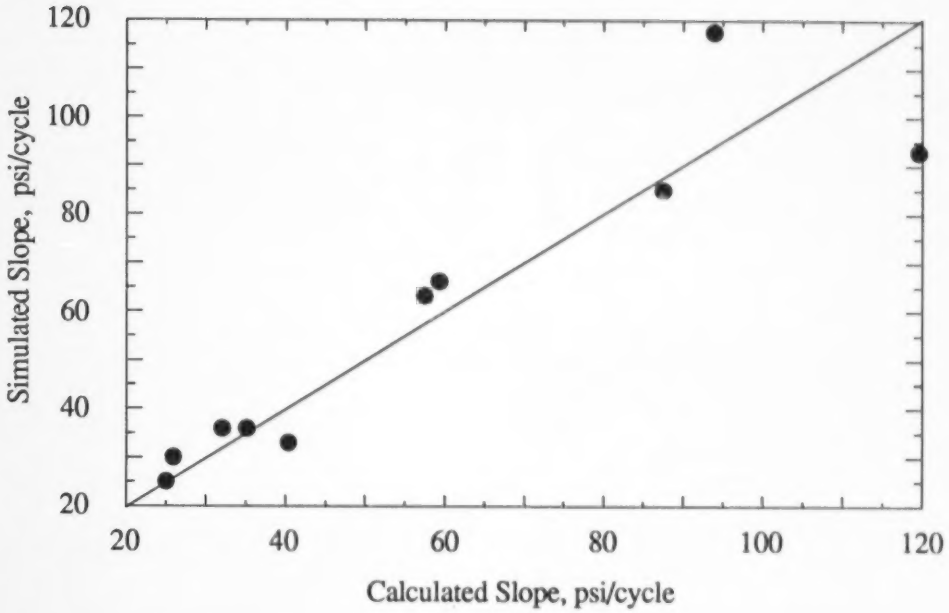

Fig. 5.14 - Comparison of simulated and calculated semi-log slopes for all simulation runs.

6. CONCLUSIONS AND RECOMMENDATIONS

This study considered the pressure transient behaviour of a horizontal well in a closed, box-shaped reservoir. Both the drawdown and buildup responses were studied. Well testing for a horizontal well under steam injection was also considered. The main focus was on the estimation of steam chamber mobility and swept volume from the well test data.

6.1 Conclusions

From the study of the pressure transient behaviour of horizontal wells, the following conclusions may be drawn regarding the drawdown response:

1. The general solution for the pressure response of a horizontal well in a closed, box-shaped reservoir[6] can be evaluated numerically, with a comparable degree of accuracy as when evaluated analytically.

2. The duration of the various transient flow periods for a horizontal well tend to be shorter, when based on the semi-log pressure derivative than when based on pressure. This conclusion is consistent with Refs. 10 and 20.

3. Changing the well location in the x- and y-directions affects the late-time flow regimes. The z-direction well location affects the early-time flow regimes.

4. The reservoir length and width affect the late-time flow behaviour, while the reservoir thickness affects the early-time flow behavior.

The following conclusions may be drawn from the buildup study:

1. Correlations have been presented that relate the deviation time (from the drawdown response) to the producing time prior to shut-in, depending on the time to pseudosteady state flow for the reservoir.

2. A pressure buildup test will not show the late linear flow regime, even if it is present on the drawdown response.

On well testing for a horizontal well under steam injection, the conclusions are:

1. The pseudosteady state method may be used to estimate the swept volume for steam injection through a horizontal well. However, swept volume may be overestimated by 10 to 60 per cent.

2. Longer injection times prior to shut-in appear to have an adverse effect on the estimation of the swept volume by the pseudosteady state method because of a more irregular swept region shape for longer injection time cases.

3. The estimate of the swept volume as well as the steam chamber mobility are sensitive to the choice of appropriate straight lines. A pressure derivative graph may be useful in identifying proper lines. This conclusion is in agreement with Ref. 33 dealing with an analysis of falloff tests for vertical steam injection wells.

4. Steam chamber mobility can be accurately estimated from the well test data.

Irregular swept region shape does not appear to have a noticeable effect on the early time well test data.

6.2 Recommendations

1. Future studies should consider simulated falloff tests from cyclic steam injection horizontal wells.

2. Simulated falloff studies of in-situ combustion through a horizontal well should be conducted to determine the accuracy to which the burned volume and its mobility could be estimated from the well test data.

3. An analytical study of the pressure behaviour of a horizontal well in a composite reservoir should be conducted for comparison with the results from the simulated falloff test.

REFERENCES

1. Goode, P. A. and Thambynayagam, R. K. M.: " Pressure Drawdown and Buildup Analysis of Horizontal Wells in Anisotropic Media," *SPE Form. Eval.* (Dec. 1987) 683-697.

2. Ozkan, E. and Raghavan, R.: " Horizontal Well Pressure Analysis," *SPE Form. Eval.* (Dec. 1989) 567-575.

3. Deviau, F., Mouronval, G., Bourdarot, G., and Curutchet, P.: " Pressure Analysis for Horizontal Wells," paper SPE 14251 presented at the SPE Annual Technical Conference and Exhibition, Las Vegas (Sept. 22-25, 1985)

4. Clonts, M. D. and Ramey, H. J., Jr.: " Pressure Transient Analysis for Wells with Horizontal Drainholes," paper SPE 15116 presented at the SPE California Regional Meeting, Oakland, CA (April 2-4, 1986)

5. Kuchuk, F. J., Goode, P. A., Wilkinson, D. J., and Thambynayagam, R. K. M.: " Pressure Transient Behaviour of Horizontal Wells With and Without Gas Cap or Aquifer," paper SPE 17413 presented at the SPE California Regional Meeting, Long Beach, CA (March 23-25, 1988)

6. Odeh, A. S. and Babu, D. K.: " Transient Flow Behavior of Horizontal Wells, Pressure Drawdown, and Buildup Analysis,"*SPE Form. Eval.*(March 1990) 7-15

7. Thompson, L. G. and Manrique, J. L.: " Efficient Algorithms for Computing the Bounded Reservoir Horizontal Well Pressure Response," paper SPE 21827 presented at the Rocky Mountain Regional Meeting and Low-Permeability Reservoir Symposium, Denver, Colorado (April 16-17, 1991)

8. Hantush, M.: *Advances in Hydroscience*, Ven Te Chow (ed.), Academic Press, New York City (1964) 281-432.

9. Agarwal, R. G.: "A New Method to Account for Producing Time Effects When Drawdown Type Curves are Used to Analyze Pressure Buildup and Other Tests Data," paper SPE 9289 presented at the 55th Annual Meeting of SPE of AIME in Dallas, TX (Sept. 21-24, 1980).

10. Aarstad, K.: " Criteria for Determining Times for End of Transient Flow and Start of Pseudosteady State Flow, " Engineer Thesis, Stanford University, Stanford, CA (Aug. 1987) p. 162

11. Ambastha, A. K. and Ramey, H. J., Jr.: " Well-Test Analysis for a Well in a Finite, Circular Reservoir, " *Proc.*, 13th Geothermal Workshop, Stanford University, Stanford, CA (Jan. 19-21, 1988)

12. Pugh, G. E.: " Drilling of Three Horizontal Wells Pattern, Fort McMurray, Alberta," paper 82-83-68 presented at the Annual Technical Meeting of the Petroleum Soc. of CIM, Calgary, Alberta (June 6-9, 1982)

13. McDonald, R. R.: " Drilling the Cold Lake Horizontal Well Pilot No. 2," *SPE Drilling Eng.* (Sept. 1987) 193-197.

14. Dietrich, J. K.: " The Kern River Horizontal Well Pilot," *SPE Reservoir Eng.* (Aug. 1988) 935-944.

15. Joshi, S. D.: " A laboratory Study of Thermal Oil Recovery Using Horizontal Wells," paper SPE 14916 presented at the SPE/DOE Fifth Symposium on Enhanced Oil Recovery, Tulsa, OK (April 20-23, 1986)

16. Butler, R. M. and Stephens, D. J.: " The Gravity Drainage of Steam Heated Heavy Oils to Parallel Horizontal Wells," *J. Can. Pet. Tech.* (April-June 1981) **20**, 90-96.

17. Butler, R. M., McNab, G. S., and Lo, H. Y.: " Theoretical Studies of the Gravity Drainage of Heavy Oils During In-Situ Steam Heating," *Cdn. J. Chem. Eng.* (Aug. 1981) **59**, 455-460.

18. Jain, S. and Khosla, A.: " Predicting Steam Recovery of Athabasca Oil Through Horizontal Wells," paper 85-36-28 presented at the 36th Annual Technical Meeting of the Petroleum Soc. of CIM, Edmonton, Alberta (June 2-5, 1985)

19. Rial, M.: " 3D Thermal Simulation Using a Horizontal Well for Steam-Flooding," paper SPE 13076 presented at the 59th Annual Technical Conference and Exhibition, Houston, TX (Sept. 16-19, 1984)

20. Ambastha, A. K. and Ramey, H. J., Jr.: " Thermal Recovery Well Test Design and Interpretation," *SPE Form. Eval.* (June 1989) 173-180.

21. van Poollen, H. K.: "Transient Tests Find Fire Front in a Combustion Project," *Oil and Gas J.* (Feb. 1965) 78-80.

22. Kazemi, H.: "Locating a Burning Front by Pressure Transient Measurements," *J. Pet. Tech.* (Feb. 1966) 227-32.

23. Bixel, H. C. and van Poollen, H. K.: " Pressure Drawdown and Buildup in the Presence of Radial Discontinuities," *SPE J.* (Sept 1967) 301-309.

24. Merrill, L. S., Hossein, K., and Gogarty, B. G.: " Pressure Falloff Analysis in Reservoirs With Fluid Banks," *J. Pet. Tech.* (July 1974) 809-818.

25. Barua, J. and Horne, R. N.: " Computerized Analysis of Thermal Recovery Well Test Data," *SPE Form. Eval.* (Dec. 1987) 560-566.

26. Eggenschwiler, M., Satman, A., and Ramey, H. J., Jr.: " Interpretation of Injection Well Pressure Transient Data in Thermal Oil Recovery," paper SPE 8908 presented at the SPE California Regional Meeting, Pasadena (April 9-11, 1980)

27. Walsh, J. W., Jr., Ramey, H. J., Jr., and Brigham, W. E., " Thermal Injection Well Falloff Testing," paper SPE 10227 presented at the SPE 56th Annual Meeting, San Antonio, TX (Oct. 5-7, 1981).

28. Messner, G. L. and Williams, R. L.: " Application of Pressure Transient Analysis in

Steam Injection Wells," paper SPE 10781 presented at the California Regional Meeting, San Francisco , CA (March 24-26, 1982)

29. Onyekonwu, M. O., Ramey, H. J. Jr., Brigham, W. E., and Jenkins, R.: "Interpretation of Simulated Falloff Tests," paper SPE 12746 presented at the California Reg. Mtg. of SPE of AIME, Long Beach, CA (April 11-13, 1984)

30. Da Prat, G., Bockh, A., and Prado, L.: " Use of Pressure Falloff Testing to Locate the Burning Front in the Miga Field, Eastern Venezuela," paper SPE 13667 presented at the California Regional Meeting, Bakersfield, CA (March 27-29, 1985)

31. Stanislav, J. F., Easwaran, C. V., and Kokal, S. L.: " Interpretation of Thermal Well Testing," *SPE Form. Eval.* (June 1989) 181-186.

32. Fassihi, M. R.: "Evaluation of an Analytic Technique for Estimating Swept Volume From Thermal Pressure Falloff Tests in Heterogeneous Systems,"*SPE Form. Eval.* (June 1988) 449-58.

33. Ambastha, A. K. and Kumar, M.: " Pressure Falloff Analysis for Steam Injection Wells in a Low-Permeability Reservoir With Steam-Induced Vertical Fractures," paper SPE 19788 presented at the 64th Annual Technical Conference and Exhibition, San Antonio, TX (Oct. 8-11, 1989)

34. Ambastha, A. K. and Ramey, H. J., Jr., " Injection -Time Effects on Falloff Responses from Composite Reservoirs," *SPE Form. Eval.* (Dec. 1990) 385-388.

35. Anon.: "In-Situ Combustion and Steam Reservoir Simulator (version 4.0)-ISCOM ," Computer Modelling Group, Calgary, Alberta (July 27, 1987)

36. Babu, D.K. and Odeh, A. S.:" Productivity of a Horizontal Well: Appendices A & B," paper SPE 18334 available at SPE, Richardson, TX (1988)

37. Miller, C. C., Dyes, A. B., and Hutchinson, C. A., Jr.: " The Estimation of Permeability and Reservoir Pressure From Bottom-Hole Pressure Buildup Characteristics, *Trans.*, AIME (1950) **189**, 91-104

38. Horner, D. R.: " Pressure Buildup in Wells," *Proc.*, Third World Pet. Cong., The Hague (1951) Sec. II, 503-523.

39. Aziz, K. and Ramesh, B.: " Fourth SPE Comparative Solution Project: A Comparison of Steam Injection Simulators," paper SPE 13510 presented at the SPE Reservoir Simulation Symposium, Dallas, TX (Feb. 10-13, 1985)

40. Bourdet, D., Ayoub, J. A., and Pirard, Y. M. : " Use of Pressure Derivative in Well-Test Interpretation," *SPE Form. Eval.* (June 1989) 293-302.

41. Tortike, W. S. and Farouq Ali, S. M.: " Saturated-Steam-Property Functional Correlations for Fully Implicit Thermal Reservoir Simulation," *SPE Res. Eng* (Nov. 1989) 471-74.

APPENDIX A

Program # 1: Pressure transient response for a horizontal well in a closed reservoir.

Program # 2: Buildup pressure derivative response for a horizontal well in a closed reservoir

```
C   PROGRAM # 1
C
C   The purpose of this program is to generate the pressure transient response
C   for a horizontal well in a closed, box-shaped reservoir.
C
C   Wellbore storage and skin are ignored.  Well produces at a constant rate.
C
C   Both drawdown pressure and pressure derivative responses are generated.

C   ***************************************************************
C   VARIABLE IDENTIFICATION LIST
C   ****************************

C   AD --- DIMENSIONLESS RESERVOIR LENGTH
C   BD --- DIMENSIONLESS RESEVOIR WIDTH
C   HD --- DIMENSIONLESS RESERVOIR HEIGHT
C  RWD--- DIMENSIONLESS WELLBORE RADIUS
C  XOD --- X-DIRECTION WELL LOCATION, DIMENSIONLESS
C  YED --- DIMENSIONLESS WELL LENGTH
C  Y1D --- STARTING POINT OF WELL IN THE Y-DIRECTION
C  Y2D --- END-POINT OF WELL IN THE Y-DIRECTION
C  ZOD --- Z-DIRECTION WELL LOCATION, DIMENSIONLESS

C  ***********************************************************
      IMPLICIT REAL*8 (A-H,O-Z)
      DIMENSION SPD(3000)

C  INPUT DATA

      DATA Q,VIS,BO,CT/800.0D+00,1.0D+00,1.25D+00,15D-06/
      DATA PMX,PMY,PMZ/400.0D+00,400.0D+00,16.0D+00/
      DATA XO,ZO,YE,PHI/1000.0D+00,100.0D+00,1000.0D+00,2D-01/
      DATA A,B,H,Y1/4000.0D+00,1000.0D+00,200.0D+00,0.0D+00/
      DATA RW,BET/2.50D-01,7.08D-03/
      PI=2.0D+00*DASIN(1.0D+00)
      RWD=RW/YE
      TOL=1.0D-15

C  CALCULATION OF DIMENSIONLESS VARIABLES

      ALP=3.79085D+03*PHI*VIS*CT
      TET=DATAN((PMZ/PMX)**2.5D-01)
      X=XO+RW*DCOS(TET)
      Y2=Y1+YE
      YO=Y1
      Y=(Y1+Y2)/2
      Z=ZO+RW*DSIN(TET)
```

```
      XD=X/YE
      XOD=XO/YE
      AD=A/YE
      G1=DSQRT(PMX/PMY)/YE
      YD=Y*G1
      YOD=YO*G1
      Y1D=Y1*G1
      Y2D=Y2*G1
      BD=B*G1
      G2=DSQRT(PMX/PMZ)/YE
      ZD=Z*G2
      ZOD=ZO*G2
      HD=H*G2
C
C     INPUT ECHO
C
      WRITE(6,11)
 11   FORMAT(' ',T20,'INPUT  DATA')
      WRITE(6,13)
 13   FORMAT(' ',T20,'==========')
      WRITE(6,15) AD,PMX
 15   FORMAT(' ',T5,'AD =',F5.2,T30,'Kx =',F6.1,1X,'md')
      WRITE(6,17) BD,PMY
 17   FORMAT(' ',T5,'BD =',F5.2,T30,'Ky =',F6.1,1X,'md')
      WRITE(6,19) HD,PMZ
 19   FORMAT(' ',T5,'HD =',F6.4,T30,'Kz =',F6.1,1X,'md')
      WLENT=YE/B
      WRITE(6,41) RWD,WLENT
 41   FORMAT(T5,'RWD =',E7.2,T30,'L/B = ',F6.3)
      WRITE(6,21)
 21   FORMAT(' ',T20,'RESULTS')
      WRITE(6,23)
 23   FORMAT(' ',T20,'=======')
      WRITE(6,25)
 25   FORMAT(' ',T5,'TD',T18,'PDP',T29,'PDP*TD',T44,'PD',T58,'T',T7
     + 0,'DP')
      WRITE(6,27)
 27   FORMAT(' ',T3,'====',T16,'======',T27,'========',T43,'====',T
     + 57,'===',T68,'======')
C
C     EVALUATION OF THE APPROPRIATE GREEN'S FUNCTIONS
C
      J=-4
      JEND=2
      ICOUNT=0
      TD=0.0D+00
      PDP1=0.0D+00
      PDP2=0.0D+00
      SUMP=0.0D+00
 9    TD=TD+10.0D+00**(J)
      ICOUNT=ICOUNT+1
      K=1000
      DYD=(Y2D-Y1D)/K
        SUM1=0
```

```
      SADD=0
      ADS1=0
      ADS2=0
      ADS3=0
      N=1
 1      TET1=N*PI*XD/AD
        TET2=N*PI*XOD/AD
        ARG=-(TD*AD*BD*(N*PI/AD)**2)
        SADD=DCOS(TET1)*DCOS(TET2)*DEXP(ARG)
        SUM1= SUM1+SADD
        ADS1=ADS2
        ADS2=ADS3
        ADS3=SADD
        IF(SUM1.EQ.0) THEN
        RATIO=1.0D+00
        ELSE
        RATIO=DABS((ADS1+ADS2+ADS3)/SUM1)
        ENDIF
        IF (RATIO.LT.TOL) GO TO 2
        IF(SUM1.EQ.0.AND.N.EQ.200) GO TO 2
        N=N+1
        GO TO 1
 2     S1D=1+2*SUM1
      DO 50 I=1,K+1
      SUM2=0
      SADD=0
      ADS1=0
      ADS2=0
      ADS3=0
      M=1
 3      TET1=M*PI*YD/BD
        TET2=M*PI*YOD/BD
        ARG=-(TD*AD*BD*(M*PI/BD)**2)
        SADD=DCOS(TET1)*DCOS(TET2)*DEXP(ARG)
        SUM2=SUM2+SADD
        ADS1=ADS2
        ADS2=ADS3
        ADS3=SADD
        IF(SUM2.EQ.0)THEN
        RATIO=1.0D+00
        ELSE
        RATIO=DABS((ADS1+ADS2+ADS3)/SUM2)
        ENDIF
        IF(RATIO.LT.TOL)GO TO 4
        IF(SUM2.EQ.0.AND.M.EQ.200) GO TO 4
        M=M+1
        GO TO 3
 4     S2D=1+2*SUM2
      SPD(I)=S2D
      YOD=Y1D+DYD*I
 50    CONTINUE
      CALL SIMPS(AREA,SPD,DYD,K)
      SUM3=0
      SADD=0
```

```
      ADS1=0
      ADS2=0
      ADS3=0
      L=1
 5      TET1=L*PI*ZD/HD
        TET2=L*PI*ZOD/HD
        ARG=-(TD*AD*BD*(L*PI/HD)**2)
        SADD=DCOS(TET1)*DCOS(TET2)*DEXP(ARG)
        SUM3=SUM3+SADD
        ADS1=ADS2
        ADS2=ADS3
        ADS3=SADD
        IF(SUM3.EQ.0)THEN
        RATIO=1.0D+00
        ELSE
        RATIO=DABS((ADS1+ADS2+ADS3)/SUM3)
        ENDIF
        IF(RATIO.LT.TOL)GO TO 6
        IF(SUM3.EQ.0.AND.L.EQ.200) GO TO 6
        L=L+1
        GO TO 5
 6      S3D=1+2*SUM3
C
C   EVALUATION OF CARTESIAN AND SEMI-LOG SLOPES
C
    PDP=2*PI*AREA*S1D*S3D
    PDPTD=PDP*TD
C
C   EVALUATION OF DIMENSIONLESS PRESSURE AND PRESSURE DROP
C
    PDP1=PDP2
    PDP2=PDP
    SUMP=SUMP+(PDP1+PDP2)*(10.0D+00**(J))/2
    PD=SUMP
    T=TD*ALP*AD*BD*YE**2/PMX
    DP=Q*VIS*BO*PD/(BET*H*PMX)
C
C   REPORT THE RESULTS
C
 WRITE(6,29) TD,PDP,PDPTD,PD,T,DP
 29   FORMAT(' ',T1,E10.4,T14,E10.4,T27,E10.4,T40,E10.4,T53,E10.4,T
   + 66,E10.4)
    IF(ICOUNT.EQ.10)THEN
      J=J+1
      ICOUNT=1
    ENDIF
    IF(J.EQ.JEND) GO TO 12
    GO TO 9
12   STOP
    END
C
C   SUBROUTINE FOR SIMPSON'S RULE INTEGRATION
C
    SUBROUTINE SIMPS(AREA,SPD,DYD,K)
```

```
      IMPLICIT REAL*8 (A-H,O-Z)
      DIMENSION SPD(3000)
      SUME=0
      SUMO=0
      DO 52 I=2,K,2
         SUME=SUME+SPD(I)
52    CONTINUE
      DO 54 I=3,K-1,2
        SUMO=SUMO+SPD(I)
54    CONTINUE
      AREA=DYD*(SPD(1)+4*SUME+2*SUMO+SPD(K+1))/3
      RETURN
      END
```

```
C     ****************************************************************
C   PROGRAM # 2
C
C   The purpose of this program is to generate the pressure buildup response
C   for a horizontal well in a closed, box-shaped reservoir.
C
C   Wellbore storage and skin are ignored.  Well produces at a constant rate
    prior to shut-in.
C
C   The dimensionless Cartesian, MDH and Agarwal  slopes are generated.

C   ****************************************************************
C   VARIABLE IDENTIFICATION LIST
C   ****************************

C      AD --- DIMENSIONLESS RESERVOIR LENGTH
C      BD --- DIMENSIONLESS RESEVOIR WIDTH
C      HD --- DIMENSIONLESS RESERVOIR HEIGHT
C    RWD  --- DIMENSIONLESS WELLBORE RADIUS
C   SCART --- CARTESIAN SLOPE
C   SMDH --- MDH SLOPE
C  SAGAR --- AGARWAL SLOPE
C     XOD --- X-DIRECTION WELL LOCATION, DIMENSIONLESS
C      YED --- DIMENSIONLESS WELL LENGTH
C      Y1D --- STARTING POINT OF WELL IN THE Y-DIRECTION
C      Y2D --- END-POINT OF WELL IN THE Y-DIRECTION
C      ZOD --- Z-DIRECTION WELL LOCATION, DIMENSIONLESS

C  *******************************************************

C


      IMPLICIT REAL*8 (A-H,O-Z)
      DIMENSION SPD(3000)

C  INPUT DATA

      DATA Q,VIS,BO,CT/800.0D+00,1.0D+00,1.25D+00,15D-06/
      DATA PMX,PMY,PMZ/400.0D+00,400.0D+00,16.0D+00/
      DATA XO,ZO,YE,PHI/1000.0D+00,100.0D+00,1000.0D+00,2D-01/
      DATA A,B,H,Y1/4000.0D+00,1000.0D+00,200.0D+00,0.0D+00/
      DATA RW,BET,TPD/2.50D-01,1.127D-03,1.00D+01/
      PI=2.0D+00*DASIN(1.0D+00)
      RWD=RW/YE
      TOL=1.0D-15
```

```
C  CALCULATION OF DIMENSIONLESS VARIABLES

      ALP=3.79085D+03*PHI*VIS*CT
      TET=DATAN((PMZ/PMX)**2.5D-01)
      X=XO+RW*DCOS(TET)
      Y2=Y1+YE
      YO=Y1
      Y=(Y1+Y2)/2
      Z=ZO+RW*DSIN(TET)
      XD=X/YE
      XOD=XO/YE
      AD=A/YE
      G1=DSQRT(PMX/PMY)/YE
      YD=Y*G1
      YOD=YO*G1
      Y1D=Y1*G1
      Y2D=Y2*G1
      BD=B*G1
      G2=DSQRT(PMX/PMZ)/YE
      ZD=Z*G2
      ZOD=ZO*G2
      HD=H*G2
C
C     INPUT ECHO
C
      WRITE(6,11)
 11   FORMAT(' ',T20,'INPUT  DATA')
      WRITE(6,13)
 13   FORMAT(' ',T20,'===========')
      WRITE(6,15) AD,PMX
 15   FORMAT(' ',T5,'AD =',F5.2,T30,'Kx =',F6.1,1X,'md')
      WRITE(6,17) BD,PMY
 17   FORMAT(' ',T5,'BD =',F5.2,T30,'Ky =',F6.1,1X,'md')
      WRITE(6,19) HD,PMZ
 19   FORMAT(' ',T5,'HD =',F6.4,T30,'Kz =',F6.1,1X,'md')
      WLENT=YE/B
      WRITE(6,41) RWD,WLENT
 41   FORMAT(T5,'RWD =',E7.2,T30,'L/B = ',F6.3)
      WRITE(6,43) TPD
 43   FORMAT(T20,'TPD = ',F12.2)
      WRITE(6,21)
 21   FORMAT(' ',T20,'RESULTS')
      WRITE(6,23)
 23   FORMAT(' ',T20,'=======')
      WRITE(6,25)
 25   FORMAT(' ',T9,'TD',T24,'SCART',T37,'SMDH',T52,'SAGAR')
      WRITE(6,27)
 27   FORMAT(' ',T7,'====',T22,'=====',T35,'=====',T50,'======')

C
      J=-4
      JEND=2
      ICOUNT=0
```

```
      TD=0.0D+00
      PDP1=0.0D+00
      PDP2=0.0D+00
      SUMP=0.0D+00
    9  TD=TD+10.0D+00**(J)
      ICOUNT=ICOUNT+1
      DO 20 IP=1,2
        IF(IP.EQ.2) THEN
         TDC=TD+TPD
        ELSE
         TDC=TD
        ENDIF
      K=1000
      DYD=(Y2D-Y1D)/K
        SUM1=0
        SADD=0
        ADS1=0
        ADS2=0
        ADS3=0
        N=1
    1     TET1=N*PI*XD/AD
          TET2=N*PI*XOD/AD
          ARG=-(TDC*AD*BD*(N*PI/AD)**2)
          SADD=DCOS(TET1)*DCOS(TET2)*DEXP(ARG)
          SUM1= SUM1+SADD
          ADS1=ADS2
          ADS2=ADS3
          ADS3=SADD
          IF(SUM1.EQ.0) THEN
          RATIO=1.0D+00
          ELSE
          RATIO=DABS((ADS1+ADS2+ADS3)/SUM1)
          ENDIF
          IF (RATIO.LT.TOL) GO TO 2
          IF(SUM1.EQ.0.AND.N.EQ.200) GO TO 2
          N=N+1
          GO TO 1
    2     S1D=1+2*SUM1
        DO 50 I=1,K+1
        SUM2=0
        SADD=0
        ADS1=0
        ADS2=0
        ADS3=0
        M=1
    3     TET1=M*PI*YD/BD
          TET2=M*PI*YOD/BD
          ARG=-(TDC*AD*BD*(M*PI/BD)**2)
          SADD=DCOS(TET1)*DCOS(TET2)*DEXP(ARG)
          SUM2=SUM2+SADD
          ADS1=ADS2
          ADS2=ADS3
          ADS3=SADD
          IF(SUM2.EQ.0)THEN
```

```
      RATIO=1.0D+00
      ELSE
      RATIO=DABS((ADS1+ADS2+ADS3)/SUM2)
      ENDIF
      IF(RATIO.LT.TOL)GO TO 4
       IF(SUM2.EQ.0.AND.M.EQ.200) GO TO 4
      M=M+1
      GO TO 3
4     S2D=1+2*SUM2
     SPD(I)=S2D
     YOD=Y1D+DYD*I
50    CONTINUE
     CALL SIMPS(AREA,SPD,DYD,K)
     SUM3=0
     SADD=0
     ADS1=0
     ADS2=0
     ADS3=0
     L=1
5       TET1=L*PI*ZD/HD
       TET2=L*PI*ZOD/HD
       ARG=-(TDC*AD*BD*(L*PI/HD)**2)
       SADD=DCOS(TET1)*DCOS(TET2)*DEXP(ARG)
       SUM3=SUM3+SADD
       ADS1=ADS2
       ADS2=ADS3
       ADS3=SADD
        IF(SUM3.EQ.0)THEN
       RATIO=1.0D+00
       ELSE
       RATIO=DABS((ADS1+ADS2+ADS3)/SUM3)
       ENDIF
       IF(RATIO.LT.TOL)GO TO 6
        IF(SUM3.EQ.0.AND.L.EQ.200) GO TO 6
       L=L+1
       GO TO 5
6       S3D=1+2*SUM3
      IF(IP.EQ.2) THEN
       PDPP=2*PI*AREA*S1D*S3D
       SCART=PDP-PDPP
       SMDH=SCART*TD
       SAGAR=SMDH*(TPD+TD)/TPD
       WRITE(6,29) TD,SCART,SMDH,SAGAR
29    FORMAT(' ',T5,E10.4,T20,E10.4,T35,E10.4,T50,E10.4)
      ELSE
       PDP=2*PI*AREA*S1D*S3D
      ENDIF
20   CONTINUE
    IF(ICOUNT.EQ.10)THEN
     J=J+1
     ICOUNT=1
    ENDIF
    IF(J.EQ.JEND) GO TO 12
    GO TO 9
```

```
 12   STOP
      END
C
      SUBROUTINE SIMPS(AREA,SPD,DYD,K)
      IMPLICIT REAL*8 (A-H,O-Z)
      DIMENSION SPD(3000)
      SUME=0
      SUMO=0
      DO 52 I=2,K,2
         SUME=SUME+SPD(I)
 52   CONTINUE
      DO 54 I=3,K-1,2
        SUMO=SUMO+SPD(I)
 54   CONTINUE
      AREA=DYD*(SPD(1)+4*SUME+2*SUMO+SPD(K+1))/3
      RETURN
      END
```

APPENDIX B

Transient Pressure Response for a Horizontal Well

(Input Data from Example 1 of Ref.6)

Input Data

AD = 4.00	Kx = 200.0 md
BD = 2.00	Ky = 200.0 md
HD =2.0000	Kz = 2.0 md
RWD =.25E-03	L/B = 0.500

Results

t_D	dp_{wD}/dt_D	$dp_{wD}/dlnt_D$	p_{wD}	t	Δp
				hrs.	psi
0.1000E-06	0.1016E+08	0.1016E+01	0.5080E+00	0.4549E-04	0.1794E+01
0.2000E-06	0.5379E+07	0.1076E+01	0.1285E+01	0.9098E-04	0.4537E+01
0.3000E-06	0.3566E+07	0.1070E+01	0.1732E+01	0.1365E-03	0.6116E+01
0.4000E-06	0.2650E+07	0.1060E+01	0.2043E+01	0.1820E-03	0.7214E+01
0.5000E-06	0.2102E+07	0.1051E+01	0.2280E+01	0.2275E-03	0.8052E+01
0.6000E-06	0.1796E+07	0.1077E+01	0.2475E+01	0.2729E-03	0.8740E+01
0.7000E-06	0.1525E+07	0.1068E+01	0.2641E+01	0.3184E-03	0.9327E+01
0.8000E-06	0.1325E+07	0.1060E+01	0.2784E+01	0.3639E-03	0.9830E+01
0.9000E-06	0.1172E+07	0.1055E+01	0.2909E+01	0.4094E-03	0.1027E+02
0.1000E-05	0.1069E+07	0.1069E+01	0.3021E+01	0.4549E-03	0.1067E+02
0.2000E-05	0.5270E+06	0.1054E+01	0.3819E+01	0.9098E-03	0.1348E+02
0.3000E-05	0.3522E+06	0.1057E+01	0.4259E+01	0.1365E-02	0.1504E+02
0.4000E-05	0.2623E+06	0.1049E+01	0.4566E+01	0.1820E-02	0.1612E+02
0.5000E-05	0.2091E+06	0.1045E+01	0.4802E+01	0.2275E-02	0.1695E+02
0.6000E-05	0.1734E+06	0.1040E+01	0.4993E+01	0.2729E-02	0.1763E+02
0.7000E-05	0.1481E+06	0.1036E+01	0.5153E+01	0.3184E-02	0.1820E+02
0.8000E-05	0.1291E+06	0.1033E+01	0.5292E+01	0.3639E-02	0.1869E+02
0.9000E-05	0.1144E+06	0.1030E+01	0.5414E+01	0.4094E-02	0.1912E+02
0.1000E-04	0.1027E+06	0.1027E+01	0.5522E+01	0.4549E-02	0.1950E+02
0.2000E-04	0.5082E+05	0.1016E+01	0.6290E+01	0.9098E-02	0.2221E+02
0.3000E-04	0.3370E+05	0.1011E+01	0.6713E+01	0.1365E-01	0.2370E+02
0.4000E-04	0.2524E+05	0.1010E+01	0.7007E+01	0.1820E-01	0.2474E+02
0.5000E-04	0.2021E+05	0.1011E+01	0.7235E+01	0.2275E-01	0.2555E+02
0.6000E-04	0.1684E+05	0.1011E+01	0.7420E+01	0.2729E-01	0.2620E+02

0.7000E-04	0.1442E+05	0.1010E+01	0.7576E+01	0.3184E-01	0.2675E+02
0.8000E-04	0.1261E+05	0.1009E+01	0.7711E+01	0.3639E-01	0.2723E+02
0.9000E-04	0.1120E+05	0.1008E+01	0.7830E+01	0.4094E-01	0.2765E+02
0.1000E-03	0.1008E+05	0.1008E+01	0.7937E+01	0.4549E-01	0.2803E+02
0.2000E-03	0.5022E+04	0.1004E+01	0.8692E+01	0.9098E-01	0.3069E+02
0.3000E-03	0.3348E+04	0.1005E+01	0.9110E+01	0.1365E+00	0.3217E+02
0.4000E-03	0.2507E+04	0.1003E+01	0.9403E+01	0.1820E+00	0.3320E+02
0.5000E-03	0.2004E+04	0.1002E+01	0.9629E+01	0.2275E+00	0.3400E+02
0.6000E-03	0.1669E+04	0.1002E+01	0.9812E+01	0.2729E+00	0.3465E+02
0.7000E-03	0.1430E+04	0.1001E+01	0.9967E+01	0.3184E+00	0.3519E+02
0.8000E-03	0.1251E+04	0.1001E+01	0.1010E+02	0.3639E+00	0.3567E+02
0.9000E-03	0.1112E+04	0.1001E+01	0.1022E+02	0.4094E+00	0.3609E+02
0.1000E-02	0.1001E+04	0.1001E+01	0.1033E+02	0.4549E+00	0.3646E+02
0.2000E-02	0.4976E+03	0.9951E+00	0.1107E+02	0.9098E+00	0.3910E+02
0.3000E-02	0.3259E+03	0.9777E+00	0.1149E+02	0.1365E+01	0.4056E+02
0.4000E-02	0.2380E+03	0.9520E+00	0.1177E+02	0.1820E+01	0.4155E+02
0.5000E-02	0.1846E+03	0.9229E+00	0.1198E+02	0.2275E+01	0.4230E+02
0.6000E-02	0.1489E+03	0.8934E+00	0.1215E+02	0.2729E+01	0.4289E+02
0.7000E-02	0.1235E+03	0.8648E+00	0.1228E+02	0.3184E+01	0.4337E+02
0.8000E-02	0.1047E+03	0.8378E+00	0.1240E+02	0.3639E+01	0.4377E+02
0.9000E-02	0.9027E+02	0.8124E+00	0.1249E+02	0.4094E+01	0.4412E+02
0.1000E-01	0.7889E+02	0.7889E+00	0.1258E+02	0.4549E+01	0.4441E+02
0.2000E-01	0.3168E+02	0.6337E+00	0.1313E+02	0.9098E+01	0.4637E+02
0.3000E-01	0.1923E+02	0.5769E+00	0.1339E+02	0.1365E+02	0.4727E+02
0.4000E-01	0.1433E+02	0.5734E+00	0.1355E+02	0.1820E+02	0.4786E+02
0.5000E-01	0.1193E+02	0.5965E+00	0.1368E+02	0.2275E+02	0.4832E+02
0.6000E-01	0.1053E+02	0.6320E+00	0.1380E+02	0.2729E+02	0.4872E+02
0.7000E-01	0.9613E+01	0.6729E+00	0.1390E+02	0.3184E+02	0.4907E+02
0.8000E-01	0.8949E+01	0.7159E+00	0.1399E+02	0.3639E+02	0.4940E+02
0.9000E-01	0.8443E+01	0.7598E+00	0.1408E+02	0.4094E+02	0.4971E+02
0.1000E+00	0.8043E+01	0.8043E+00	0.1416E+02	0.4549E+02	0.5000E+02

APPENDIX C

Development of Design Equations for Horizontal Well Testing

This appendix presents the development of time criteria for the occurrence of the transient flow regimes based on the dimensionless semi-log pressure derivative response. Also presented are design equations for buildup pressure derivative analysis of horizontal wells. Accuracy of the design equations is investigated.

1. Early Radial Flow Period

This period is characterized by a zero-slope (flat line) on a log-log graph of $dp_{wD}/dlnt_D$ vs. t_D. The end of the period is defined by the dimensionless time by which the semi-log pressure derivative is within 5% of the correct value. Data for the end of the early radial period are shown in Table C1. From Table C1, the end of the early radial flow period can be approximated by:

$$(t_{end})_D = \text{minm} \left[0.25\, d_{zD}^2 ,\ 0.033\, L_D^2 \right] \qquad \text{(C-1)}$$

Table C1: Data for estimating the time to the end of the early radial flow period

d_{zD}	L_D	t_D	t_D/d_{zD}^2	t_D/L_D^2
0.05	1	0.0006	0.24	0.0006
0.1	1	0.0025	0.25	0.0025
0.15	1	0.006	0.26	0.006
0.2	1	0.01	0.25	0.01
0.25	1	0.0165	0.26	0.0165
0.3	1	0.0237	0.26	0.0237
0.35	1	0.04	0.33	0.04
0.4	1	0.034	0.21	0.034
0.45	1	0.033	0.16	0.033
0.5	1	0.033	0.13	0.033
0.5	0.8	0.021	0.084	0.033
0.5	0.5	0.0081	0.032	0.032

2. Early Linear Flow Period

This period is characterized by a slope of 0.5 on a log-log graph of $dp_{wD}/dlnt_D$ vs. t_D. Data for the start and end of the early linear period are shown in Tables C2 and C3, respectively. For this period, the dimensionless time for which the slope of the log-log graph of $dp_{wD}/dlnt_D$ vs. t_D is within 5% of 0.5 are approximately:

$$(t_{start})_D = 0.6\, D_{zD}^2 \text{, and} \qquad \text{(C-2)}$$

$$(t_{end})_D = 0.02\, L_D^2 \qquad \text{(C-3)}$$

Table C2: Data for estimating the time to the start of the early linear flow period

h_D	D_{ZD}	t_D	t_D/D_{ZD}^2
0.1	0.05	0.00015	0.6
0.2	0.1	0.006	0.6
0.3	0.15	0.015	0.66

Table C3: Data for estimating the time to the end of the early linear flow period

a_D	b_D	h_D	L_D	t_D	t_D/L_D^2
4	4	0.1	1	0.02	0.02
4	4	0.2	1	0.02	0.02
4	4	0.3	1	0.02	0.02
6	4	0.2	1	0.02	0.02
4	5	0.2	1	0.02	0.02
8	8	0.2	2	0.08	0.02
14	16	0.2	4	0.3	0.019

3. Late Pseudo-Radial Flow Period

The dimensionless semi-log pressure derivative is equal to 0.5 during the late pseudo-radial flow. Tables C4 and C5 show data for estimating the start and end of the flow period, respectively. The dimensionless times by which the dimensionless semi-log pressure derivative is within 5% of 0.5 are:

$$(t_{start})_D = 0.4\ L_D^2 \text{ ,and} \qquad \text{(C-4)}$$

$$(t_{end})_D = \text{minm}\left[\ 0.333\ (d_{yD} + L_D/4)^2\ ,\ 0.27\ d_{xD}^2\ \right] \qquad \text{(C-5)}$$

Table C4: Data for estimating the time to the start of the late pseudo radial flow period

a_D	b_D	h_D	L_D	t_D	t_D/L_D^2
14	2	0.2	0.5	0.10	0.4
14	3	0.2	1	0.35	0.35
14	4	0.2	1	0.4	0.4
14	5	0.2	1	0.4	0.4
14	6	0.2	1	0.4	0.4
14	7	0.2	1	0.4	0.4
14	8	0.2	1	0.4	0.4
14	8	0.2	2	1.6	0.4

Table C5: Data for estimating the time to the end of the late pseudo radial flow period

d_{xD}	d_{yD}	L_D	$(d_{yD}+L_D/4)$	t_D	$t_D/(d_{yD}+L_D/4)^2$	t_D/dx_D^2
7	0.75	0.5	0.875	0.25	0.33	0.005
7	1.5	1	1.75	1.1	0.36	0.022
7	2	1	2.25	1.67	0.33	0.034
7	2.5	1	2.75	2.31	0.31	0.047
7	3	1	3.25	3.35	0.32	0.068
7	3.5	1	3.75	4.37	0.31	0.089
7	3	2	3.5	4.00	0.33	0.082
2	3.5	1	3.75	1.14	0.081	0.285
2.5	3.5	1	3.75	1.71	0.121	0.273
3	3.5	1	3.75	2.41	0.172	0.27
3.5	3.5	1	3.75	3.13	0.22	0.26
4	3.5	1	3.75	4.10	0.29	0.26

4. Late Linear Flow Period

The slope of the log-log graph of $dp_{wD}/dlnt_D$ vs. t_D during the late linear period is 0.5. From Tables C6 and C7, the dimensionless times by which the slope of the log-log graph of $dp_{wD}/dlnt_D$ vs. t_D is within 5% of 0.5 are approximately:

$$(t_{start})_D = \text{maxm}\left[\, 0.88\, D_{yD}^2 \,,\, 0.63\, D_{zD}^2 \,\right], \text{ and} \qquad \text{(C-6)}$$

$$(t_{end})_D = 0.162\, d_{xD}^2 \qquad \text{(C-7)}$$

Table C6: Data for estimating the time to the start of the late linear flow period

D_{yD}	D_{zD}	t_D	t_D/D_{yD}^2	t_D/D_{zD}^2
1.5	0.1	2	0.89	200
2	0.1	3.5	0.88	350
2.5	0.1	5	0.80	500
3	0.1	8	0.88	800
3.5	0.1	10	0.82	1000
1.5	2.5	4	1.77	0.64
1.5	3.0	5.5	2.44	0.61
1.5	3.5	7.5	5.0	0.61
1.5	4.0	9	6.0	0.64

Table C7: Data for estimating the time to the end of the late linear flow period

a_D	d_{xD}	t_D	t_D/d_{xD}^2
10	5	4	0.16
11	5.5	5	0.165
12	6	6	0.166
13	6.5	7	0.166
14	7	8	0.163
15	7.5	9	0.160
16	8	10	0.156

5. Design equations for buildup pressure derivative analysis

Table C8 presents $(\Delta t_{DA})_{dev}$ values by which the MDH slope has deviated by 5% from the drawdown slope. Dimensionless time to pseudosteady state $(t_{DA})_{pss}$ for the drawdown solution of the reservoir of Table C8 is 0.1.

Table C8: Comparison of deviation times predicted by Eq. (C-8) with the actual deviation times (MDH slope within 5% of drawdown slope)

t_{pDA}	$(\Delta t_{DA})_{dev}$ actual	$(\Delta t_{DA})_{dev}$ from Eq. (C-8)
0.001	0.00007	-0.001
0.01	0.00055	0.0006
0.1	0.0025	0.0024
1	0.004	0.0041

Based on the actual $(\Delta t_{DA})_{dev}$ values of Table C8, a design equation for the deviation time of the MDH slope from the drawdown slope is:

$$(\Delta t_{DA})_{dev} = 0.00407 + 0.00172 \log (t_{pDA}) , \quad \text{for} \quad 0.001 \le t_{pDA} \le 0.1 . \qquad \text{(C-8)}$$

The $(\Delta t_{DA})_{dev}$ values from Eq. (C-8) are presented in the third column of Table C8, for comparison with the actual $(\Delta t_{DA})_{dev}$ values in the second column. Eq. (C-8) applies for a horizontal well in a closed, box-shaped reservoir of dimensions $a_D = 1$, $b_D = 1$, and $h_D = 1$. The horizontal well is centrally-located and fully-penetrating.

Table C9 presents $(\Delta t_{DA})_{dev}$ values for a reservoir configuration whose $(t_{DA})_{pss}$ for the drawdown solution is 4.0. Reservoir dimensions are $a_D = 4$, $b_D = 1$, and $h_D = 1$. The horizontal well is off-centered and fully penetrating.

Table C9: Comparison of deviation times predicted by Eq. (C-9) with the actual deviation times (MDH slope within 5% of drawdown slope)

t_{pDA}	$(\Delta t_{DA})_{dev}$ actual	$(\Delta t_{DA})_{dev}$ from Eq. (C-9)
0.01	0.0005	0.0005
0.1	0.002	0.002
1	0.0035	0.0035
10	0.004	0.005

Based on the actual $(\Delta t_{DA})_{dev}$ values of Table C9, a design equation for the deviation time of the MDH slope from the drawdown slope as a function of t_{pDA} is:

$$(\Delta t_{DA})_{dev} = 0.0035 + 0.0015 \log (t_{pDA}) , \qquad \text{for } 0.01 \leq t_{pDA} \leq 4 . \qquad \text{(C-9)}$$

The second and third columns of Table C9 compare the actual $(\Delta t_{DA})_{dev}$ values with the $(\Delta t_{DA})_{dev}$ values from Eq. (C-9).

For selected values of t_{pDA} ,Table C10 presents $(\Delta t_{DA})_{dev}$ values for a reservoir whose $(t_{DA})_{pss}$ for the drawdown response is 0.6.

Table C10: Comparison of deviation times predicted by Eq. (C-10) with the actual deviation times. (MDH slope within 5% of drawdown slope)

t_{pDA}	$(\Delta t_{DA})_{dev}$ actual	$(\Delta t_{DA})_{dev}$ from Eq. (C-10)
0.001	0.00002	-0.0003
0.01	0.0005	0.0009
0.1	0.0025	0.0022
1	0.0035	0.0035

Based on the actual $(\Delta t_{DA})_{dev}$ values of Table C10, a design equation for the deviation time of the MDH slope from the drawdown slope as a function of t_{pDA} is:

$$(\Delta t_{DA})_{dev} = 0.00347 + 0.00127 \log (t_{pDA}), \quad \text{for} \quad 0.001 \leq t_{pDA} \leq 0.6 . \qquad \text{(C-10)}$$

The second and third columns of Table C10 compare the actual $(\Delta t_{DA})_{dev}$ values with the $(\Delta t_{DA})_{dev}$ values from Eq. (C-10). Eq. (C-10) applies for a horizontal well in a closed, box-shaped reservoir of dimensions $a_D = 10$, $b_D = 4$, and $h_D = 0.2$.

APPENDIX D

Further Analysis Equations for Thermal Horizontal Well Testing

A Cartesian graph of p_{ws} vs. Δt, during the wellbore storage-dominated period, results in a straight line of slope, m_{cw}, which can be used to calculate the dimensionless wellbore storage coefficient, C_D, as:

$$C_D = \frac{q_s B_g}{24(2\pi)(\phi c_t L r_{we}^2) m_{cw}} \quad , \tag{D-1}$$

where:

$$r_{we}^2 = \frac{(\Delta x \Delta z)_w}{\pi} \quad . \tag{D-2}$$

If the total simulated swept volume (V_s) is defined to include both the steam zone (V_{st}) and the hot water zone (V_{hw}), then the total system compressibility, c_t, is given by[29]:

$$c_t = \frac{V_{st}}{V_s} c_{ts} + \frac{V_{hw}}{V_s} c_{thw} \quad , \tag{D-3}$$

where:

c_{ts} = total compressibility in the steam zone $\approx c_{2\phi}$ as defined by Eq. (5.2),

$V_{hw} = V_s - V_{st}$, and (D-4)

$$c_{thw} = c_f + c_w S_w + c_o S_o \ . \qquad \text{(D-5)}$$

For early radial flow, the skin factor, s, is given by[6]:

$$s = 1.151 \left[\frac{(p_{ws} - p_{wfs})}{m_{s1}} - \log\left(\frac{k_{rg}\sqrt{k_x k_z}\Delta t}{\phi \mu c_t r_{we}^2} \right) + 3.23 \right] . \qquad \text{(D-6)}$$

APPENDIX E

Figures for Analysis of Horizontal Thermal Well Test Data

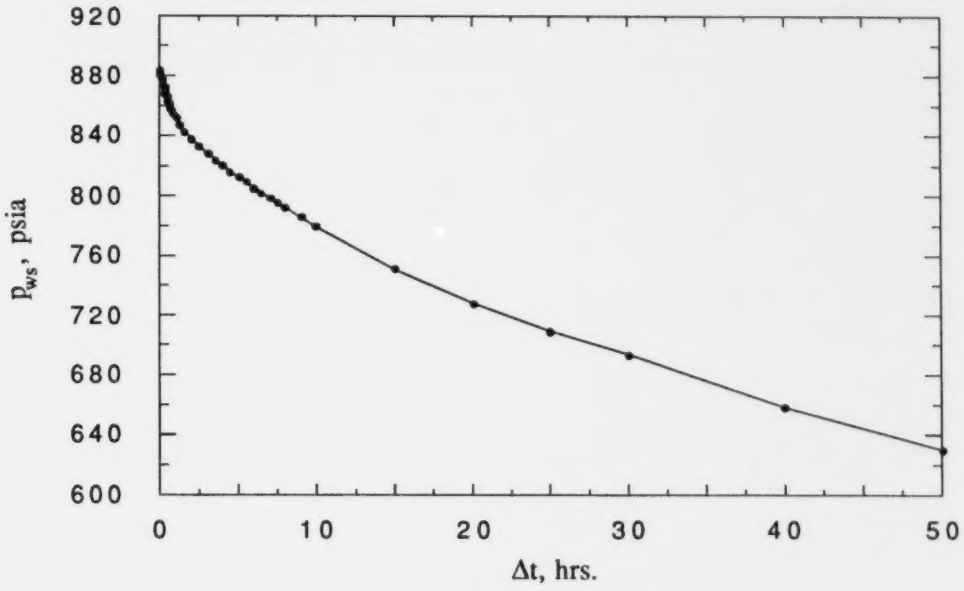

Fig. E1a - Falloff response from simulator for Run 1

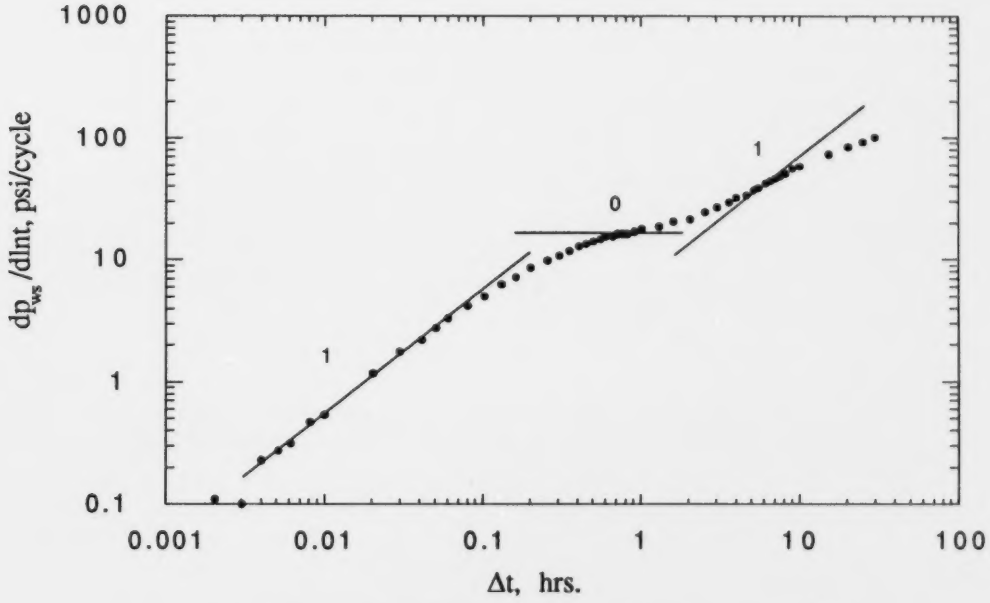

Fig. E1b - Semi-log pressure derivative response from falloff data for Run 1

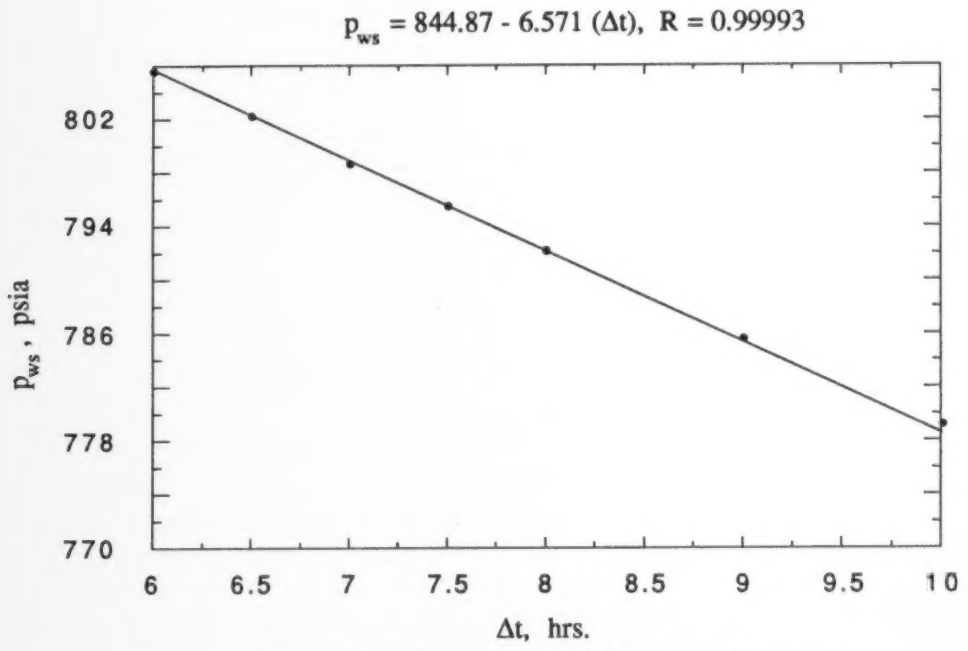

Fig. E1c - Cartesian graph of falloff data for Run 1

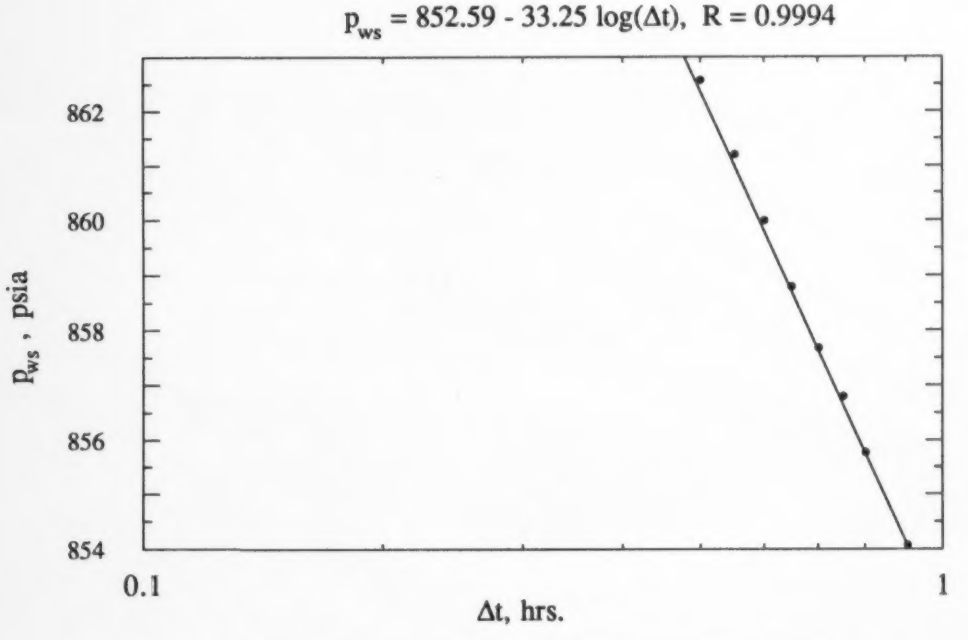

Fig. E1d - Semi-log graph of falloff data for Run 1

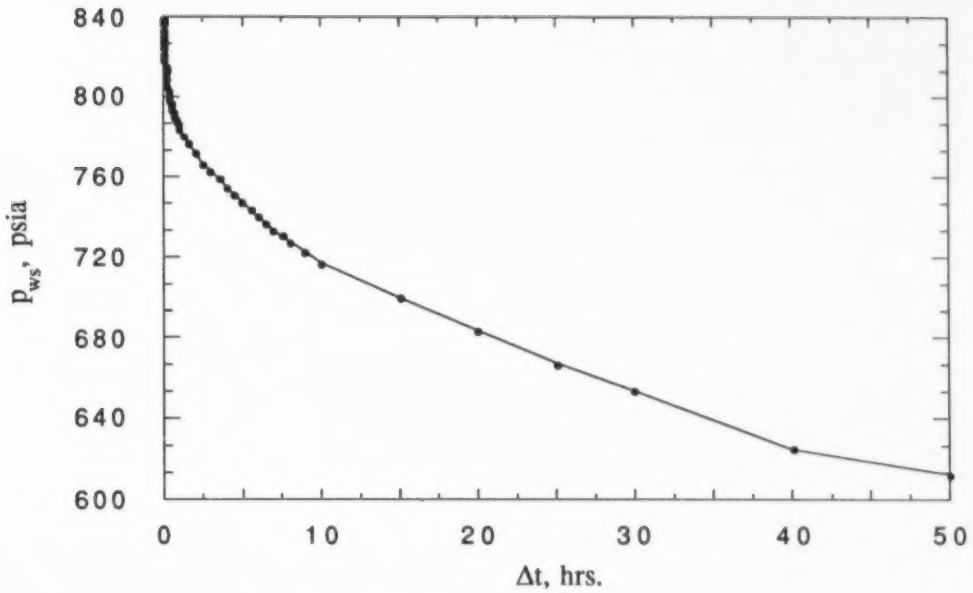

Fig. E2a - Falloff response from simulator for Run 2

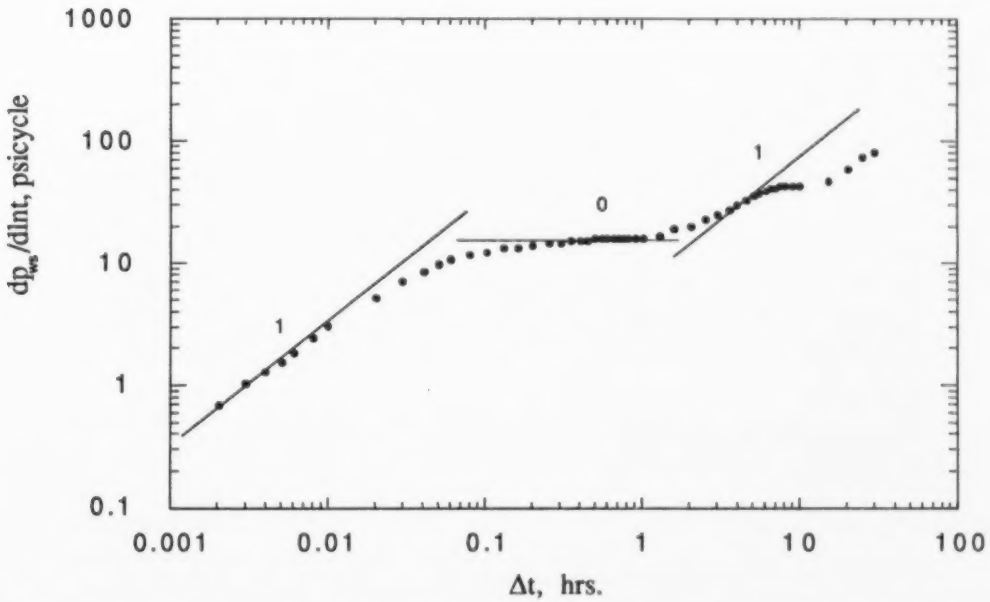

Fig. E2b - Semi-log pressure derivative response from falloff data for Run 2

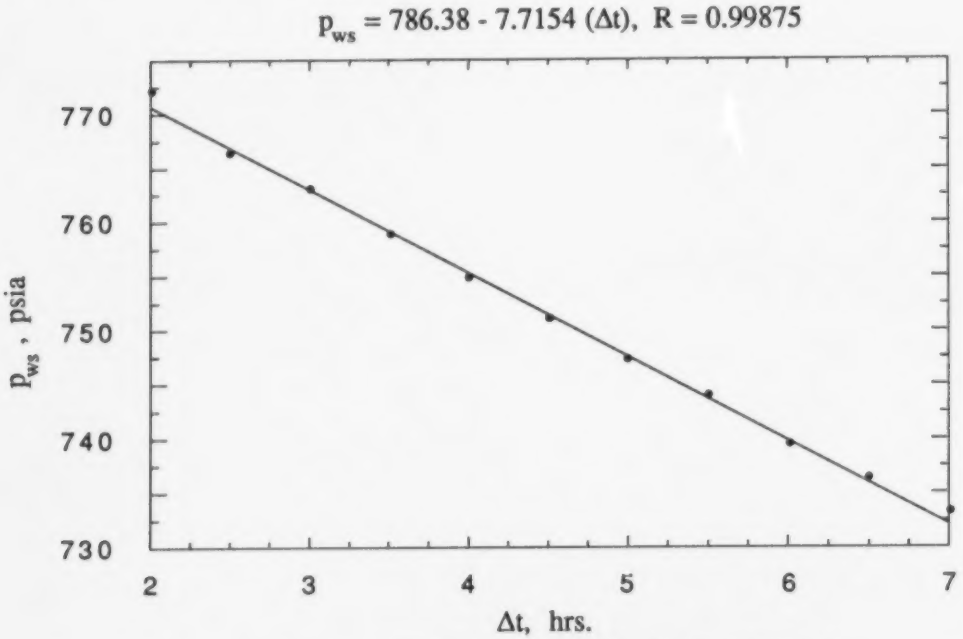

Fig. E2c - Cartesian graph of falloff data for Run 2

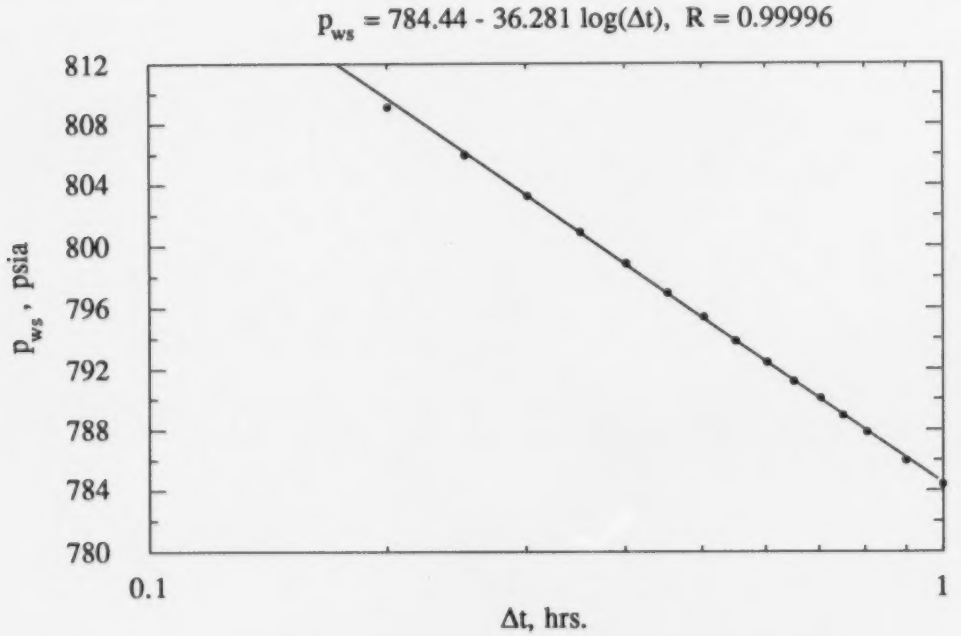

Fig. E2d - Semi-log graph of falloff data for Run 2

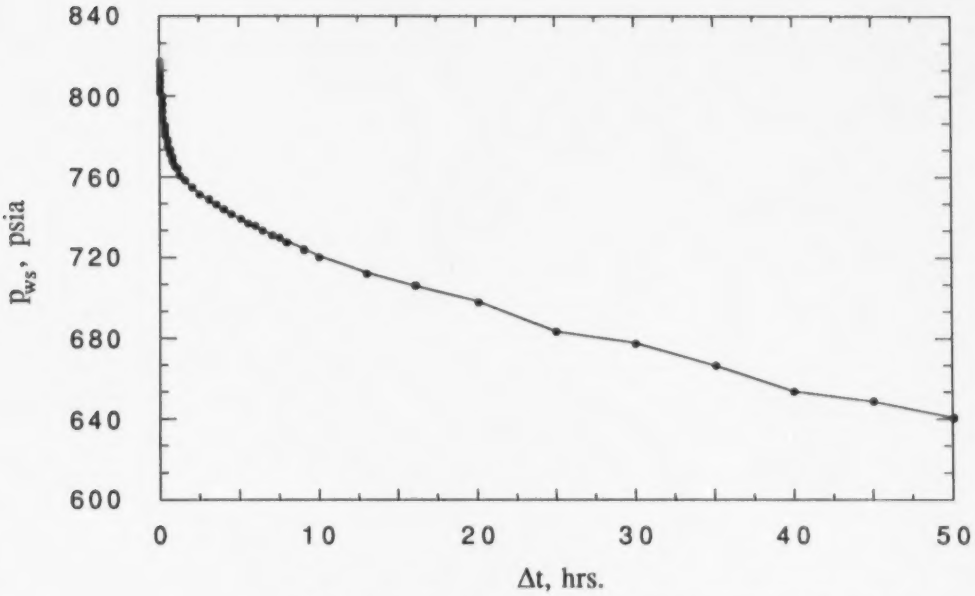

Fig. E3a - Falloff response from simulator for Run 3

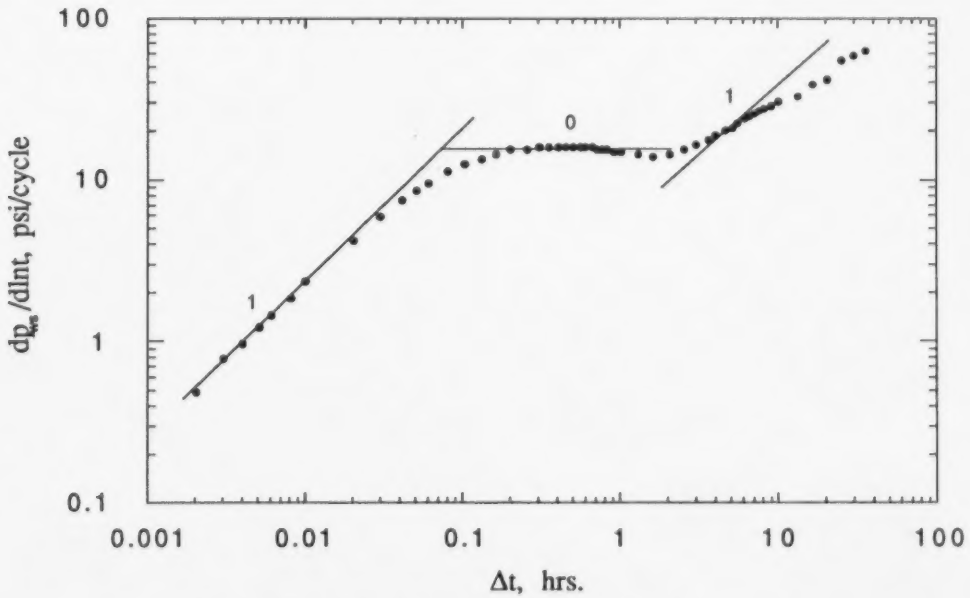

Fig. E3b - Semi-log pressure derivative response from falloff data for Run 3

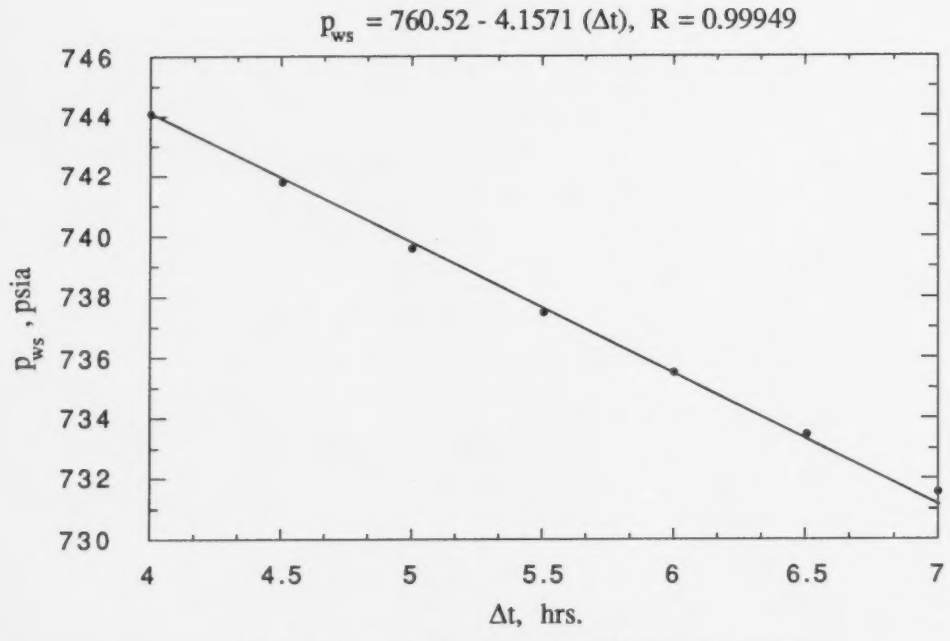

Fig. E3c - Cartesian graph of falloff data for Run 3

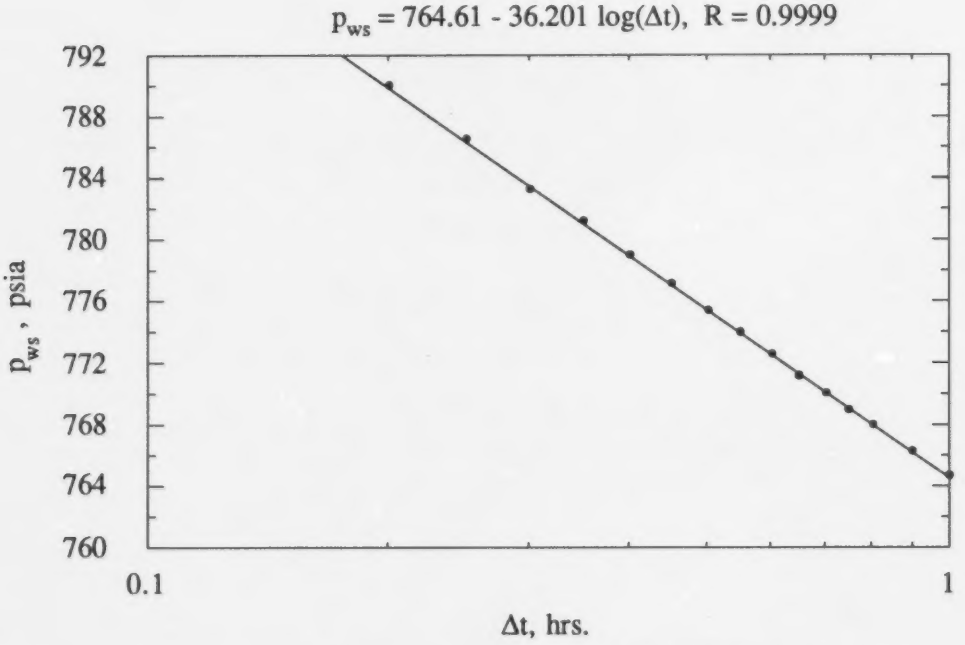

Fig. E3d - Semi-log graph of falloff data for Run 3

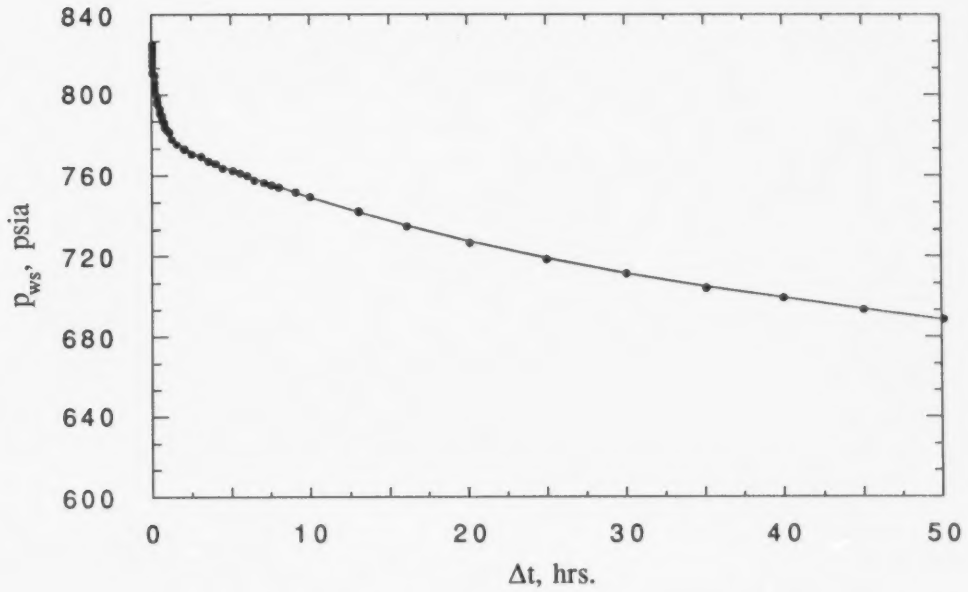

Fig. E4a - Falloff response from simulator for Run 4

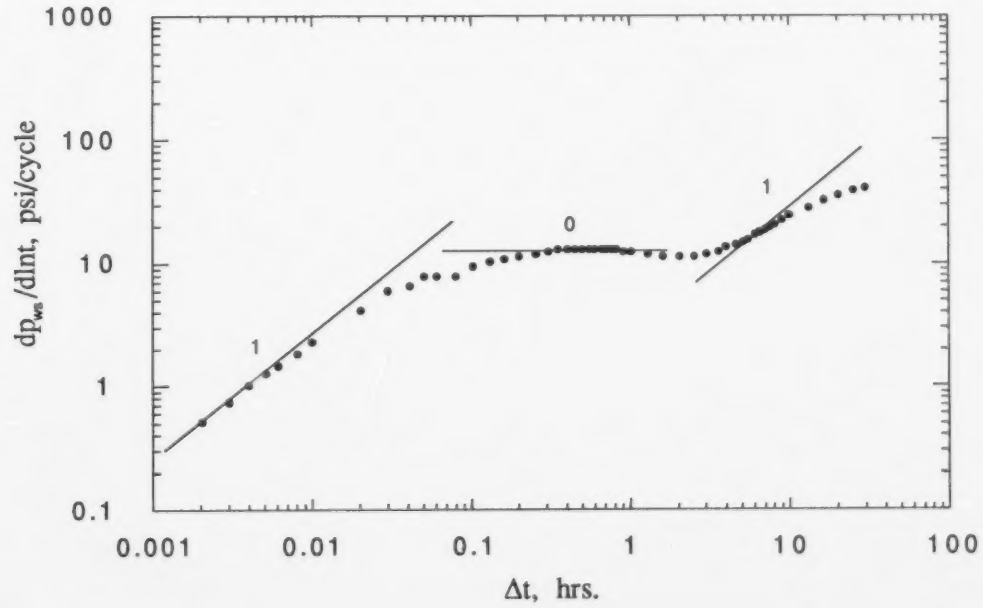

Fig. E4b - Semi-log pressure derivative response from falloff data for Run 4

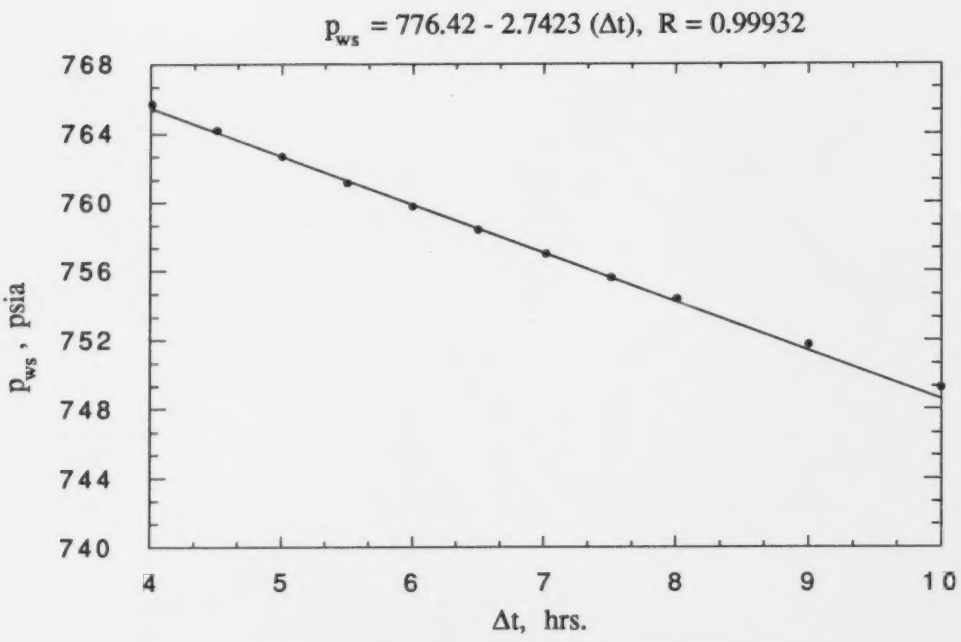

Fig. E4c - Cartesian graph of falloff data for Run 4

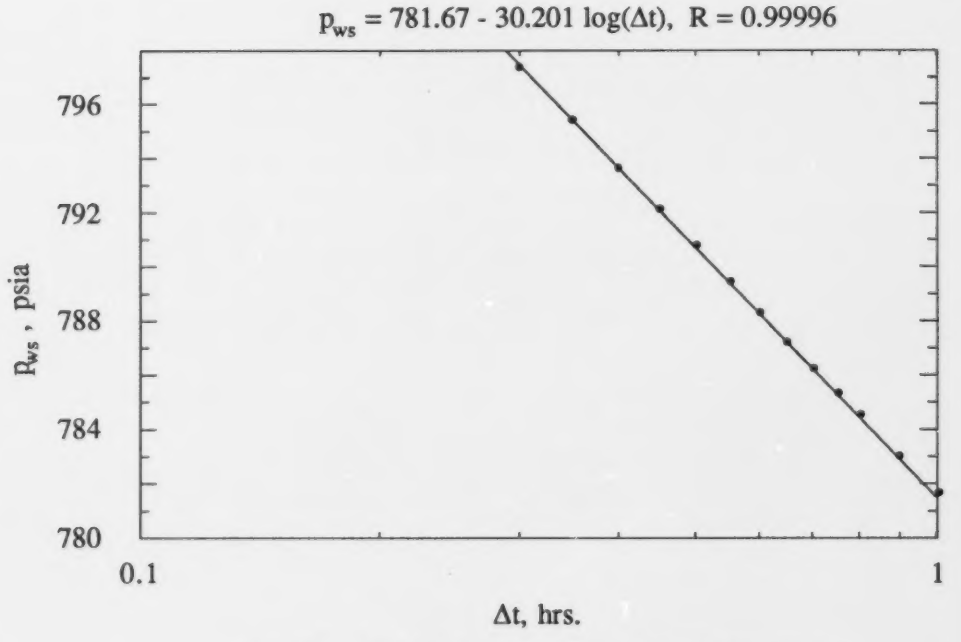

Fig. E4d - Semi-log graph of falloff data for Run 4

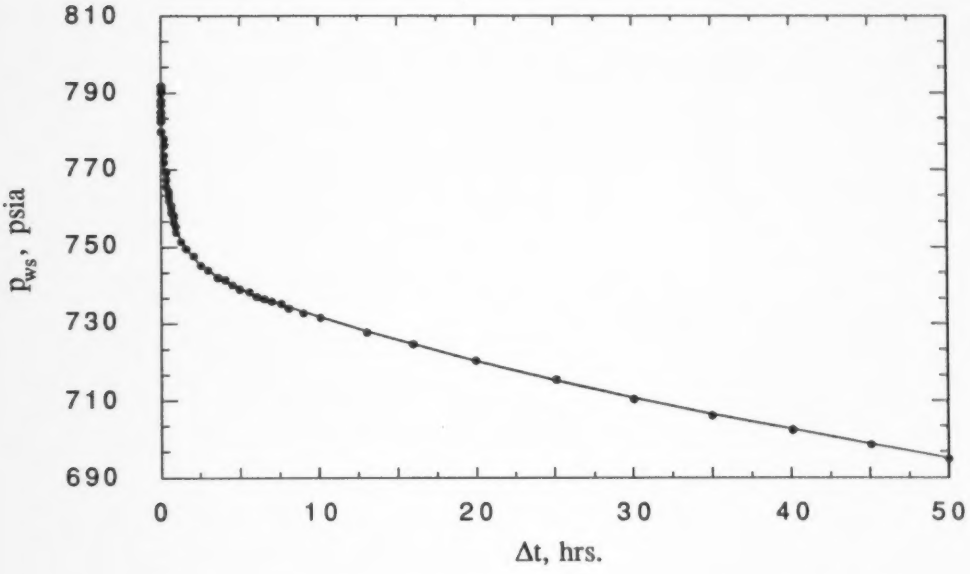

Fig. E5a - Falloff response from simulator for Run 5

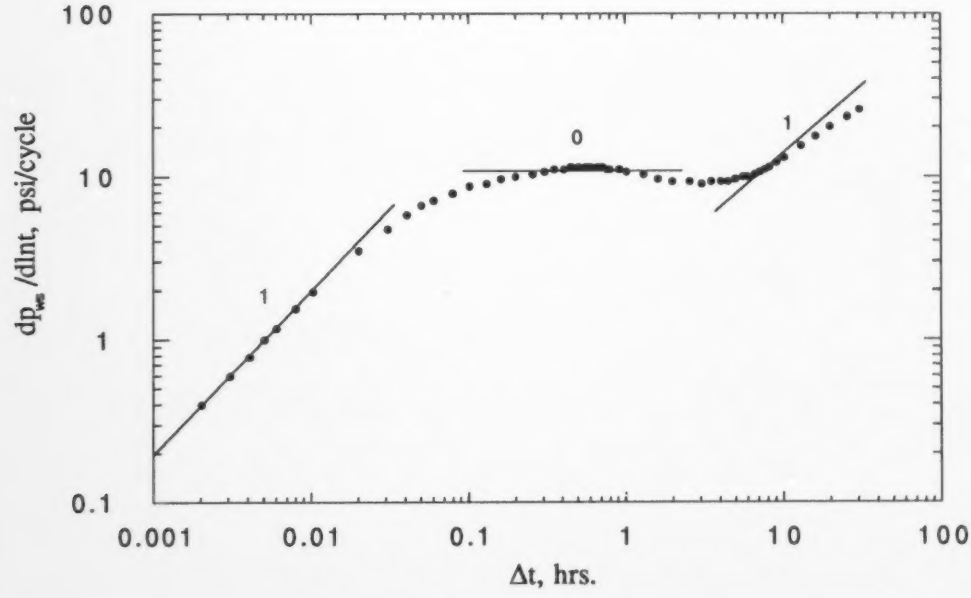

Fig. E5b - Semi-log pressure derivative response from falloff data for Run 5

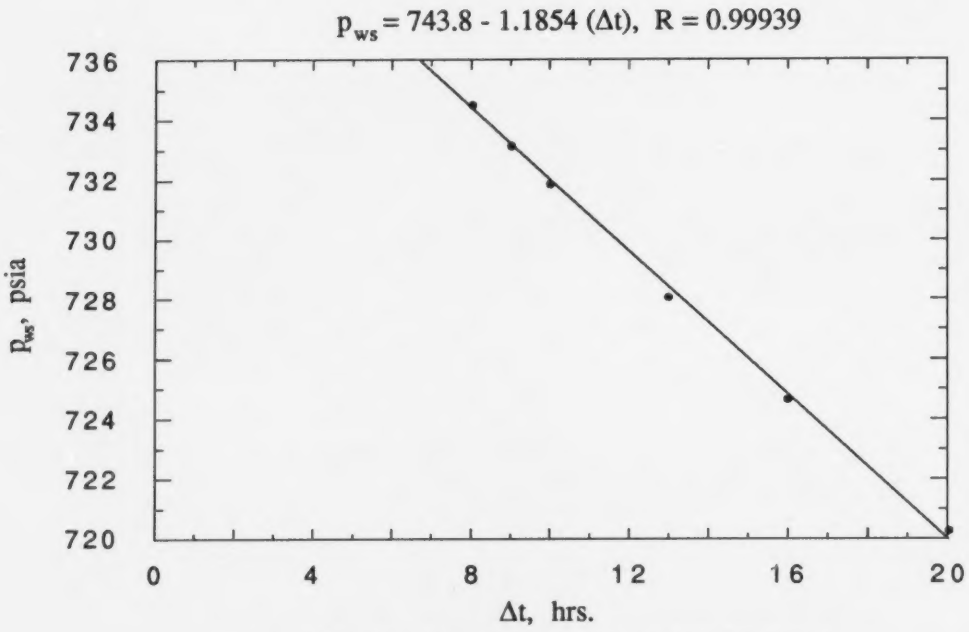

Fig. E5c - Cartesian graph of falloff data for Run 5

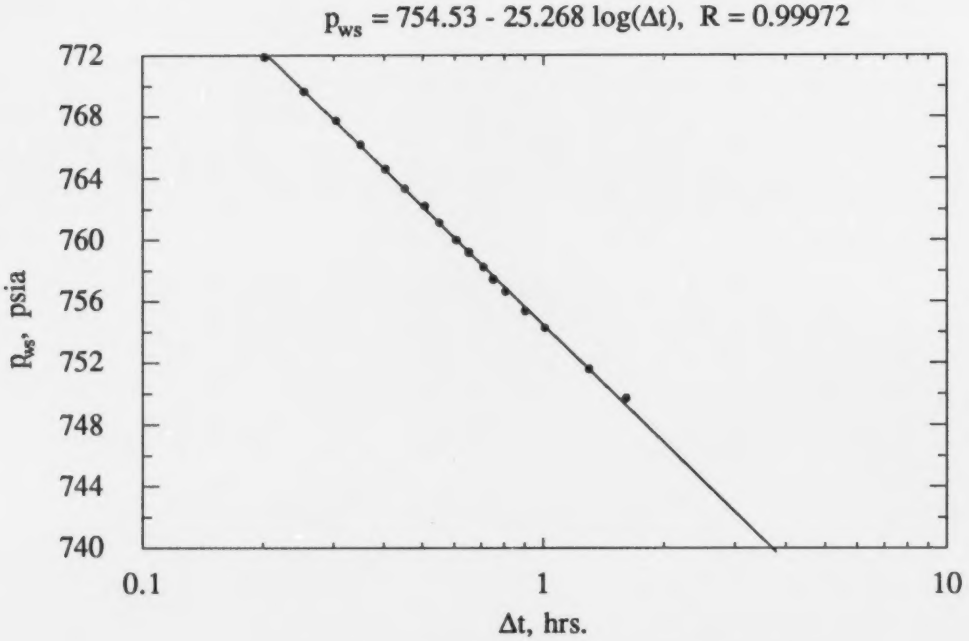

Fig. E5d - Semi-log graph of falloff data for Run 5

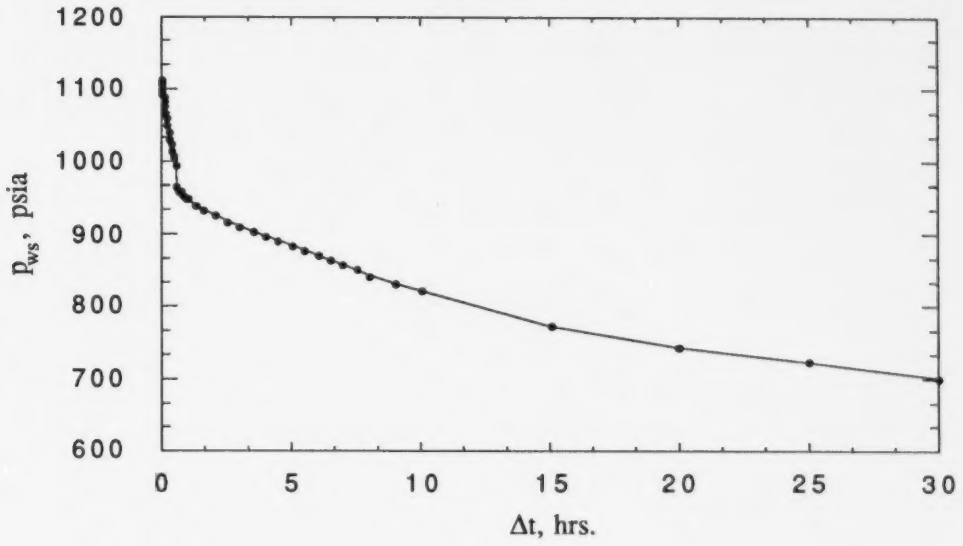

Fig. E6a - Falloff response from simulator for Run 6

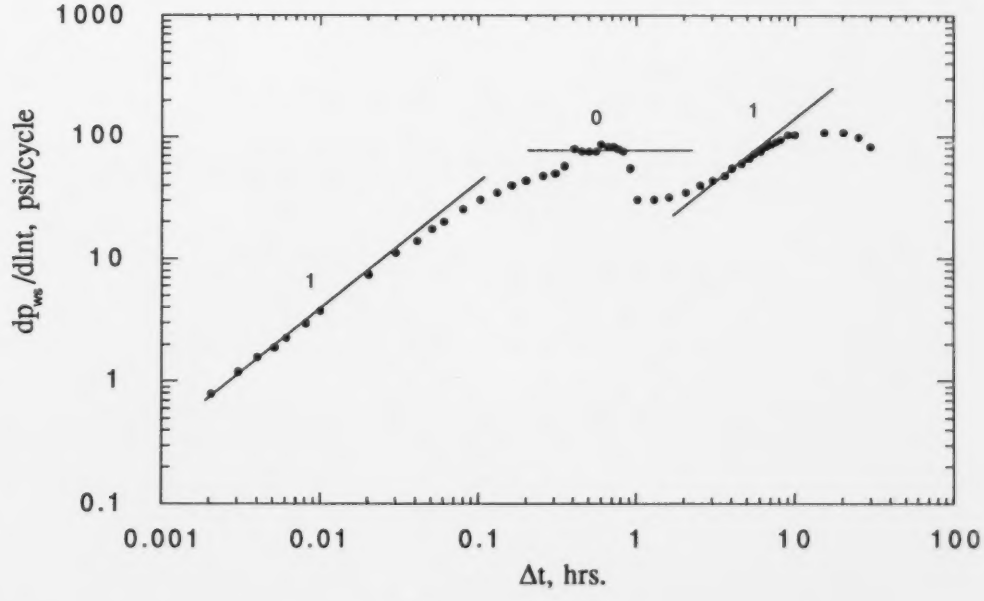

Fig. E6b - Semi-log pressure derivative response from falloff data for Run 6

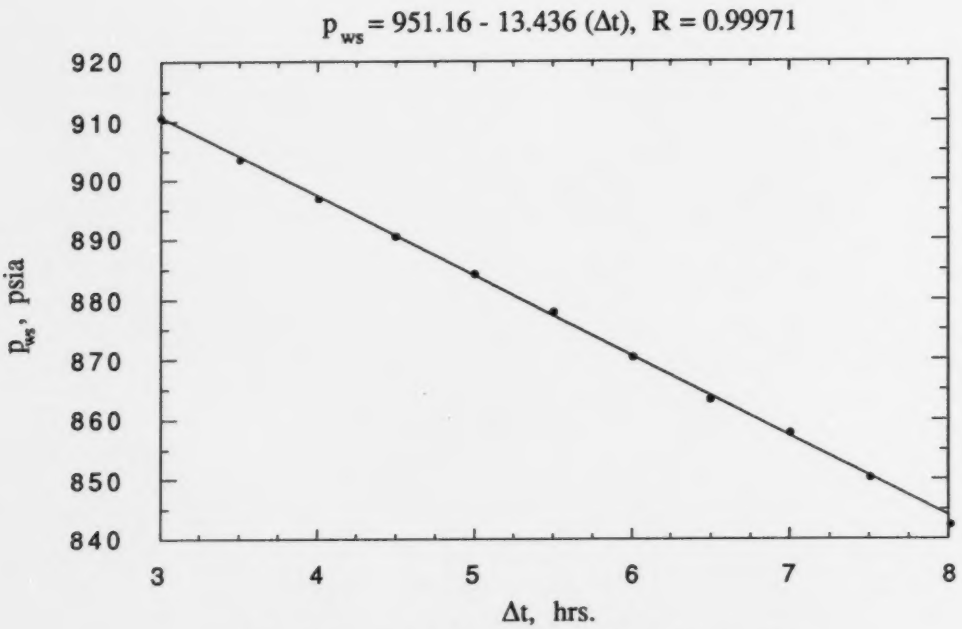

Fig. E6c - Cartesian graph of falloff data for Run 6

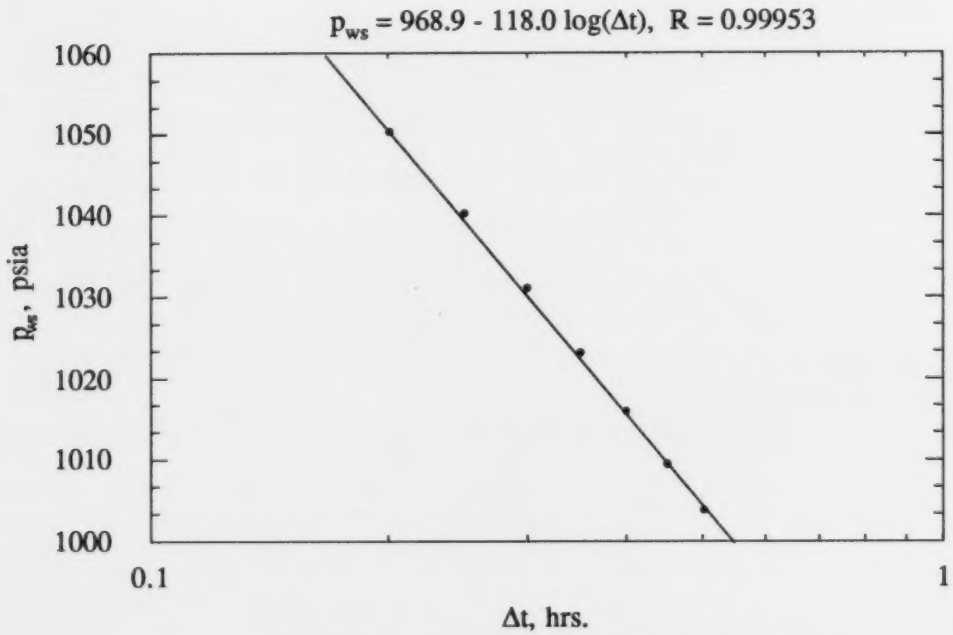

Fig. E6d - Semi-log graph of falloff data for Run 6

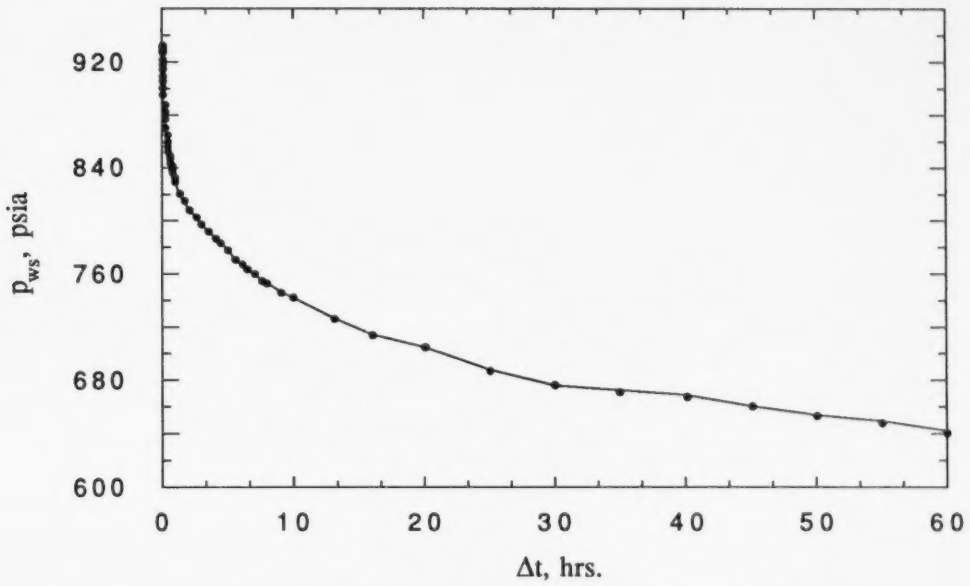

Fig. E7a - Falloff response from simulator for Run 7

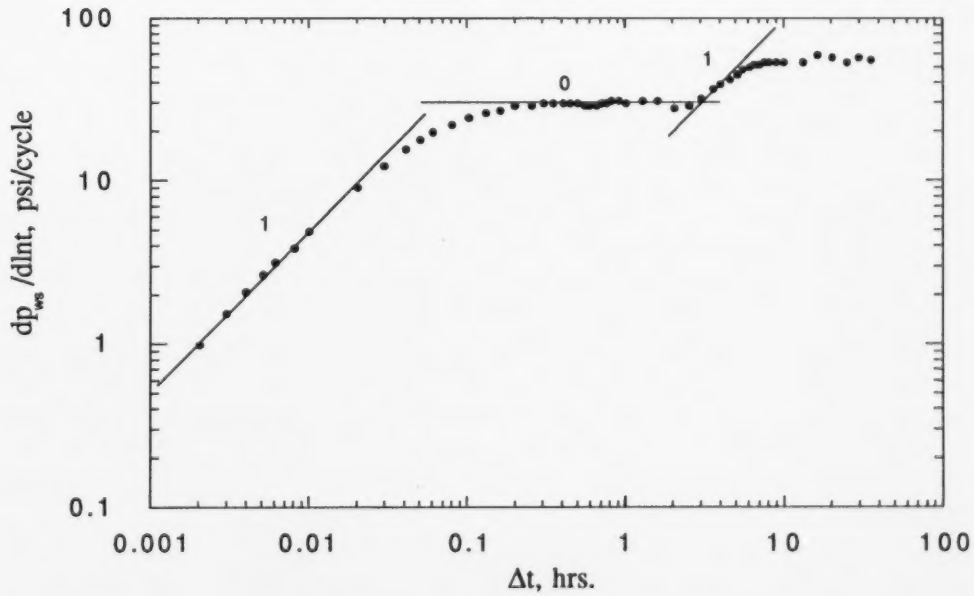

Fig. E7b - Semi-log pressure derivative response from falloff data for Run 7

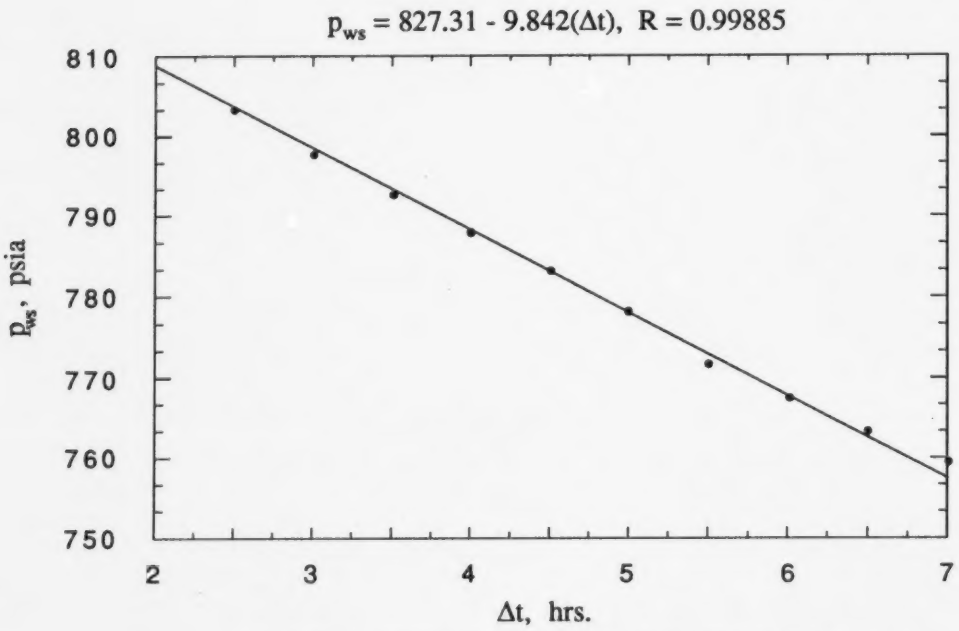

Fig. E7c - Cartesian graph of falloff data for Run 7

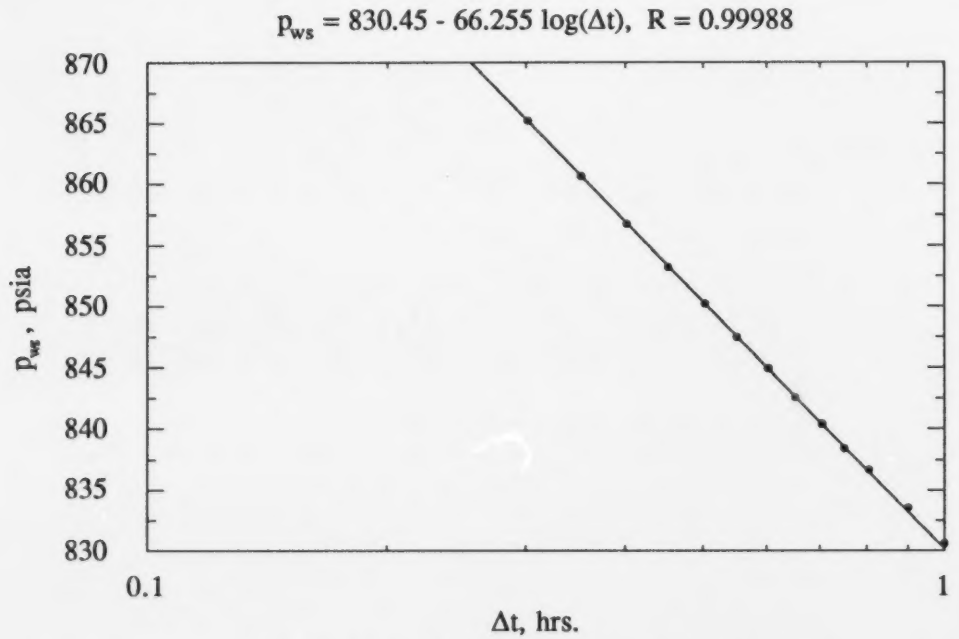

Fig. E7d - Semi-log graph of falloff data for Run 7

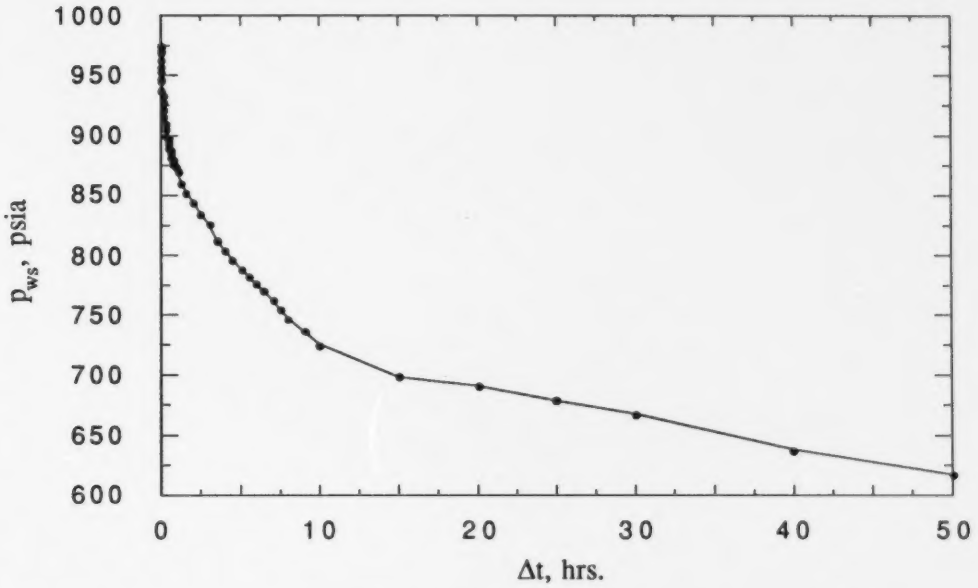

Fig. E8a - Falloff response from simulator for Run 8

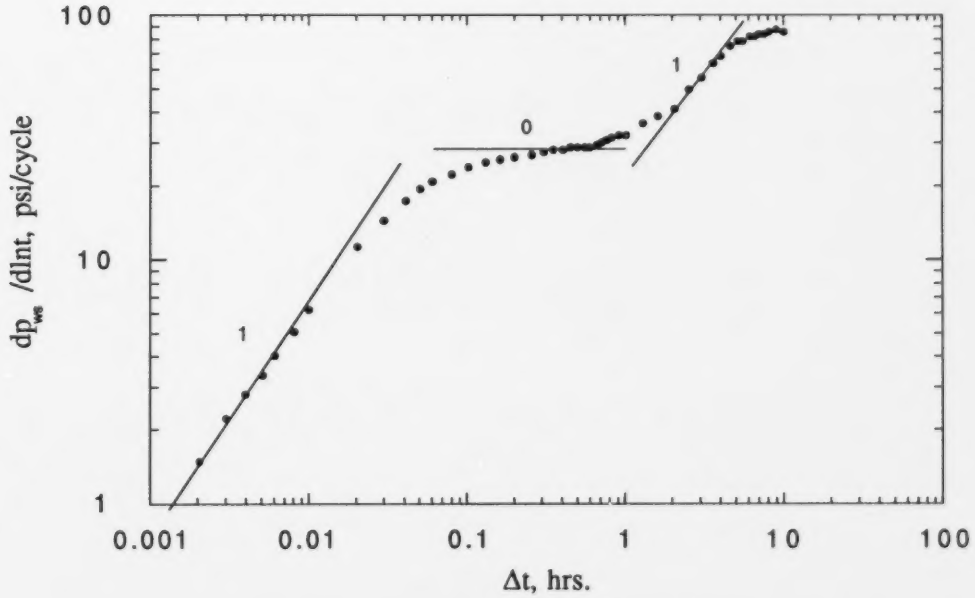

Fig. E8b - Semi-log pressure derivative response from falloff data for Run 8

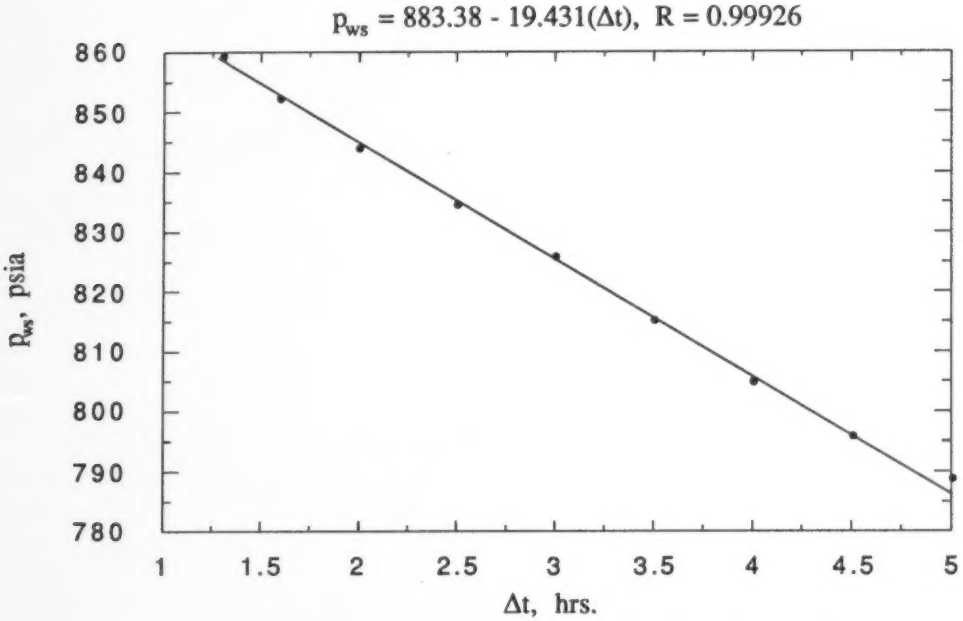

Fig. E8c - Cartesian graph of falloff data for Run 8

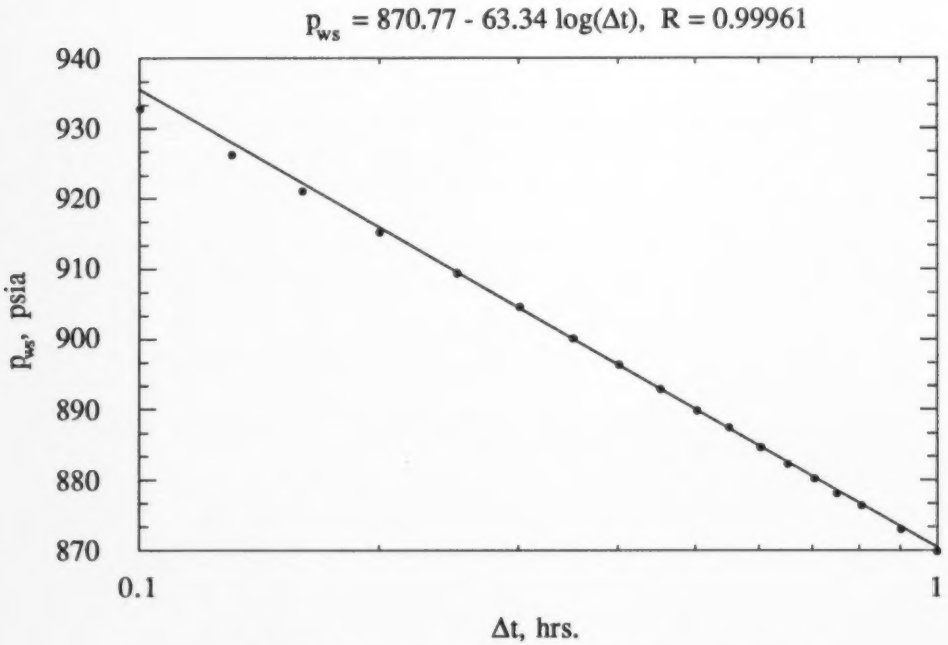

Fig. E8d - Semi-log graph of falloff data for Run 8

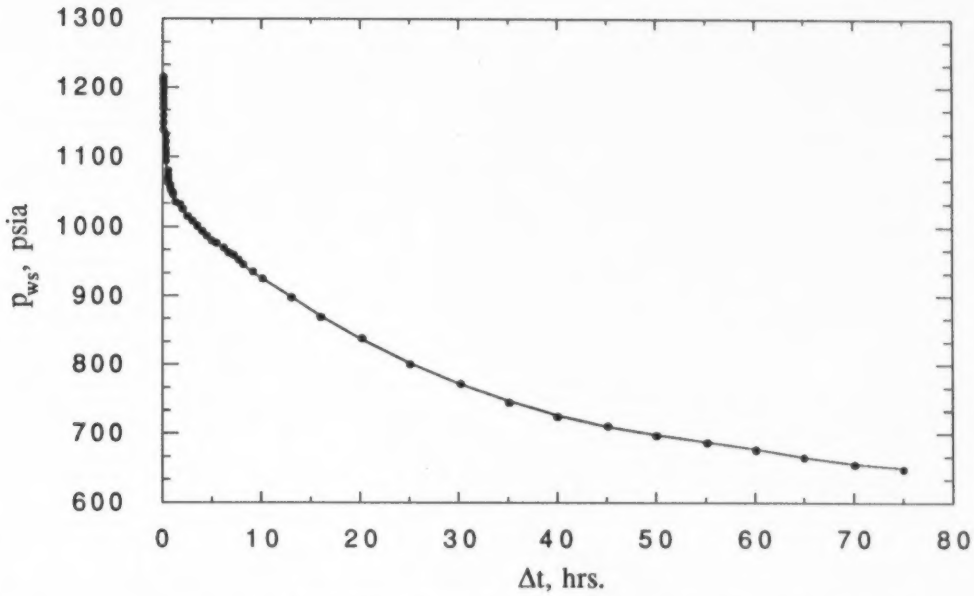

Fig. E9a - Falloff response from simulator for Run 9

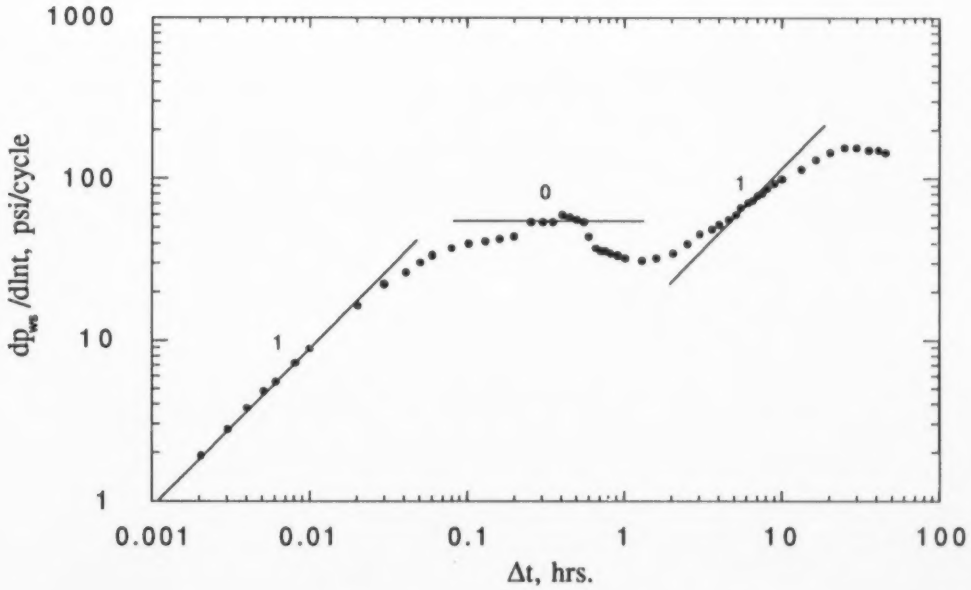

Fig. E9b - Semi-log pressure derivative response from falloff data for Run 9

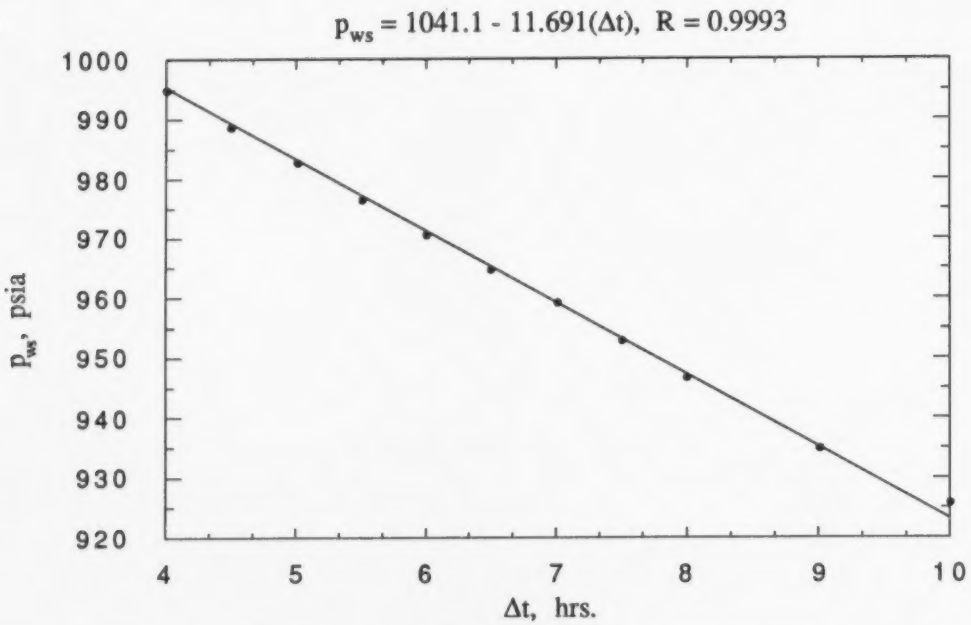

Fig. E9c - Cartesian graph of falloff data for Run 9

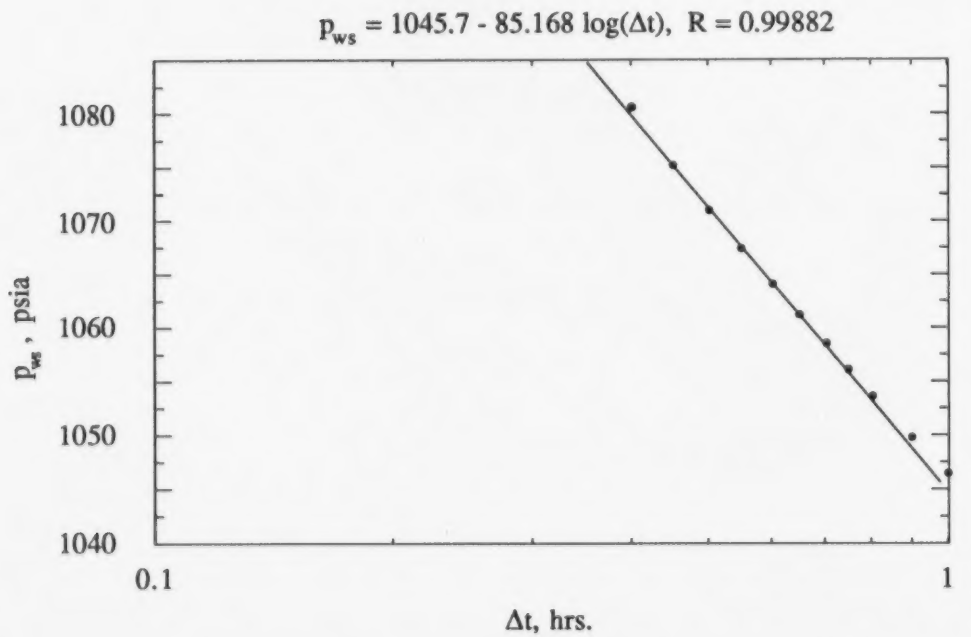

Fig. E9d - Semi-log graph of falloff data for Run 9

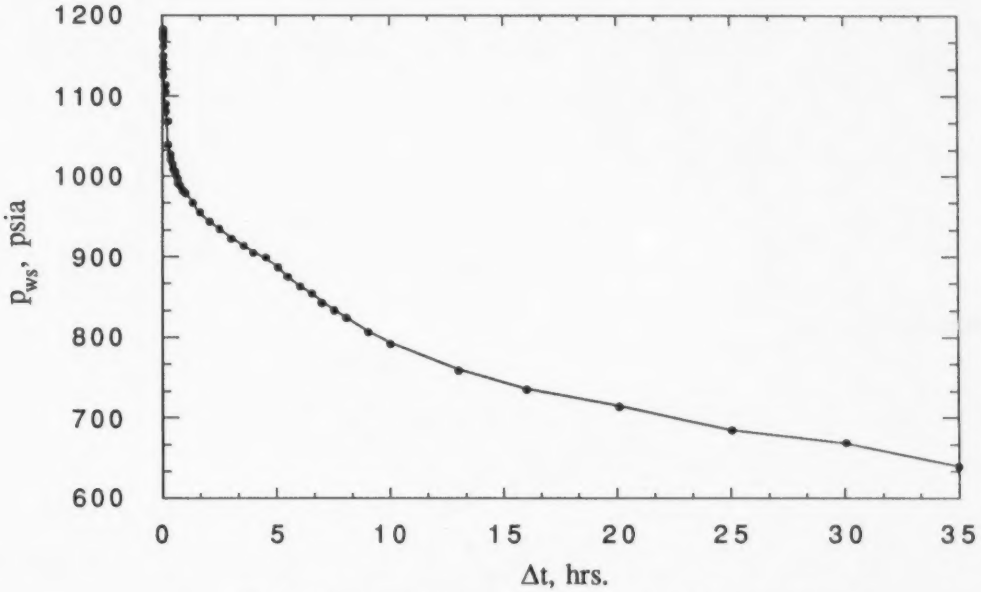

Fig. E10a - Falloff response from simulator for Run 10

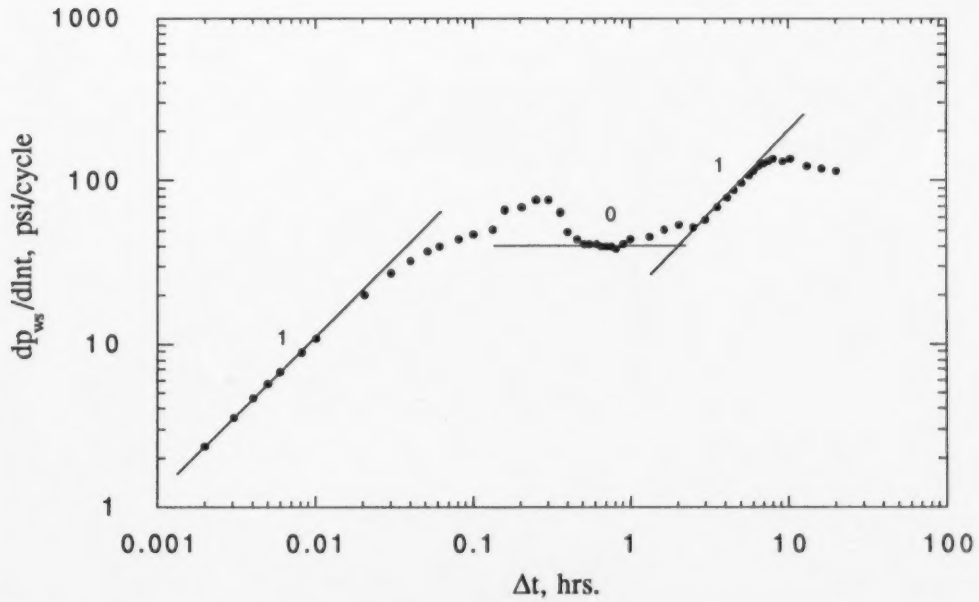

Fig. E10b - Semi-log pressure derivative response from falloff data for Run 10

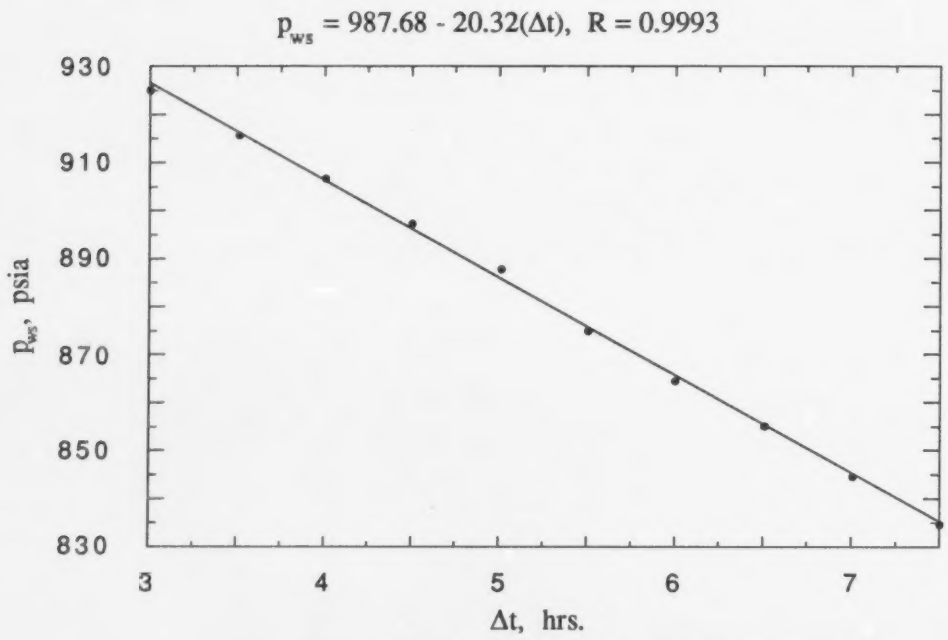

Fig. E10c - Cartesian graph of falloff data for Run 10

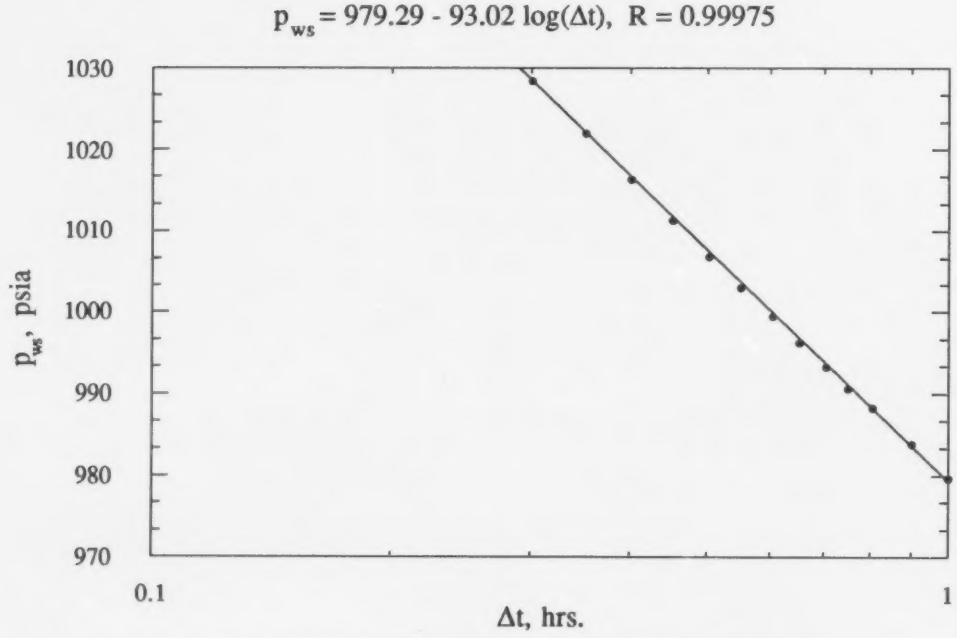

Fig. E10d - Semi-log graph of falloff data for Run 10